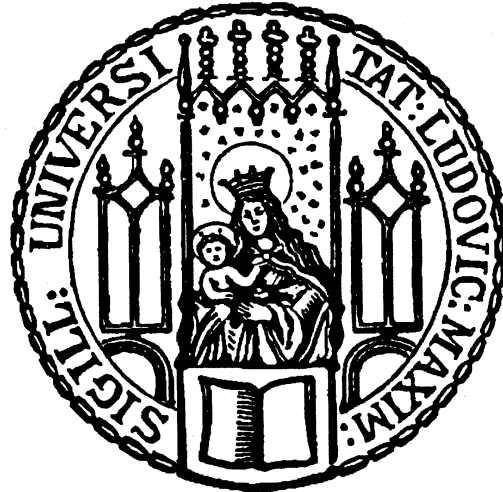


Tensor Networks for the Simulation of Strongly Correlated Systems



Dissertation der Fakultät für Physik
der
Ludwig-Maximilians-Universität München

vorgelegt von Stefan Depenbrock
aus Dortmund

München, den 10. Mai 2013

Erstgutachter: Prof. Dr. U. Schollwöck
Zweitgutachter: Prof. Dr. M. M. Wolf
Datum der mündlichen Prüfung: 22. Juli 2013

Zusammenfassung

In dieser Dissertation wird die klassische Simulation von stark wechselwirkenden Quantenvielteilchensystemen in mehr als einer Dimension mittels Matrixproduktzuständen und den allgemeineren Tensorproduktzuständen untersucht. Im Gegensatz zu klassischen Systemen besitzen Quantenvielteilchensysteme exponentiell mehr Freiheitsgrade, womit die numerische Beschreibung auf klassischen Computern erheblich erschwert wird.

Für diese Arbeit wurden zwei verschiedene Darstellungen von Vielteilchensystemen benutzt. Die erste davon sind die sogenannten Matrixproduktzustände (MPS), welche die Basis der sehr erfolgreichen Dichtematrixrenormierungsgruppe (DMRG) bilden. Obwohl sie ursprünglich für eindimensionale Systeme entwickelt wurden, können MPS im Prinzip beliebige Quantenvielteilchensysteme beschreiben. Mithilfe der Quanteninformationstheorie ist es möglich zu zeigen, dass MPS eine Darstellung dieser Systeme bilden, die lediglich polynomial in der Anzahl der Teilchen skaliert und somit eine effiziente Simulation von 1D-Systemen auf klassischen Computern ermöglicht. Eines der Schlüsselergebnisse dieser Arbeit ist, dass diese Darstellung tatsächlich so effizient ist, dass sogar große Systeme in zwei Dimensionen beschrieben werden können, womit ihre Simulation mittels DMRG ermöglicht wird.

Als Vorführung der Möglichkeiten der DMRG, wird diese auf den Heisenberg-Antiferromagneten mit Spin $S = 1/2$ auf dem kagome-Gitter angewandt. Der Grundzustand dieses Modells wird schon lange gesucht, mit Vorschlägen die von statischen Spinkonfigurationen bis hin zu sogenannten Spinflüssigkeiten reichen. In diesen exotischen Zuständen zerstören Quantenfluktuationen sämtliche konventionelle Ordnung und erzeugen so exotische Quantenordnungen. Mittels einer $SU(2)$ -symmetrischen Implementierung der DMRG ist es uns gelungen das exponentielle Wachstum der Verschränkung zu beschreiben und den Grundzustand dieses Modells für Zylinder mit bis zu 700 Spins zu berechnen. Obwohl wir einen eigentlich eindimensionalen Algorithmus für dieses zweidimensionale System benutzt haben, waren wir dennoch in der Lage die Anregungslücke zur ersten spin-haften Anregung zu berechnen. Gleichzeitig konnten wir die Grundzustandseigenschaften, wie z.B. Korrelationsfunktionen, statische Spinstrukturfaktoren und die Struktur und Verteilung von nächste-Nachbar Spin-Spin-Korrelationen untersuchen. Indem wir zusätzlich noch die aus der Quanteninformationstheorie bekannte topologische Verschränkungsentropie, ausgewertet haben, konnten wir mit großer Zuversicht zeigen, dass der Grundzustand dieses Systems eine topologisch geordnete Z_2 Quantenspinflüssigkeit ist.

Diese Studie wird ergänzt durch die Erweiterung von MPS zu höheren Dimensionen, die als Tensorproduktzustände bekannt sind. Wir haben einen Optimierungsalgorithmus für diese Zustände implementiert und ihn auf das bilineare-biquadratische-bikubische Heisenberg-Modell auf dem $z = 3$ Bethe-Gitter angewendet. Durch sorgfältige Analyse der Simulationsdaten konnten wir zeigen, dass die analytisch vorhergesagte Haldane-Phase tatsächlich ausgedehnten Raum im Phasendiagramm einnimmt. Schlüsseigenschaften dieser von Symmetrie beschützten topologischen Ordnung beinhalten eine Verdopplung der Niveaus im Verschränkungsspektrum und die Präsenz von Randspins, welche beide in unseren Simulationen gefunden wurden.

Abstract

This thesis treats the classical simulation of strongly-interacting many-body quantum-mechanical systems in more than one dimension using matrix product states and the more general tensor product states. Contrary to classical systems, quantum many-body systems possess an exponentially larger number of degrees of freedom, thereby significantly complicating their numerical treatment on a classical computer.

For this thesis two different representations of quantum many-body states were employed. The first, the so-called matrix product states (MPS) form the basis for the extremely successful density matrix renormalization group (DMRG) algorithm. While originally conceived for one-dimensional systems, MPS are in principle capable of describing arbitrary quantum many-body states. Using concepts from quantum information theory it is possible to show that MPS provide a representation of one-dimensional quantum systems that scales polynomially in the number of particles, therefore allowing an efficient simulation of one-dimensional systems on a classical computer. One of the key results of this thesis is that MPS representations are indeed efficient enough to describe even large systems in two dimensions, thereby enabling the simulation of such systems using DMRG.

As a demonstration of the power of the DMRG algorithm, it is applied to the Heisenberg antiferromagnet with spin $S = 1/2$ on the kagome lattice. This model's ground state has long been under debate, with proposals ranging from static spin configurations to so-called quantum spin liquids, states where quantum fluctuations destroy conventional order and give rise to exotic quantum orders. Using a fully $SU(2)$ -symmetric implementation allowed us to handle the exponential growth of entanglement and to perform a large-scale study of this system, finding the ground state for cylinders of up to 700 sites. Despite employing a one-dimensional algorithm for a two-dimensional system, we were able to compute the spin gap (i.e. the energy gap to the first spinful excitation) and study the ground state properties, such as the decay of correlation functions, the static spin structure factors, and the structure and distribution of the nearest-neighbor spin-spin correlations. Additionally, by applying a new tool from quantum information theory, the topological entanglement entropy, we could also with high confidence demonstrate the ground state of this model to be the elusive gapped Z_2 quantum spin liquid with topological order.

To complement this study, we also considered the extension of MPS to higher dimensions, known as tensor product states (TPS). We implemented an optimization algorithm exploiting symmetries for this class of states and applied it to the bilinear-biquadratic-bicubic Heisenberg model with spin $S = 3/2$ on the $z = 3$ Bethe lattice. By carefully analyzing the simulation data we were able to determine the presence of both conventional and symmetry-protected topological order in this model, thereby demonstrating the analytically predicted existence of the Haldane phase in higher dimensions within an extended region of the phase diagram. Key properties of this symmetry-protected topological order include a doubling of the levels in the entanglement spectrum and the presence of edge spins, both of which were confirmed in our simulations. This finding simultaneously validated the applicability of the novel TPS algorithms to the search for exotic order.

Publications

The following parts of this thesis have been published elsewhere:

1. The chapter on the spin liquid ground state of the antiferromagnetic Heisenberg model on kagome cylinders (Chap. 3) has been published in PRL:
Nature of the Spin Liquid Ground State of the $S = 1/2$ Kagome Heisenberg Model
S. Depenbrock, I. McCulloch, and U. Schollwöck
Phys. Rev. Lett. 109, 067201 (2012)
2. The chapter on the phase diagram of the bilinear-biquadratic-bicubic Heisenberg model on the $z = 3$ Bethe lattice (Chap. 4) has been submitted to PRB for publication and is available online at the arXiv:
Phase diagram of the Isotropic Spin-3/2 Model on the $z = 3$ Bethe Lattice
S. Depenbrock and F. Pollmann
arXiv:1303.1110

Contents

Zusammenfassung	I
Abstract	III
Publications	V
1 Introduction	1
2 Methods	5
2.1 Introduction	5
2.2 Matrix Product States	6
2.2.1 Schmidt decomposition	6
2.2.2 Construction of MPS	8
2.2.3 Canonical forms of MPS	12
2.2.4 Mixed canonical form	13
2.2.5 Construction of iMPS	15
2.2.6 Canonical form of iMPS	17
2.3 Tensor Product States	18
2.3.1 Tree tensor networks	19
2.3.2 Projected entangled-pair states	21
2.3.3 Fermionic tensor networks	25
2.4 Symmetries	28
2.5 Matrix Product Operators	30
2.6 Optimization Procedures	31
2.6.1 Imaginary-time evolution	32
2.6.2 Variational optimization	33
2.6.3 Single-site DMRG	35
2.6.4 Two-site DMRG	36
2.7 Parallelization	37
2.7.1 Shared-Memory Parallelization	38
2.7.2 Real-Space Parallelization	38
2.8 DMRG in Two Dimensions	43
3 The Kagome Heisenberg Antiferromagnet	45
3.1 Review of Published Results for the Kagome Heisenberg Antiferromagnet	47
3.1.1 Classical ground state	49
3.1.2 Valence bond crystals	49
3.1.3 Quantum spin liquids	50

3.1.4	Numerical results	53
3.1.5	Experimental realizations	55
3.2	Methodology	57
3.2.1	Mapping the lattice	57
3.2.2	Simulation details	57
3.2.3	Entanglement entropy	59
3.3	Nature of the Spin Liquid Ground State of the $S = 1/2$ Kagome Heisenberg Model	61
4	Symmetry-Protected Topological Phases and the Bethe Lattice	71
4.1	Haldane Phase and Haldane Conjecture	72
4.2	Phase Diagram of the Isotropic Spin-3/2 Model on the $z = 3$ Bethe Lattice	74
5	Summary and Outlook	83
	Bibliography	85
	Curriculum Vitae	109
	Acknowledgments	111

1 Introduction

Some of the most elemental and ubiquitous features of physics are phases and the transitions between them. For a long time it was thought that Landau's theory of symmetry breaking, together with the Fermi-liquid theory of metals composed a framework in which all states of matter could be described using e.g. renormalization group techniques [1]. Examples of this include superconductivity [2], Bose-Einstein condensation [3], and superfluidity [4].

This picture was shattered when the fractional quantum Hall effect and high-temperature superconductivity [5] were discovered. Fractional quantum Hall (FQH) states for example exhibit non-Fermi liquid behavior, while simultaneously different fractional quantum Hall states break the same symmetries, thereby falling out of both Fermi liquid theory and the Landau-Ginzburg paradigm of symmetry breaking.

By the study of so-called chiral spin liquids in high-temperature superconductors it was realized that there exists a large class of phases beyond the paradigm of symmetry breaking, most of which are magnetically disordered insulators [6–11]. These new phases beyond Landau theory can be described by the concept of quantum order [12], the most prominent example of which is known as topological order [13, 14]. Instead of being characterized by a broken symmetry, these phases are rather described by an underlying structure in virtual gauge fields that distinguishes them from other, topologically trivial phases.

The defining property of these new types of order is entanglement [12, 15–17]. Whereas conventional order is usually carried by short-range entanglement and long-range correlations, this picture reverses itself for quantum orders which are carried by short-range correlations and long-range entanglement [12, 18–20]. Somewhere in-between these concepts lies a hybrid class of order known as symmetry-protected topological order, which exhibits both short-range entanglement and short-range correlations, while still being topologically ordered and thereby outside the reach of Landau theory.

Some of these new orders were initially studied due to their link to high-temperature superconductivity [8, 21–26], but physicists soon realized these states to be interesting in their own right as they display bewildering new physics such as fractionalized excitations [6, 9, 27] (e.g. magnetic monopoles) or non-trivial ground state degeneracy [11, 28]. Aside from a possible explanation of high- T_c , some of these new states (i.e. topological states) also offer a different route to quantum computing. It has been proposed [29, 30] to employ their topologically protected degenerate ground states to store information in the form of topological qubits. These can then be used for topological quantum computing which is expected to be fault-tolerant due to the topological protection of the ground state, further increasing the interest in these phases.

The key aspect of these new and exotic states of matter is that they are not created by external symmetries such as lattice symmetries, but instead many of these fascinating phases come about as a result of strong correlations that are frustrated due to geometry or competing interactions. The collaborative effects of strong interactions then create phase-coherent correlations which give rise to new exotic physics in insulating systems.

This leads us to one of the most exciting problems of condensed matter theory: while metals are well-understood, the theory of magnetically disordered insulators is much more complicated and less-understood. The complications in understanding insulating phases of matter are related to the sheer number of different parameter sets realizing these phases. Well-known examples of insulating phases include the Mott insulator, where charge carriers are localized due to electron-electron interactions, and topological insulators that only carry current on their surface due to a symmetry-protected gapped bulk. These two examples already exemplify the sheer abundance of different concepts and mechanisms underlying insulated phases. One of the most fruitful fields in this context is the field of strongly correlated frustrated magnetism, where competing interactions and/or geometric frustration cause Hamiltonian terms to be incompletely fulfilled, i.e. to be frustrated. These frustration-induced quantum fluctuations then lead to new states of matter and strong entanglement.

Although these strong correlations and interactions enable fascinating new phenomena, they also pose the biggest hindrance in trying to understand the underlying theory. Whereas many conventional phases can be understood in a framework of almost free (or weakly correlated) particles the same approach often fails for strongly interacting systems, where contributions from many energy and length scales have to be taken into account. Examples of these are e.g. strongly correlated transition metal oxides (e.g. *NiO*) which form Mott insulators or high-temperature superconductors, where weakly correlated approximations such as Hartree-Fock or density functional theory with the local density approximation routinely fail. Since many of these phenomena are related to the inherently quantum property of entanglement, semi-classical techniques that do not account for this property also often break down at absolute zero, thus failing to determine the correct ground state. Analytical methods on the other hand usually have to make gross approximations, causing them to miss the essential physics of quantum orders thereby yielding misleading answers.

On the experimental front, the study of cold atom gases has given experimentalists a number of new methods to analyze this behavior [31], as it is possible to directly simulate theoretical models in these systems. In optical lattices, many theoretical models (e.g. the 2D-Hubbard model [32]) can be experimentally realized [33] and observed for signs of high-temperature superconductivity or topological order. However, in order to identify the interesting parameter ranges for these experiments, a better understanding of the models thought to describe the physical systems is desirable.

In some other cases there are condensed matter compounds which can be studied using e.g. neutron scattering [34–36] or angle-resolved photoemission spectroscopy (ARPES) [37–39]. Although these experimental techniques allow some insight in the bulk behavior of a sample, they still face the challenge of correctly interpreting the data, based on an approximative model. The determination of the parameters

of these models is again subject to the same problems an exact theory faces. New approaches and techniques are therefore necessary.

Complementing analytical and experimental investigations are numerical techniques, which aim to determine a system's ground state properties numerically. But computational physics struggles with parametrizing the exponentially large size of the Hilbert space in quantum many-body problems on a classical computer. Despite the existence of a multitude of well-established numerical techniques, such as exact diagonalization [40], quantum Monte Carlo calculations [41, 42], series expansion [43], or linked-cluster expansion [44], to name just some, a large class of two-dimensional many-particle systems involving frustrated spins or fermions remains essentially unsolved. It is therefore of strong interest for numerical physicists to develop techniques that can efficiently parametrize the relevant aspects of the problem and compute an approximate solution.

Such a method is the density matrix renormalization group (DMRG) that was introduced by S.R. White in 1992 [45], which relies on a highly efficient parametrization of a one-dimensional system's Hilbert space known as matrix product states (MPS) [46–48] to calculate the ground state [49, 50]. In recent years there have been extensions of the class of ansatz states underlying DMRG to higher dimensions, known as tensor product or tensor network states [51–83].

In this thesis we will showcase the application of two of these algorithms to problems in more than one dimension. First we apply DMRG to a very hard two-dimensional system, the Heisenberg antiferromagnet on the kagome lattice. The ground state of this model has been investigated for more than two decades and we can show it to be topologically ordered using MPS techniques. In a second application we used one of the extensions of DMRG to higher dimensions, namely tensor product states for tree tensor networks, to study a strongly correlated spin model on the $z = 3$ Bethe lattice. Within this model's phase diagram we found both conventionally ordered phases and a symmetry-protected topological phase.

This thesis is organized as follows: In the first part (Chap. 2), we introduce the numerical tools we used to simulate strongly correlated many-body systems. This also includes a discussion on how simulations in the space of MPS can be performed that make use of shared-memory and real-space parallelization while exploiting symmetries. Chapter 3 is then devoted to the kagome lattice Heisenberg antiferromagnet, introducing topological order and giving an overview of current results in the process. That study is followed by Chapter 4, where the simulations on the Bethe lattice and symmetry-protected topological order are discussed. This thesis is then wrapped up by Chapter 5, which summarizes the key aspects.

2 Methods

Note that parts of this chapter were adapted from

S. Depenbrock and F. Pollmann, arXiv:1303.1110

In this rather technical chapter we offer a concise introduction to matrix product states (MPS), tensor product states (TPS), and some of the algorithms operating on these ansatz states with special attention given to the density matrix renormalization group (DMRG) [45]. We will also describe some recent developments such as parallelization and fermionic tensor networks. We will not cover the classical representation of DMRG in terms of blocks or try to be exhaustive on DMRG since there is a host of literature available on these topics, e.g. Schollwöck's reviews of DMRG [49, 50].

After a short review of the construction of MPS and their elemental properties and manipulations we proceed to introduce TPS, followed by a compact discussion of symmetries and fermionic tensor networks. With these tools we go on to describe Matrix Product Operators (MPOs), one of the basic building blocks of state of the art implementations of DMRG. We then present some of the numerous optimization procedures for these states before expanding on recent progress in the field with a focus on the real-space parallelization of DMRG.

2.1 Introduction

Quantum many-body systems consist of a large number of degrees of freedom, as the dimension of the Hilbert space \mathcal{H} grows exponentially with the number of particles contained within. Consider e.g. a simple spin-1/2 spin chain of length L . The full Hilbert space \mathcal{H} is then given by the tensor product of the single-particle Hilbert spaces:

$$\mathcal{H} = \bigotimes_{i=1}^L \mathcal{H}_0 \quad (2.1)$$

where \mathcal{H}_0 denotes the single-particle Hilbert space. The dimension of the Hilbert space therefore scales exponentially with the number of particles,

$$\dim \mathcal{H} = (\dim \mathcal{H}_0)^L = 2^L \quad (2.2)$$

for spin-1/2 particles. Finding the ground state in such a huge space rigorously is exponentially hard, but for one-dimensional quantum lattice models there exists a method, the DMRG, that manages to efficiently find the ground state even of large systems. DMRG was originally introduced by Steve White [45] as a modification of the numerical renormalization group and relies on a highly efficient parametrization

of the Hilbert space known as matrix product states [46, 47, 84]. In fact, this representation allows the calculation of almost arbitrary expressions with only modestly scaling numerical resources.

The excellent performance of DMRG has been shown to be closely linked to the scaling of entanglement in one-dimensional gapped systems [15–17, 85–87]. For these systems, the scaling of entanglement obeys an area law, i.e. it does not grow with the system size in 1D [88]. But this reasoning only applies to ground states and does not hold for excited states or even critical systems where there are logarithmic corrections to the area law [89]. Indeed the growth of entanglement is the limiting factor for the application of DMRG to other problems.

Still, DMRG has been overwhelmingly successful, with extensions to the simulation of time-dependent problems [90, 91] and dynamical quantities being introduced in the last years [92]. It can even be employed to perform calculations at finite temperatures, for quantum chemistry, or to some extent in two dimensions [93–102]. In the following we will introduce DMRG’s basis states, the matrix product states, followed by their extension to infinite systems and two dimensions. Afterwards we will introduce matrix product operators and finally describe the DMRG optimization scheme for these ansatz states.

2.2 Matrix Product States

2.2.1 Schmidt decomposition

The Schmidt decomposition [103, 104] forms the basis for the class of states known as matrix product states, making it one of the most important tools in the field of matrix product algorithms. Among its many applications is the construction of matrix product states (MPS) and the characterization of multipartite quantum systems. Here we will give a short outline of this decomposition’s theoretical background and usage, roughly following Ref. [105].

Consider a quantum system that is in one of N states $|\psi_i\rangle$, with respective probabilities p_i , where $i \in \{1, \dots, N\}$. Then the set of pairs $\{p_i|\psi_i\rangle\}$ is called an *ensemble of pure states* and the system’s *density matrix* is defined by the equation

$$\rho := \sum_{i=1}^N p_i |\psi_i\rangle\langle\psi_i|. \quad (2.3)$$

The density matrix is a positive operator and always satisfies $\text{Tr}(\rho) = 1$. If a quantum system is in a state $|\psi\rangle$ with probability 1, its state is exactly known and it is said to be in a *pure state* where its density matrix is given by $\rho = |\psi\rangle\langle\psi|$. Otherwise, if the system described by ρ is in a mixture of the different pure states in the ensemble for ρ , it is called a *mixed state*. For a pure state $\text{Tr}(\rho^2) = 1$ holds, whereas for a mixed state $\text{Tr}(\rho^2) < 1$ holds.

Since any unitary transformation of the density operator’s basis generates a new density matrix, there is no unique density operator. Two different sets $|\psi_i\rangle$ and

$|\tilde{\Phi}_j\rangle$ generate the same density matrix if and only if $|\tilde{\psi}_i\rangle = \sum_j u_{ij}|\tilde{\Phi}_j\rangle$, where u_{ij} is a unitary matrix of complex numbers and we append additional vectors with probability 0 to whichever set of vectors $|\tilde{\psi}_i\rangle$ and $|\tilde{\Phi}_j\rangle$ is smaller so that the two sets have the same number of elements.

Nevertheless the system can be completely characterized by its density matrix, as all the system's properties can be determined from ρ . This can be shown by rewriting the postulates of quantum mechanics in the terminology of the density operator. Therefore an equivalent description of the system is given by ρ instead of the wave function ψ .

For the algorithms described in this thesis, one of the most important applications of the density matrix is as a descriptive tool for *subsystems* of a composite quantum system, which is provided by the so-called *reduced density matrix*. The state space of a composite physical system is given by the tensor product of the state spaces of the component physical systems, i.e. it is given by the tensor product of the Hilbert spaces of the constituent systems: $\mathcal{H} = \mathcal{H}_1 \otimes \mathcal{H}_2 \otimes \dots \otimes \mathcal{H}_N$. Suppose now, that we have two physical systems A and B , whose state is given by the density matrix $\rho^{[AB]}$. The reduced density matrix for subsystem A is then defined as $\rho^{[A]} = \text{Tr}_B(\rho^{[AB]})$, where Tr_B is a map of operators known as the *partial trace* over subsystem B . The partial trace is defined by

$$\text{Tr}_B(|a_1\rangle\langle a_2| \otimes |b_1\rangle\langle b_2|) = |a_1\rangle\langle a_2| \text{Tr}(|b_1\rangle\langle b_2|), \quad (2.4)$$

with a_1, a_2 in the state space of A and b_1, b_2 in the state space of subsystem B . The trace operation appearing on the right side is the usual trace operation for subsystem B , i.e. $\text{Tr}(|b_1\rangle\langle b_2|) = \langle b_2|b_1\rangle$. By additionally requiring the partial trace to be linear in its input, the partial trace is uniquely defined.

With these building blocks at hand we have the necessary ingredients to introduce the *Schmidt Decomposition* [105] which is an indispensable tool for the description of quantum systems. Suppose $|\psi^{[AB]}\rangle$ describes a pure state of the composite system AB , then there exist orthonormal states $|\Phi^{[A]}\rangle$ for subsystem A and orthonormal states $|\Phi^{[B]}\rangle$ for subsystem B such that

$$|\psi^{[AB]}\rangle = \sum_{i=1}^{\kappa} \Lambda_i |\Phi_i^{[A]}\rangle |\Phi_i^{[B]}\rangle, \quad (2.5)$$

where the Λ_i are non-negative real numbers satisfying $\sum_i \Lambda_i^2 = 1$ known as *Schmidt coefficients*. Mathematically the Schmidt Decomposition is equivalent to a Singular Value Decomposition (SVD), enabling us to efficiently compute this decomposition numerically. The two bases $|\Phi_i^{[A]}\rangle$ and $|\Phi_i^{[B]}\rangle$ for the sub-systems are called the *Schmidt bases* for A and B respectively, and the number of non-zero values Λ_i is called the *Schmidt number* or *Schmidt rank* for $|\psi^{[AB]}\rangle$. The Schmidt number is an interesting property of a composite quantum system, as it can be used to quantify the amount of entanglement between the sub-systems A and B [106]. As a direct consequence of the Schmidt decomposition it follows that the state $|\psi^{[AB]}\rangle$ of a composite system AB is a product state if and only if it has a Schmidt rank of 1. The

converse also holds true, i.e. $|\psi^{[AB]}\rangle$ is a product state if and only if $\rho^{[A]}$ and $\rho^{[B]}$ are pure states.

A common measure for the entanglement of two subsystems is the *von-Neumann entropy* which can be computed from the Schmidt coefficients. It is given by

$$S = - \sum_{i=1}^{\kappa} \alpha_i \log_2 \alpha_i, \quad (2.6)$$

where the α_i are given by the Schmidt decomposition: $\alpha_i = \Lambda_i^2$, where the Λ_i are the Schmidt coefficients of the Schmidt decomposition according to this bipartition. The entropy is therefore confined to the interval

$$0 \leq S \leq - \sum_{i=1}^{\kappa} \frac{1}{\kappa} \log_2 \frac{1}{\kappa} = \log_2 \kappa, \quad (2.7)$$

i.e. the maximum entropy increases with the Schmidt rank κ . To put it in other words, the entanglement between the two sub-systems is upper-bounded by the Schmidt rank κ .

Let now $|\psi^{[AB]}\rangle$ be a pure state of a composite system AB . Then, by calculating the Schmidt decomposition, we obtain $\rho^{[A]} = \sum_i \Lambda_i^2 |\Phi_i^{[A]}\rangle \langle \Phi_i^{[A]}|$ and $\rho^{[B]} = \sum_i \Lambda_i^2 |\Phi_i^{[B]}\rangle \langle \Phi_i^{[B]}|$, therefore the eigenvalues of $\rho^{[A]}$ and $\rho^{[B]}$ are identical, namely Λ_i^2 for both density matrices.

2.2.2 Construction of MPS

The description of quantum many-body systems is extremely hard in general, as the state space accessible to the system grows exponentially with the size of the system. This growth of the underlying Hilbert space allows for highly entangled states which are intractable classically. This problem can be circumvented by considering the distribution of the states in Hilbert space. Since these states often arise from local interactions and local correlations, a description of the states that has this locality built in may be a good solution. Such a representation is given by matrix product states (MPS) [48, 49, 84, 107, 108]. Here we will introduce the construction of MPS and discuss some of their properties that are relevant to this thesis.

Let us consider a state $|\psi\rangle \in (\mathcal{H}^d)^{\otimes N}$ of N sites defined on an one-dimensional chain, where each site is described by a d -dimensional Hilbert space \mathcal{H}^d . The state $|\psi\rangle$ can then be expanded in the local basis of the sites:

$$|\psi\rangle = \sum_{i_1=1}^d \cdots \sum_{i_N=1}^d c_{i_1 \dots i_N} |i_1\rangle \otimes \dots \otimes |i_N\rangle. \quad (2.8)$$

The Schmidt decomposition (SD) of $|\psi\rangle$ according to some bipartition $A : B$ then

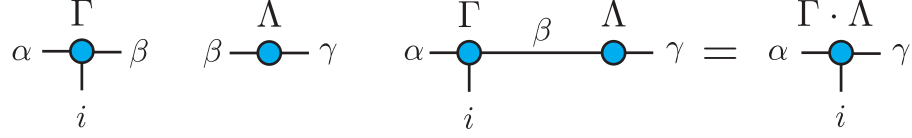
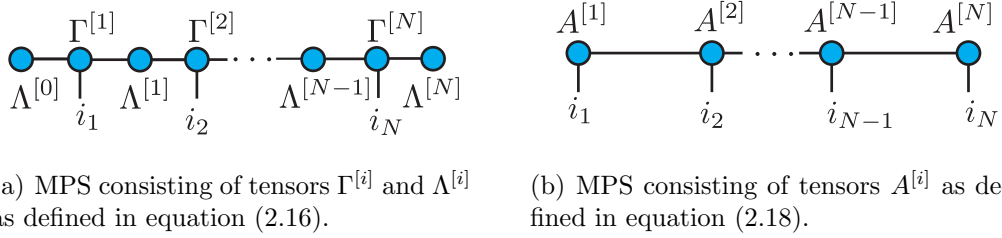


Figure 2.1: Diagrammatic representation of the tensors Γ (left) and Λ (middle) with physical index i and two virtual indices α and β and β and γ respectively. Tensors are represented by circles and their indices by legs. A leg connecting two circles corresponds to a *bond index* shared by two tensors that is summed over. An open leg corresponds to an uncontracted index.



(a) MPS consisting of tensors $\Gamma^{[i]}$ and $\Lambda^{[i]}$ as defined in equation (2.16).

(b) MPS consisting of tensors $A^{[i]}$ as defined in equation (2.18).

Figure 2.2: The state $|\psi\rangle$ represented in terms of different tensors for open boundary conditions.

reads

$$|\psi\rangle = \sum_{\alpha=1}^{\kappa} \Lambda_{\alpha} |\Phi_{\alpha}^{[A]}\rangle \otimes |\Phi_{\alpha}^{[B]}\rangle, \quad (2.9)$$

where $|\Phi_{\alpha}^{[A]}\rangle$ ($|\Phi_{\alpha}^{[B]}\rangle$) are the eigenvectors of the reduced density matrix $\rho^{[A]}$ ($\rho^{[B]}$) respectively with eigenvalues $|\Lambda_{\alpha}|^2 > 0$ and κ is again the Schmidt rank of the decomposition. By computing a succession of Schmidt decompositions for this state, we can then obtain a more local description of the system. Assuming the Schmidt rank for each decomposition is χ , the coefficients for this representation are given by

$$c_{i_1 \dots i_N} = \sum_{\alpha_0, \dots, \alpha_N=1}^{\chi} \Lambda_{\alpha_0} \Gamma_{\alpha_0 \alpha_1}^{[1] i_1} \Lambda_{\alpha_1}^{[1]} \Gamma_{\alpha_1 \alpha_2}^{[2] i_2} \Lambda_{\alpha_2}^{[2]} \Gamma_{\alpha_2 \alpha_3}^{[3] i_3} \Lambda_{\alpha_3}^{[3]} \dots \Gamma_{\alpha_{N-1} \alpha_N}^{[N] i_N} \Lambda_{\alpha_N}. \quad (2.10)$$

This representation employs N three-index tensors $\{\Gamma^{[1]} \dots \Gamma^{[N]}\}$ and $N+1$ diagonal matrices $\{\Lambda^{[0]} \dots \Lambda^{[N]}\}$, whose indices i_l and α_l take values in $\{1, \dots, d\}$ and $\{1, \dots, \chi\}$ respectively [109]. The diagonal tensors Λ_0 and Λ_N in this representation are scalars which are introduced for reasons which will become apparent later on. There is a very efficient diagrammatic representation of these decompositions which is introduced in Fig. 2.1.

To obtain this representation, $N-1$ Schmidt decompositions have to be concatenated. More explicitly, first the SD according to the bipartition of the system into

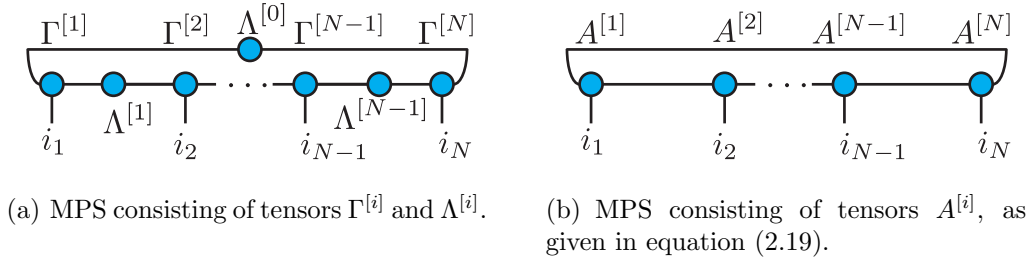


Figure 2.3: Diagrammatic representation of the state $|\psi\rangle$ in terms of different tensors for periodic boundary conditions.

site 1 and the $N - 1$ remaining sites is calculated:

$$|\psi\rangle = \sum_{\alpha_1=1}^{\chi} \Lambda_{\alpha_1}^{[1]} |\Phi_{\alpha_1}^{[1]}\rangle \otimes |\Phi_{\alpha_1}^{[2\dots N]}\rangle. \quad (2.11)$$

We then expand the first Schmidt vector $|\Phi_{\alpha_1}^{[1]}\rangle$ in terms of the local basis vectors $|i_1\rangle$ of the first site:

$$|\Phi_{\alpha_1}^{[1]}\rangle = \sum_{i_1=1}^d \Gamma_{\alpha_1}^{[1]i_1} |i_1\rangle. \quad (2.12)$$

Following this, the next Schmidt vector is expanded in the second site's local basis:

$$|\Phi_{\alpha_1}^{[2\dots N]}\rangle = \sum_{i_2=1}^d |i_2\rangle \otimes |\tau_{\alpha_1 i_2}^{[3\dots N]}\rangle. \quad (2.13)$$

With a succession of further Schmidt decompositions of $|\psi\rangle$, we can then recursively express every newly constructed vector $|\tau_{\alpha_1 i_2}^{[3\dots N]}\rangle$ in terms of at most χ Schmidt vectors $\{|\Phi_{\alpha_2}^{[3\dots N]}\rangle\}_{\alpha_2=1}^{\chi}$ and the corresponding Schmidt coefficients $\Lambda_{\alpha_2}^{[2]}$:

$$|\tau_{\alpha_1 i_2}^{[3\dots N]}\rangle = \sum_{\alpha_2=1}^{\chi} \Gamma_{\alpha_1 \alpha_2}^{[2]i_2} \Lambda_{\alpha_2}^{[2]} |\Phi_{\alpha_2}^{[3\dots N]}\rangle. \quad (2.14)$$

In the last step Eq. (2.14) is substituted in Eq. (2.13) and the result is introduced into Eq. (2.12) to obtain

$$|\psi\rangle = \sum_{i_1, i_2=1}^d \sum_{\alpha_1, \alpha_2=1}^{\chi} \Gamma_{\alpha_1}^{[1]i_1} \Lambda_{\alpha_1}^{[1]} \Gamma_{\alpha_1 \alpha_2}^{[2]i_2} \Lambda_{\alpha_2}^{[2]} |i_1\rangle \otimes |i_2\rangle \otimes |\Phi_{\alpha_2}^{[3\dots N]}\rangle. \quad (2.15)$$

By iterating this procedure for the remaining Schmidt vectors we can now express the state $|\psi\rangle$ as in Eq. (2.10), representing the state $|\psi\rangle$ in terms of the tensors $\Gamma^{[l]}$ and the diagonal matrices $\Lambda^{[l]}$. A particularly useful feature of the description of $|\psi\rangle$ in terms of the tensors Γ and Λ is that it readily gives the SD of $|\psi\rangle$ according to the

bipartition $[1 \dots l] : [(l+1) \dots N]$.

In the context of DMRG a slightly different notation is usually employed to describe MPS and will be used for this purpose throughout this thesis [50, 107]. In this representation the Λ -matrices are multiplied with the adjoining Γ -tensors, leading to a more compact representation consisting only of general linear maps $A_{\alpha_{l-1}\alpha_l}^{[l]i_l} = \Lambda_{\alpha_{l-1}}^{[l-1]i_l} \Gamma_{\alpha_{l-1}\alpha_l}^{[l]i_l}$ to describe site l :

$$|\psi\rangle = \sum_{i_1 \dots i_N} \sum_{\{\alpha\}} \Lambda_{\alpha_0}^{[0]i_1} \Gamma_{\alpha_0\alpha_1}^{[1]i_1} \Lambda_{\alpha_1}^{[1]i_1} \Gamma_{\alpha_1\alpha_2}^{[2]i_2} \Lambda_{\alpha_2}^{[2]i_2} \dots \Gamma_{\alpha_{N-1}\alpha_N}^{[N]i_N} \Lambda_{\alpha_N}^{[N]i_N} |i_1\rangle \otimes \dots \otimes |i_N\rangle \quad (2.16)$$

$$= \sum_{i_1 \dots i_N} \sum_{\{\alpha\}} A_{\alpha_0\alpha_1}^{[1]i_1} A_{\alpha_1\alpha_2}^{[2]i_2} \dots A_{\alpha_{N-1}\alpha_N}^{[N]i_N} |i_1\rangle \otimes \dots \otimes |i_N\rangle \quad (2.17)$$

$$= \sum_{i_1 \dots i_N} \text{Tr} (A^{[1]i_1} A^{[2]i_2} \dots A^{[N]i_N}) |i_1\rangle \otimes \dots \otimes |i_N\rangle \quad (2.18)$$

where the dummy matrix $\Lambda^{[N]} = 1$ was multiplied with the last site tensor. This expression describes a wave function $|\psi\rangle$ with open boundary conditions. A diagrammatic representation of this state is depicted in Figure 2.2. For periodic boundary conditions the construction procedure results in a representation analytically given by

$$|\psi\rangle = \sum_{i_1 \dots i_N} \sum_{\alpha_1, \dots, \alpha_N}^{\chi} A_{\alpha_1\alpha_2}^{[1]i_1} A_{\alpha_2\alpha_3}^{[2]i_2} \dots A_{\alpha_N\alpha_1}^{[N]i_N} |i_1\rangle \otimes \dots \otimes |i_N\rangle \quad (2.19)$$

$$= \sum_{i_1 \dots i_N} \text{Tr} (A^{[1]i_1} A^{[2]i_2} \dots A^{[N]i_N}) |i_1\rangle \otimes \dots \otimes |i_N\rangle, \quad (2.20)$$

and diagrammatically shown in Figure 2.3.

We can therefore express every state as a MPS by writing $A^{[l]i_l}$ for the $D_l \times D_{l+1}$ matrix with elements $A_{\alpha\beta}^{[l]i_l}$ belonging to site l [110]. Note that in general ψ is neither normalized nor is its MPS representation unique. This representation is most efficient and natural for one-dimensional systems though, where the entanglement scales in a way that is favorable for MPS.

As determined by the Schmidt decomposition, the amount of entanglement that can be carried by a MPS is limited by its bond dimension. For gapped one-dimensional systems the entanglement has been shown to scale as the surface area of the bipartition, i.e. $\mathcal{S} \propto L^{d-1}$ where L denotes the linear dimension of the surface area and d is the dimensionality of the system. Then it follows that the entropy for a one-dimensional system saturates, i.e. $\mathcal{S} \propto L^0 = \text{const.}$ In one dimension MPS are therefore able to capture all the entanglement present in the system, as long as the bond dimension can be increased sufficiently.

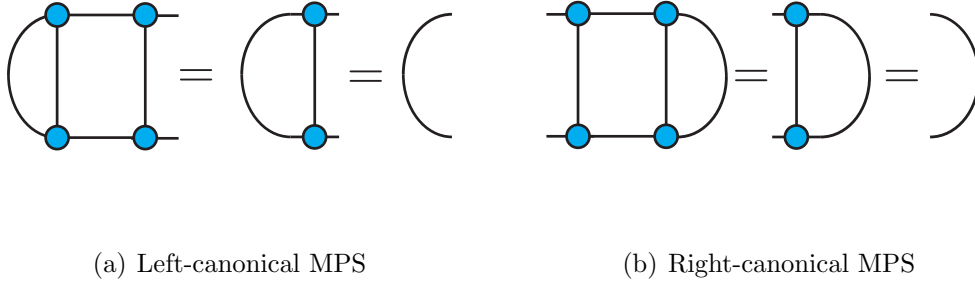


Figure 2.4: Diagrammatic representation of the canonical forms of MPS: Here the contraction of a MPS with its hermitian conjugate results in the identity, allowing us to avoid the actual calculation if the canonical form is maintained.

2.2.3 Canonical forms of MPS

As noted above, the representation of a given state ψ in terms of MPS is not unique. This is immediately obvious by realizing that we can at any point in the MPS insert a product of a matrix and its inverse without changing the state: $A^{[i]}A^{[i+1]} = (A^{[i]}X)(X^{-1}A^{[i+1]})$. By defining a canonical form, this freedom in the representation can be eliminated [86, 107], effectively fixing the gauge degree of freedom for this MPS.

Consider a state ψ with open boundary conditions in its MPS representation

$$|\psi\rangle = \sum_{i_1, \dots, i_N=1}^d \text{Tr} (A^{[1]i_1} A^{[2]i_2} \dots A^{[N-1]i_{N-1}} A^{[N]i_N}) |i_1 \dots i_N\rangle, \quad (2.21)$$

where the $A^{[m]i_m}$ are $D_m \times D_{m+1}$ matrices with $D_1 = D_N = 1$. If $D = \max_m D_m$ the state is said to have the bond dimension D . The bond dimension D is usually known as m in DMRG literature and χ in the context of tensor product algorithms. It can be shown [109] that any state $\psi \in (\mathbb{C}^d)^{\otimes N}$ has a MPS representation of the form of equation (2.21) with bond dimension $D \leq d^{\lfloor N/2 \rfloor}$ that satisfies

1. $\sum_i A^{[m]i} (A^{[m]i})^\dagger = \mathbb{1}_{D_m} \quad \forall \quad 1 \leq m \leq N,$
2. $\sum_i (A^{[m]i})^\dagger \Lambda^{[m-1]} A^{[m]i} = \Lambda^{[m]} \quad \forall \quad 1 \leq m \leq N,$
3. $\Lambda^{[0]} = \Lambda^{[N]} = 1$ and each $\Lambda^{[m]}$ is a $D_{m+1} \times D_{m+1}$ diagonal matrix which is positive, has full rank and fulfills the condition $\text{Tr} \Lambda^{[m]} = 1$. This, of course, is only true if there is no truncation involved in the Schmidt decomposition.

These conditions follow immediately from the construction of a MPS by the concatenation of singular value decompositions (SVDs). A matrix product state that satisfies these conditions is said to be in its *canonical form*. In practice it is sufficient

to ensure the first condition for MPS with open boundary conditions, the remaining conditions then follow by construction.

But even the canonical form is only unique up to permutations and degeneracies in the Schmidt decomposition as follows from construction. In this representation, the matrix $\Lambda^{[m]}$ is the diagonal matrix of non-zero eigenvalues of the reduced density operator $\rho_m = \text{Tr}_{m+1, \dots, N} |\psi\rangle\langle\psi|$.

A state given in its MPS representation can always be transformed to its canonical form using successive SVDs following the prescription for the original construction of the MPS. Suppose a state with open boundary conditions is given by

$$|\psi\rangle = \sum_{i_1, \dots, i_N=1}^d \text{Tr} (B^{[1]i_1} B^{[2]i_2} \dots B^{[N-1]i_{N-1}} B^{[N]i_N}) |i_1 \dots i_N\rangle. \quad (2.22)$$

Then, there must exist matrices Y^j and Z^j with $Y^j Z^j = \mathbb{1}$ such that, if we define

$$\begin{aligned} A^{[1]i} &= B^{[1]i} Z^1 \\ A^{[m]i} &= Y^{m-1} B^{[m]i} Z^m \\ A^{[N]i} &= Y^{N-1} B^{[N]i} \end{aligned}$$

for $1 < m < N$, the canonical form of $|\psi\rangle$ is given by

$$|\psi\rangle = \sum_{i_1, \dots, i_N=1}^d \text{Tr} (A^{[1]i_1} A^{[2]i_2} \dots A^{[N-1]i_{N-1}} A^{[N]i_N}) |i_1 \dots i_N\rangle. \quad (2.23)$$

In general one distinguishes between two distinct variants of the canonical form. By iterating the construction prescription for a canonical MPS as above, from left to right, we arrive at a left-canonical, i.e. left-orthonormalized MPS description of our state. The same procedure can instead be iterated starting from the right end of the wave function, thereby yielding a right-canonical state. Here, we follow Ref. [50] in denoting right-orthonormal matrices as B and left-orthonormal matrices as A . In this notation the orthonormality conditions can simply be written as

$$\sum_{\sigma} A^{\sigma\dagger} A^{\sigma} = \mathbb{1} \quad \text{for left-canonical, and as} \quad (2.24)$$

$$\sum_{\sigma} B^{\sigma} B^{\sigma\dagger} = \mathbb{1} \quad \text{for right-canonical matrices.} \quad (2.25)$$

These conditions become particularly obvious when considering a MPS in the Γ - Λ -notation, where $A = \Lambda\Gamma$ and $B = \Gamma\Lambda$.

2.2.4 Mixed canonical form

While in theory a left- or right-canonical form is very useful, in practice a mixing of the two forms has many advantages. Most operations on MPS are performed as local

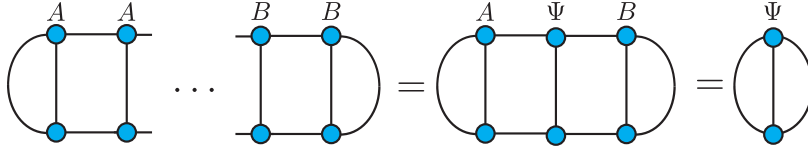


Figure 2.5: Diagrammatic representation of the mixed canonical form of a MPS. Key to this representation is the presence of a orthonormalization center Ψ . To the left of Ψ , all sites are left-orthonormal, to the right all sites are right-orthonormal, enabling the efficient evaluation of expressions centered on this site.

updates, therefore having access to a well-defined local basis is highly desirable. To that end, we write the wave function in the so-called *mixed canonical form*, which provides us with that well-defined basis (see Fig. 2.5). The mixed canonical form is obtained by singling out a single site k as the *center site* and writing the state $|\psi\rangle$ as

$$\begin{aligned}
 |\psi\rangle &= \sum_{\sigma} \Lambda^{[0]} \Gamma^{[1]\sigma_1} \dots \Gamma^{[k-1]\sigma_{k-1}} \Lambda^{[k-1]} \Gamma^{[k]\sigma_k} \Lambda^{[k]} \Gamma^{[k+1]\sigma_{k+1}} \dots \Gamma^{[N]\sigma_N} \Lambda^{[N]} |\sigma\rangle \\
 &= \sum_{\sigma} A^{[1]\sigma_1} \dots A^{[k-1]\sigma_{k-1}} \Lambda^{[k-1]} \Gamma^{[k]\sigma_k} \Lambda^{[k]} B^{[k+1]\sigma_{k+1}} \dots B^{[N]\sigma_N} |\sigma\rangle \\
 &= \sum_{a_{k-1}, \sigma_k, a_{k+1}} \Psi_{a_{k-1} a_{k+1}}^{[k]\sigma_k} |a_{k-1}\rangle \otimes |\sigma_k\rangle \otimes |a_{k+1}\rangle,
 \end{aligned}$$

where the center site's tensor is written as $\Psi_{a_{k-1} a_{k+1}}^{[k]\sigma_k}$. Here we can expand the left or right basis and write it as

$$\begin{aligned}
 |l_k\rangle &= |a_{k-1}\rangle \otimes |\sigma_k\rangle \quad \text{or} \\
 |r_k\rangle &= |\sigma_k\rangle \otimes |a_{k+1}\rangle.
 \end{aligned}$$

This way we obtain a local description of state $|\psi\rangle$ in terms of a single $d\chi \times \chi$ -dimension center matrix Ψ . Note that this representation is closely related to the traditional DMRG representation. By including two Γ -matrices instead of one in the center matrix one arrives at the two-site center matrix used in traditional DMRG.

In this form it is also obvious that the A - (B -) matrices serve to transform the tensor product of the truncated left (right) basis with the local basis into the new truncated left (right) basis. One of the main advantages of this mixed canonical form is that the evaluation of a single-site operator $\hat{\mathbf{O}}^{[k]}$ reduces to calculations involving only the operator and the center matrix, i.e. $\langle\psi|\hat{\mathbf{O}}^{[k]}|\psi\rangle = \sum \Psi^{[k]\dagger} \mathbf{O}^{[k]} \Psi^{[k]}$ as can be seen in Fig. 2.6.

Furthermore, if the state is given in the center matrix description for site k , it is now straightforward to switch the representation to site $k \pm 1$ with the corresponding new basis sets $|l_{k \pm 1}\rangle$, $|\sigma_{k \pm 1}\rangle$, and $|r_{k \pm 1}\rangle$. All we have to do is perform one single

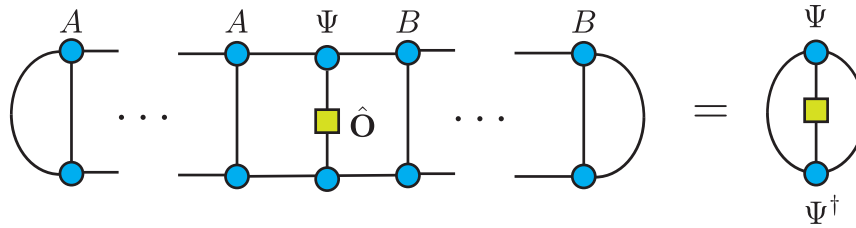


Figure 2.6: Diagrammatic representation of the evaluation of an observable in the mixed canonical form of a MPS. Since all tensors to the left (right) of the center matrix are left- (right-) orthonormal, the evaluation of a single site operator only requires the contraction over the center site and its conjugate.

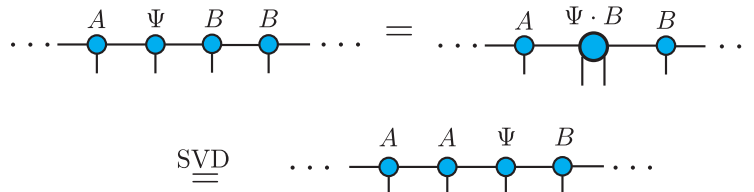


Figure 2.7: Diagrammatic representation of shifting the center matrix to the right in the mixed canonical form. We first contract it with its right neighbor and then perform a SVD, yielding a new left-orthonormal site A . By multiplying the remaining parts of the SVD, i.e. $S \cdot V^\dagger$, to the right we obtain a new center matrix $\Psi = S \cdot V^\dagger \cdot B$.

canonization step. Suppose for example we want to move from site k to site $k + 1$, then we simply compute the SVD of the center matrix $\Psi^{[k]} = USV^\dagger$ and multiply SV^\dagger with $B^{[k+1]}$ and write U as $A^{[k]\sigma_k}$, arriving at the mixed canonical form with $\Psi^{[k+1]} = SV^\dagger B^{[k+1]}$ (see also Fig. 2.7).

2.2.5 Construction of iMPS

The elimination of finite-size effects in the simulation of quantum mechanical systems often requires a tedious finite-size scaling. From the early days of DMRG the infinite-size algorithm (iDMRG) was known and used to grow a system to the intended size for later optimization with finite-size DMRG. Recently the iTEBD [111] algorithm was proposed, which makes use of a system's translational invariance to reduce the number of tensors necessary to store the state. This in turn allows a highly efficient representation of the quantum state consisting only of the system's unit cell. This special case of a matrix product representation is now known as an infinite matrix product state (iMPS) and also lies at the heart of the reformulated iDMRG [45, 112]

algorithm used for variational ground state calculations in the thermodynamic limit [113, 114]. Here, we will briefly review how those states are constructed and used.

Consider a one-dimensional quantum many-body state defined on an infinite lattice, where each site r , $r \in \mathbb{Z}$ is described by a Hilbert space $\mathcal{H}^{[r]} \cong \mathbb{C}^d$ of finite dimension d . Let the vector $|\psi\rangle \in \bigotimes_{r \in \mathbb{Z}} \mathcal{H}^{[r]} \cong \bigotimes_{r \in \mathbb{Z}} \mathbb{C}^d$ denote a pure state of the lattice that is invariant under translations by n sites. For the purpose of introducing the iMPS formalism we will restrict this to the simplest case of $n = 1$, but the extension to arbitrary n is straightforward.

Splitting the chain, we denote the resulting semi-infinite sublattices made of sites $\{-\infty, \dots, r\}$ and $\{r + 1, \dots, \infty\}$ with $[\langle r]$ and $[r + 1 \triangleright]$, respectively. Using the Schmidt decomposition

$$|\psi\rangle = \sum_{\alpha=1}^{\chi} \Lambda_{\alpha}^{[r]} |\Phi_{\alpha}^{[\langle r]}\rangle \otimes |\Phi_{\alpha}^{[r+1 \triangleright]}\rangle, \quad (2.26)$$

(according to this bipartition, where we assume the Schmidt rank χ to be finite), we can calculate the spectral decomposition of the reduced density matrices for the left and right semi-infinite sublattices:

$$\rho^{[\langle r]} = \sum_{\alpha=1}^{\chi} (\Lambda_{\alpha}^{[r]})^2 |\Phi_{\alpha}^{[\langle r]}\rangle \langle \Phi_{\alpha}^{[\langle r]}| \quad (2.27)$$

$$\rho^{[r+1 \triangleright]} = \sum_{\alpha=1}^{\chi} (\Lambda_{\alpha}^{[r]})^2 |\Phi_{\alpha}^{[r+1 \triangleright]}\rangle \langle \Phi_{\alpha}^{[r+1 \triangleright]}|. \quad (2.28)$$

As in the finite case, we now use a three-index tensor $\Gamma_{\alpha\beta}^{[r]i}$ to expand the Schmidt bases $|\Phi^{[r]}\rangle$ in terms of the local basis vectors $|i^{[r]}\rangle$:

$$|\Phi_{\alpha}^{[\langle r+1]}\rangle = \sum_{\beta=1}^{\chi} \sum_{i=1}^d \Lambda_{\beta}^{[r]} \Gamma_{\beta\alpha}^{[r+1]i} |\Phi_{\beta}^{[\langle r]}\rangle |i^{[r+1]}\rangle \quad (2.29)$$

$$|\Phi_{\alpha}^{[r \triangleright]}\rangle = \sum_{\beta=1}^{\chi} \sum_{i=1}^d \Gamma_{\alpha\beta}^{[r+1]i} \Lambda_{\beta}^{[r]} |i^{[r]}\rangle |\Phi_{\beta}^{[r+1 \triangleright]}\rangle. \quad (2.30)$$

Using this, we can expand $|\psi\rangle$ in the local basis $|i^{[r]}\rangle$ for site r and the coefficients Γ :

$$|\psi\rangle = \sum_{\alpha,\beta=1}^{\chi} \sum_{i=1}^d \Lambda_{\alpha}^{[r]} \Gamma_{\alpha\beta}^{[r+1]i} \Lambda_{\beta}^{[r+1]} |\Phi_{\alpha}^{[\langle r]}\rangle |i^{[r]}\rangle |\Phi_{\beta}^{[r+1 \triangleright]}\rangle. \quad (2.31)$$

For sites $\{r, r + 1\}$, this decomposition reads

$$|\psi\rangle = \sum_{\alpha,\beta,\gamma=1}^{\chi} \sum_{i,j=1}^d \Lambda_{\alpha}^{[r]} \Gamma_{\alpha\beta}^{[r+1]i} \Lambda_{\beta}^{[r+1]} \Gamma_{\beta\gamma}^{[r+2]j} \Lambda_{\gamma}^{[r+2]} |\Phi_{\alpha}^{[\langle r]}\rangle |i^{[r]}\rangle |j^{[r+1]}\rangle |\Phi_{\gamma}^{[r+2 \triangleright]}\rangle. \quad (2.32)$$

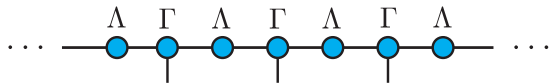


Figure 2.8: Diagrammatic representation of an iMPS consisting of alternating copies of the tensors Γ and Λ . Due to the translational invariance, the state $|\psi\rangle$ is completely determined by these two tensors.

We can now simplify this representation by assuming the state to be invariant under shifts, which translates into the conditions $\Gamma^{[r]} = \Gamma^{[r+1]}$ and $\Lambda^{[r]} = \Lambda^{[r+1]}$.

By iterating this construction we can now write any state $|\psi\rangle$ that is translationally invariant under shifts by n sites as a tensor network of n Γ -tensors and $n + 1$ Λ -matrices. We observe, that iMPS are always bounded on both ends by non-trivial Λ -matrices, whereas MPS with open boundary conditions end in scalar Λ -matrices. Fig. 2.8 shows a diagrammatic representation of iMPS invariant under shifts by one site.

2.2.6 Canonical form of iMPS

Evaluating arbitrary observables in the framework of iMPS results in the contraction of an infinite one-dimensional tensor network consisting of alternating copies of the tensors Γ and Λ . Since this contraction is in principle intractable exactly, it is useful to employ tensors that obey some kind of orthonormality condition. In Ref. [115] such a form is proposed as the *canonical form* of an iMPS, analogous to the finite-size variant.

An infinite MPS $|\psi\rangle$ described by tensors $\{\Gamma, \Lambda\}$ is said to be in its canonical form, if the diagonal matrix Λ on each bond is related to the Schmidt spectrum resulting from the Schmidt decomposition of $|\psi\rangle$:

$$|\psi\rangle = \sum_{\alpha=1}^{\chi} \Lambda_{\alpha}^{[r]} |\Phi_{\alpha}^{[<r]}\rangle \otimes |\Phi_{\alpha}^{[r+1>]}\rangle. \quad (2.33)$$

Λ therefore contains the decreasingly ordered Schmidt coefficients (i.e. eigenvalues of the reduced density matrix) and the vectors $|\Phi\rangle$ form orthonormal sets with

$$\langle \Phi_{\alpha}^{[<r]} | \Phi_{\alpha'}^{[<r]} \rangle = \langle \Phi_{\alpha}^{[r+1>} | \Phi_{\alpha'}^{[r+1>} \rangle = \delta_{\alpha\alpha'}.$$

While this condition is mathematically correct, it is not computationally available since the vectors $|\Phi\rangle$ describe semi-infinite sublattices. Since we cannot compute the expression a different way to enforce this condition has to be derived. Assuming $|\psi\rangle$ is invariant under shifts by one lattice site, we can write ψ as an iMPS consisting of

just the two tensors Γ and Λ . Defining matrices R and L as

$$R_{(\alpha\alpha')(\beta\beta')} = \sum_{i=1}^d (\Gamma_{\alpha\beta}^i \Lambda_{\beta'}^i) (\Gamma_{\alpha'\beta'}^i \Lambda_{\beta'}^i)^*, \quad (2.34)$$

$$L_{(\alpha\alpha')(\beta\beta')} = \sum_{i=1}^d (\Lambda_{\alpha} \Gamma_{\alpha\beta}^i) (\Lambda_{\alpha'} \Gamma_{\alpha'\beta'}^i)^*, \quad (2.35)$$

the canonical form corresponds to the conditions

$$\sum_{\beta, \beta'=1}^{\chi} R_{(\alpha\alpha')(\beta\beta')} \delta_{\beta\beta'} = \eta \delta_{\alpha\alpha'} \quad (2.36)$$

$$\sum_{\alpha, \alpha'=1}^{\chi} \delta_{\alpha, \alpha'} L_{(\alpha\alpha')(\beta\beta')} = \eta \delta_{\beta, \beta'}, \quad (2.37)$$

where $\eta \in \mathbb{C}$ and the symbols $(\alpha\alpha')$ and $(\beta\beta')$ indicate composite indices. In other words, the identity matrix is a left (right) eigenvector of matrix L (R) with eigenvalue $\eta \in \mathbb{C}$, where $\eta = 1$ if and only if $|\psi\rangle$ is normalized.

Forcing the iMPS representation of state $|\psi\rangle$ to be in its canonical form, we can discard all tensors of the iMPS that are not contained within the unit cell when evaluating operators. In this representation it is therefore sufficient to contract only the unit cell consisting of Γ and Λ to evaluate an operator $\hat{O}^{[r]}$ (see also Figure 2.9(a)):

$$\langle \psi | \hat{O}^{[r]} | \psi \rangle = \sum_{i,j=1}^d \sum_{\alpha, \beta=1}^{\chi} \Lambda_{\alpha}^{[r-1]} \Gamma_{\alpha\beta}^{[r]i} \Lambda_{\beta}^{[r]} \hat{O}_{ij}^{[r]} \left(\Lambda_{\alpha}^{[r-1]} \Gamma_{\alpha\beta}^{[r]j} \Lambda_{\beta}^{[r]} \right)^*. \quad (2.38)$$

Analogously we can compute correlation functions (Fig. 2.9(b)) and other expectation values. Note that these contraction formulas are only valid if the iMPS is in its canonical form [115].

Due to the construction, the canonical form of an iMPS is unique only up to a choice of phases $e^{i\phi_{\alpha}}$. Suppose two canonical forms for $|\psi\rangle$ are given by the tensors $\{\Gamma, \Lambda\}$ and $\{\Gamma', \Lambda'\}$ respectively. Then the relations

$$(\Gamma')_{\alpha\beta}^i = e^{i\phi_{\alpha}} \Gamma_{\alpha\beta}^i e^{-i\phi_{\beta}}, \quad (2.39)$$

$$\Lambda' = \Lambda \quad (2.40)$$

hold.

2.3 Tensor Product States

Since matrix product states proved to be extremely successful in capturing the essential physics of one-dimensional systems, there have been many attempts to extend them to higher-dimensional systems. While the naive extension of DMRG to two-

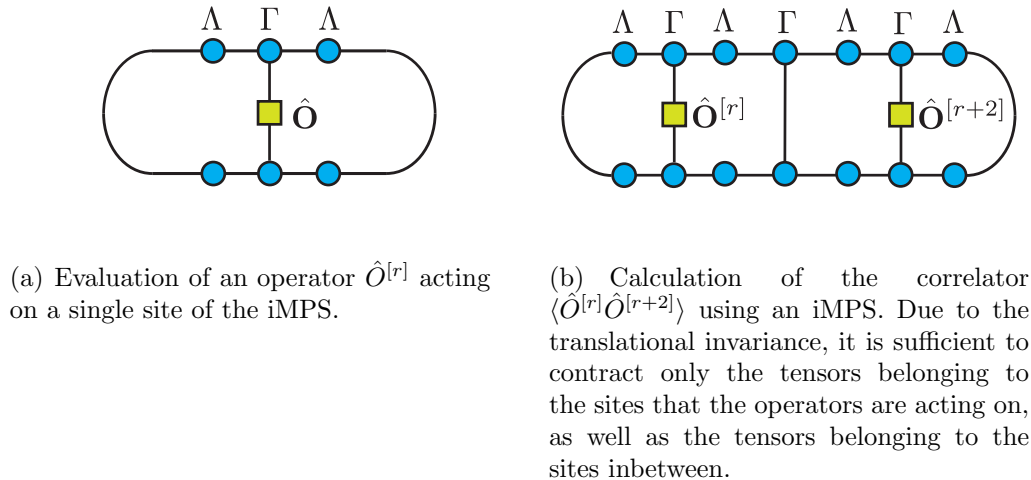


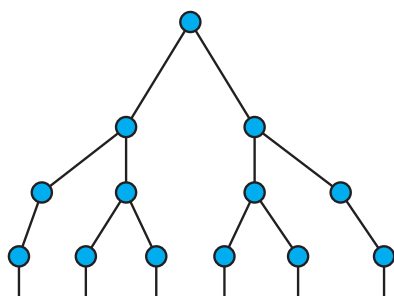
Figure 2.9: Calculation of observables and correlators for an iMPS constructed from the two tensors Γ and Λ .

dimensional systems is surprisingly useful (see also Sec. 2.8), it is still severely limited. The failing of DMRG in 2D can be attributed to the area law of entanglement, which MPS can not fulfill [77]. Therefore a generalized MPS ansatz that is able to capture the entanglement growth in higher dimensions is desirable. One such ansatz are tensor network states [116], which can be broadly classified into two ansätze: On the one hand there are those like the multi-scale entanglement renormalization ansatz (MERA) [52, 53, 58, 62, 63, 72, 117–119] that attempt to model the entanglement structure and on the other hand there are those like the projected entangled pair-states (PEPS) [75, 78, 79, 107, 120–123] that endeavor to model the real-space structure of the lattice systems under consideration. Note that in one dimension MERA is still bound by the area law since it can be mapped directly to a PEPS [124]. In this thesis we will focus on the latter kind, as it is more closely related to the idea behind DMRG.

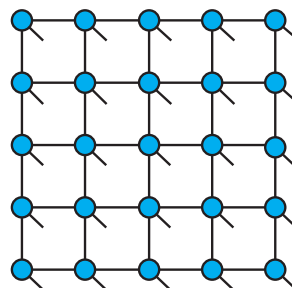
First we will introduce the notion of tree tensor networks, which are a straightforward generalization of MPS to tree networks. We then proceed to explain the construction of PEPS, followed by a short introduction to the ideas behind fermionic tensor product states.

2.3.1 Tree tensor networks

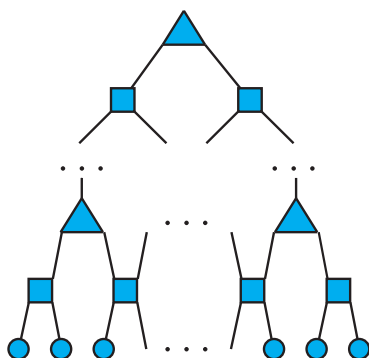
One of the most useful properties of matrix product states is the fact that one can always transform the wave function's basis into a well-defined orthonormal basis, allowing well-defined truncations in the Schmidt decomposition and stable optimization. The logical extension of states with this property is given by so-called tree tensor networks (TTN), i.e. states that are defined on a tree geometry. The construction of these states is based on the bipartite nature of trees, allowing them to be split into



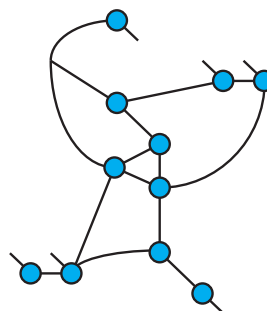
(a) Tree tensor network, where each branch can have up to two leaves.



(b) Projected entangled-pair states for the square lattice.



(c) Multi-scale entanglement renormalization ansatz (MERA), where the triangles are isometries and the squares denote disentanglers.



(d) General tensor product state. The connections and dimensionality of the tensors in a general tensor network state can be chosen arbitrarily.

Figure 2.10: Diagrammatic representation of different tensor networks. As in the case of MPS, uncontracted indices are depicted as open-ended lines. These are usually the physical indices.

two subsystems via the Schmidt decomposition, analogous to one-dimensional chains. Thus the generalization of the one-dimensional construction to trees is straightforward but in order to introduce the ansatz and the notation, we will cover it here as well.

To describe a tree of coordination number z (i.e. each vertex has z nearest neighbors), we place tensors $\Gamma^{[i]}$ of order $z + 1$ on the vertices and vectors Λ^k on the edges of the tree graph in Figure 2.11(a). We then connect the tensor's indices in a way that mimics the model's underlying lattice structure. A state $|\psi\rangle$ on the $z = 3$ Bethe lattice can in this representation be written as

$$|\psi\rangle = \left(\prod_{k \in \text{bonds}} \sum_{a_k < \chi} \Lambda_{a_k}^k \right) \times \left(\prod_{i \in \text{sites}} \sum_{s_i < d} \Gamma_{a_i a_m a_n}^{[i] s_i} \right) |\dots\rangle |s_i\rangle |\dots\rangle.$$

While the dimension d of the physical indices s_i is dictated by the model, the dimension χ of the virtual indices a_k can be chosen arbitrarily and is only limited by computational resources. This ansatz can easily be extended to lattices with a higher coordination number but for the sake of simplicity we will only cover the case of $z = 3$ here.

Analogous to MPS, the tensors in a tree tensor network can then be chosen such that they satisfy the conditions for a canonical tensor network:

$$\sum_{a_k} \Lambda_{a_k}^2 = 1 \quad (2.41)$$

$$\sum_{s_i} \sum_{a_k a_l} \Gamma_{a_k a_l a_m}^{s_i} \Lambda_{a_k}^2 \Lambda_{a_l}^2 \left(\Gamma_{a_k a_l a'_m}^{s_i} \right)^* = \delta_{a_m a'_m}. \quad (2.42)$$

The advantages of the canonical form of TTN are the same as for MPS, i.e. the canonical form provides a well-defined basis for evaluations of observables and the imaginary-time evolution.

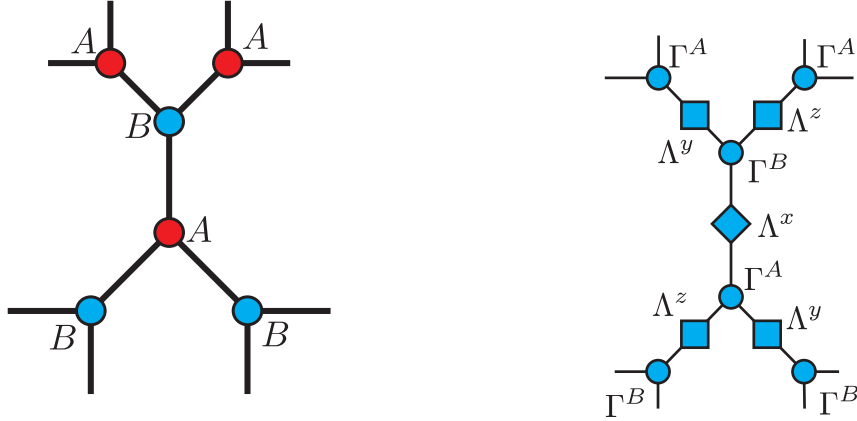
2.3.2 Projected entangled-pair states

As noted above, while MPS are the natural choice of ansatz state for one-dimensional systems, they are eminently unsuitable for large higher-dimensional systems. For these systems the ideas behind MPS can be generalized to create a new class of states known as tensor product (TPS) [121–123] or projected entangled-pair states (PEPS) [61, 77, 78].

Consider a pure state $|\psi\rangle$ of N spins on a two-dimensional lattice where each site, labeled by a vector $\mathbf{r} = (x, y)$, is described by a finite-dimensional local Hilbert space $\mathcal{H}^{[r]} \cong \mathbb{C}^d$ of dimension d . This state can always be written as

$$|\psi\rangle = \sum_{i_1 \dots i_N} c_{i_1 i_2 \dots i_N} |i_1 i_2 \dots i_N\rangle, \quad (2.43)$$

allowing a decomposition into local subsystems. To determine the decomposition we



(a) A tree tensor network ansatz with a two-site unit cell for the $z = 3$ Bethe lattice.

(b) The structure of the TTN for the Bethe lattice. Note the introduction of Λ -tensors on each bond.

Figure 2.11: Diagrammatic representation of the description of the Bethe lattice in terms of tensor product states.

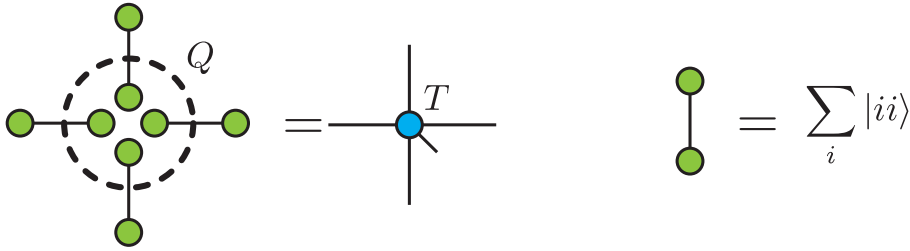


Figure 2.12: Sketch of the construction of PEPS. The map Q maps the maximally entangled pairs $\sum_i |ii\rangle$ to a tensor T .

concentrate on a single site. For each neighboring site \mathbf{r}' we now introduce auxiliary systems $a^{[\mathbf{r}']}, b^{[\mathbf{r}']}, \dots$. Each of these auxiliary systems is in a maximally entangled state $|I\rangle = \sum_{i=1}^D |ii\rangle$ with its neighboring site in such a way that it mimics the lattice structure (see Fig. 2.12).

By applying a linear map $Q^{[\mathbf{r}]}$, we can now map these auxiliary systems onto the physical systems, leading to a representation of $|\psi\rangle$ in terms of the linear maps $Q^{[\mathbf{r}]}$. This procedure allows a decomposition of the coefficients $c_{i_1 i_2 \dots i_N}$ in terms of local tensors

$$T_{ab\dots}^{i_k} = \langle i_k | Q | ab \dots \rangle \quad (2.44)$$

for each site k . By tracing out the auxiliary systems we arrive at a representation of

$|\psi\rangle$ given by the tensors T :

$$|\psi\rangle = \sum_{i_1 \dots i_N} \text{Tr} \left(T_{a \dots}^{[1]i_1} \dots T_{b \dots}^{[N]i_N} |i_1 \dots i_N\rangle \right) \quad (2.45)$$

which becomes exact in the limit of large virtual bond dimension D . The tensors $T^{[\mathbf{r}]}$ are called site tensors and are associated with a lattice site \mathbf{r} . Each site tensor projects the auxiliary systems of dimension D down to the local state space of dimension d . A state described by these site tensors is usually known as a projected entangled-pair state (PEPS) or simply as a tensor product state (TPS).

Placing site tensors on each site \mathbf{r} of a lattice and entangling them with their neighbors via auxiliary systems can be generalized to arbitrary lattices in a straightforward manner and has in fact been done for the square, honeycomb, and triangular lattices. In general, any state defined on a lattice with coordination number z can be written as a tensor product state consisting of tensors of rank $z+1$. Here, we will focus on the square lattice with open boundary conditions where the states can be decomposed in terms of rank five tensors, defined via

$$T_{udlr}^{[\mathbf{r}]i_k} = \langle k | Q^{[\mathbf{r}]} | udlr \rangle, \quad (2.46)$$

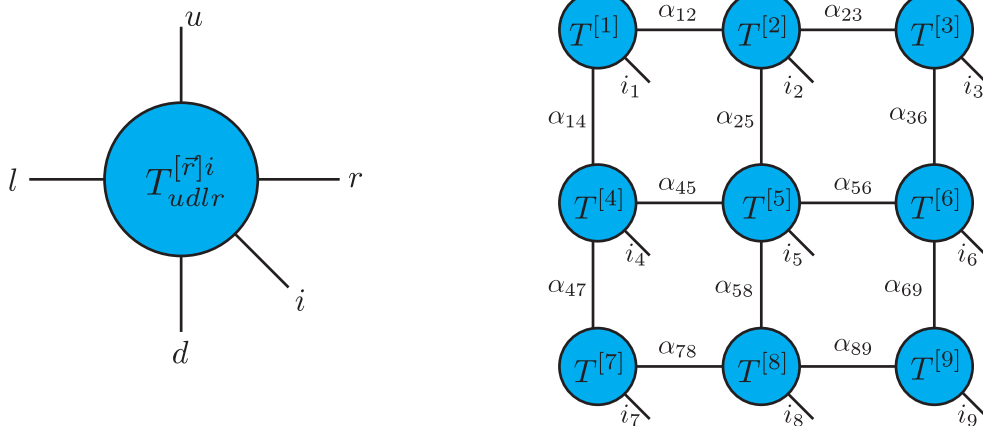
where u (up), d (down), l (left), and r (right), denote the auxiliary systems connecting the site with its nearest neighbors.

TPS are conceptually highly appealing as they fulfill the area law of entanglement by construction [77]. In this sense they can be seen as a generalization of MPS to higher dimensions. While MPS capture the entanglement of one-dimensional systems efficiently, TPS are well-suited to doing the same in two dimensions. PEPS can therefore exactly reproduce the area law scaling of the block entropy in higher-dimensional systems.

But where MPS can be rigorously constructed using the Schmidt decomposition, there is no such general prescription for tensor product states. While this may seem a minor drawback it actually connects to the much larger issue of evaluation and optimization of ansatz states. The canonical form of MPS as defined by the Schmidt decomposition always offer a single orthonormalization center. Therefore, a MPS can always be brought in a form where a single bond corresponds to the Schmidt decomposition relative to this bond. In this basis, the state is in a well defined basis, where one can e.g. directly truncate the spectrum of the density matrix. Such a single orthonormalization center can not be consistently defined for generic lattices with loops.

Additionally, the contraction or multiplication of two matrices results in a new matrix, making matrix product states efficient to evaluate. The contraction of two tensors with higher rank $r, r > 2$ on the other hand results in a bigger tensor of rank $2r - 2$. This makes the evaluation (i.e. contraction) of general tensor networks both an extremely hard problem. In fact, the problem of optimal contraction order is already NP hard.

Therefore one of the most important questions in current research on tensor net-



(a) Diagrammatic representation of one site tensor A . As before, we represent tensors with circles. The diagonal leg represents the uncontracted physical index, while the other four legs are bond indices.

(b) A tensor product state with open boundary conditions defined on a 3×3 lattice.

Figure 2.13: Diagrammatic representation of PEPS and TPS tensors.

works is the search for good contraction strategies. All of the different competing schemes are approximate contractions, as the exact contraction usually scales exponentially in the number of tensors. One of the most popular approximate contraction schemes involves treating rows of tensors as MPOs and applying them to border MPS. In some cases these contractions can be accelerated by making use of stochastic methods [73]. But even when the optimal contraction is known and can be computed, it is still not known how to optimize the wave function optimally. For MPS we can always stick to the canonical form where we have access to a well-defined orthonormal basis, which is not possible for an arbitrary higher-dimensional TPS. This lack of an orthonormal basis lies at the heart of the problems in dealing numerically with TPS, as it makes the evaluation of a tensor network both hard and ill-defined at once. But even with these drawbacks there are extremely interesting applications of tensor network algorithms. One of the most promising approaches, known as the *infinite projected entangled-pair state algorithm* (iPEPS), involves the generalization of TPS to infinite systems, analogous to the generalization of MPS to iMPS [59, 61]. This class of ansatz states has been applied to many problems with some success [57, 125–128].

One of the biggest problems of TPS is the lack of an efficient optimization scheme. Since the exact evaluation scales exponentially, approximate contraction techniques have to be employed. But even with approximate evaluation schemes the numerical cost still scales with a high power of the truncated bond dimension χ , ranging from χ^7 (scale-invariant MERA with stochastic updates [129]) over χ^{10} (iPEPS [130]) to χ^{15} (2D MERA [62]). These costs can be reduced by further approximations which reduce both numerical cost and the algorithm's precision. Still, owing to their appealing concepts tensor networks are a very promising line of research and have been applied

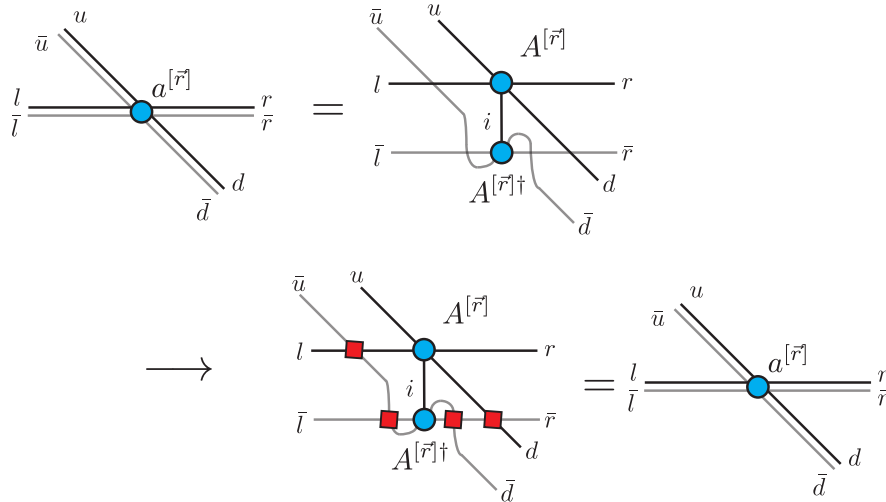


Figure 2.14: Sketch of the construction of fermionic PEPS. By inserting swap gates at every crossed bond and summing over the physical index, we can reduce the contraction of a fermionic tensor network to a contraction of a generic bosonic network.

to continuous systems, quantum chemistry problems, as well as topological problems.

Today there exist a variety of optimization and contraction schemes for both finite and infinite systems on different lattices. The description of these schemes extends well beyond the scope of this work, we will therefore limit ourselves to a short description of fermionic tensor networks and the implementation of symmetries in tensor networks.

2.3.3 Fermionic tensor networks

Generic tensor networks are defined for spin systems, but many interesting models are defined for fermionic particles. For one-dimensional systems this poses no problem as fermions can be mapped to bosonic particles via a Jordan-Wigner transform in a straightforward manner. For two-dimensional problems though it is not clear how this mapping can be done without a high computational cost. Therefore, one of the most interesting extensions of tensor networks in recent years has been the advent of fermionic tensor networks. For a more general derivation and introduction consider e.g. references [131–136]. A conceptually different approach to deduce identical relations is given by the Grassmann tensor networks [74, 137] which can also be expressed in terms of fermionic tensor networks. The aim of this introduction is therefore rather to provide a short guide to the ideas behind fermionic tensor networks and how the sign structure depends on the contractions.

There have been a variety of approaches to fermionic tensor networks. The first to simulate fermions with tensor product states were Corboz *et al* who derived a fermionic formulation of MERA [134]. Shortly thereafter Kraus and coworkers con-

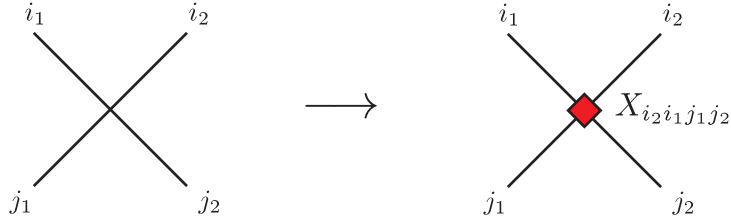


Figure 2.15: Sketch of the swap gate for fermionic PEPS. In order to create a fermionic tensor network, we have to insert a so-called swap gate at every bond crossing.

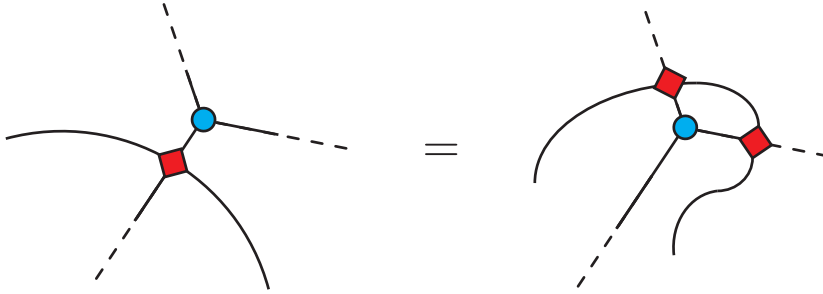


Figure 2.16: Sketch of the jump move for fermionic PEPS. The jump move allows changes in contraction order by inserting additional swap gates.

ceived a different flavor of fermionic PEPS where they dealt with the fermionic sign structure by inserting an additional bond, thereby increasing the rank of the site tensors [136]. At the same time Barthel *et al* introduced the notion of fermionic operator circuits [131, 138] which is the most general derivation of sign rules for fermionic tensor networks today. Further schemes have been published by Corboz *et al* who use graphical rules [132–134] and Pizorn *et al* who employ a derivation in terms of fermionic creation and annihilation operators [135]. This multitude of approaches all aim to reduce the non-local nature of the fermionic sign structure to local operations. By rewriting the derivations, one can show them to be equivalent, which we will do here for the case of fermionic operator circuits and the explicit construction of fermionic site tensors. First let us review the generic case of fermionic operator circuit calculus.

Consider the set of operators $\{\hat{A} : \mathcal{F}_n \rightarrow \mathcal{F}_m\}$ that map the Fock space \mathcal{F}_n to the Fock space \mathcal{F}_m which is spanned by the basis states

$$|n\rangle = |n_1 \dots n_{|n|}\rangle = (f_{n_1}^\dagger)^{n_1} \dots (f_{n_{|n|}}^\dagger)^{n_{|n|}} |0\rangle \quad (2.47)$$

with $\{f_i, f_j^\dagger\} = \delta_{ij}$. In this basis every operator \hat{A} can be expressed as a matrix with coefficients $J_{m,n}(\hat{A}) = \langle n | \hat{A} | m \rangle$.

Fermionic tensors obey the statistics of such systems, i.e. they are antisymmetric. Due to this antisymmetry the calculus of fermionic tensors is non-trivial. Consider e.g. the contraction of some outgoing modes of an operator $\hat{A} : \mathcal{F}_m \rightarrow \mathcal{F}_{n \cup p}$ with the corresponding incoming modes of an operator $\hat{B} : \mathcal{F}_{m \cup q} \rightarrow \mathcal{F}_k$:

$$\begin{aligned}
 \hat{C} &= \hat{B} \cdot \hat{A} \\
 &= |k\rangle \langle k| B |n'q\rangle \langle n'q| \cdot |np\rangle \langle np| A |m\rangle \langle m| \\
 &= |k\rangle \langle k| B |n'q\rangle \langle np| A |m\rangle \langle 0| F_q F_{n'} F_n^\dagger F_p^\dagger |0\rangle \langle m| \\
 &= |k\rangle \langle k| B |n'q\rangle \langle np| A |m\rangle \langle 0| F_p^\dagger F_{n'} F_n^\dagger F_q (-1)^{\bar{p}\bar{q} + (\bar{p} + \bar{q})(\bar{n} + \bar{n}')} |0\rangle \langle m| \\
 &= |k\rangle \langle k| B |nq\rangle \langle np| A |m\rangle \langle p| \delta_{n,n'} (-1)^{\bar{p}\bar{q} + 2\bar{n}(\bar{p} + \bar{q})} |q\rangle \langle m| \\
 &= |k\rangle |q\rangle \langle k| B |nq\rangle \langle np| A |m\rangle \delta_{n,n'} (-1)^{\bar{p}\bar{q}} \langle p| \langle m| \\
 &= |kp\rangle \langle kp| C |mq\rangle \langle mq|
 \end{aligned}$$

where the term $\langle k| B |nq\rangle \langle np| A |m\rangle \delta_{n,n'} (-1)^{\bar{p}\bar{q}}$ was contracted to form the matrix element $\langle kp| C |mq\rangle$.

Consider now a tensor network consisting of 5-index tensors A . These tensors can be written as a product of fermionic creation and annihilation operators, where the horizontal modes are created by α^\dagger and the vertical modes by γ^\dagger :

$$\hat{A}_{ij} = \sum A_{u_{ij} d_{ij} l_{ij} r_{ij}}^{[ij] s_{ij}} (c^\dagger)^{s_{ij}} (\alpha_{i,j}^\dagger)^{r_{ij}} (\gamma_{i,j}^\dagger)^{d_{ij}} (\gamma_{i-1,j})^{u_{ij}} (\alpha_{i,j-1})^{l_{ij}} \quad (2.48)$$

This tensor has two incoming modes (labeled by u and l) and two outgoing modes (labeled by d and r) as well as a physical mode labeled by s .

Contracting some outgoing indices of A_{ij} with some incoming indices of its next horizontal neighbor $A_{i,j+1}$ (i.e. the same contraction as above) would now look like this:

$$\begin{aligned}
 &\hat{A}_{i,j+1} \cdot \hat{A}_{ij} \\
 &= (|s_{i,j+1} r_{i,j+1} d_{i,j+1}\rangle A^{[i,j+1]} \langle u_{i,j+1} l_{i,j+1}|) \cdot (|s_{ij} r_{ij} d_{ij}\rangle A^{[ij]} \langle u_{ij} l_{ij}|) \\
 &= \left(|s_{i,j+1} r_{i,j+1} d_{i,j+1}\rangle A^{[i,j+1]} A^{[i,j]} \langle 0| \gamma_{i-1,j+1}^{u_{i,j+1}} \alpha_{i,j}^{l_{i,j+1}} (c^\dagger)^{s_{i,j}} (\alpha_{i,j}^\dagger)^{r_{ij}} (\gamma_{i,j}^\dagger)^{d_{ij}} |0\rangle \langle u_{ij} l_{ij}| \right) \\
 &= \left(|s_{i,j+1} r_{i,j+1} d_{i,j+1}\rangle A^{[i,j+1]} A^{[i,j]} \langle u_{i,j+1} | |s_{i,j} d_{i,j}\rangle \langle u_{ij} l_{ij}| \right) \cdot (-1)^{\bar{r}_{i,j}(\bar{s}_{i,j} + 2\bar{d}_{i,j})} \delta_{\bar{r}_{i,j}, \bar{l}_{i,j+1}} \\
 &= (-1)^{\bar{s}_{i,j} \bar{r}_{i,j}} A^{[i,j+1]} A^{[i,j]} \delta_{\bar{r}_{i,j}, \bar{l}_{i,j+1}} |s_{i,j+1} r_{i,j+1} d_{i,j+1} s_{i,j} d_{i,j}\rangle \langle u_{i,j+1} u_{ij} l_{i,j}| \\
 &= \hat{C}
 \end{aligned}$$

Therefore deriving the signs for a given operation on the tensors A constructed using fermionic creation operators is equivalent to the derivation of the same operation for generic fermionic operator circuits. The equivalence of this derivation can be shown

to hold also for the other elemental operations on fermionic tensor networks, making the choice of fermionic framework one of personal preference.

This equivalence also allows us to greatly simplify the evaluation of fermionic tensor networks. As has been observed by Corboz *et al* [132–134] the sign structure can be derived diagrammatically by considering only line crossings in the contraction scheme and introducing so-called *swap gates* at these crossings. This scheme assumes explicit conservation of the parity of the wave function (see Sec. 2.4 on how to do this) thereby giving access to the parity quantum number at any point. The swap gate now modifies the sign of any index in a line crossing where both indices are of odd parity, according to the prescription

$$X_{i_2 i_1 j_1 j_2} = \delta_{i_1 j_2} \delta_{i_2 j_1} P(i_1, i_2), \quad (2.49)$$

where $P(i_1, i_2) = -1$ if the parity of both i_1 and i_2 is odd and $P(i_1, i_2) = 1$ otherwise.

The placement of these swap gates has to be derived according to the graphic rules, following which one can modify the placement of the swap gates using so-called *jump moves*. These moves enable the placement of the swap gates in such a way that the swap gates can be absorbed in the reduced site tensors. Once this sign structure has been computed, the tensor network can be evaluated in the same way as a tensor network for spin systems. For further details on swap gates and fermionic tensor networks we refer to the literature.

2.4 Symmetries

The number of parameters required to describe a generic many-body state grows exponentially with the number of particles contained within that state. While this cost is mediated in large part by only considering a small part of the total Hilbert space in the form of MPS or TPS, the numerical cost of manipulating these states is still steep. But the computational cost can be further reduced by also considering the symmetries of the system.

When a many-body Hamiltonian H is invariant under certain transformations, these transformations form a symmetry group G . This symmetry group then divides the total Hilbert space into separate subspaces, i.e. symmetry sectors labeled by quantum numbers or conserved charges. For a model defined on a lattice we can distinguish internal and space symmetries. Whereas space symmetries correspond to some permutation of the lattice sites, internal symmetries correspond to transformations on the local vector space of each lattice site. An example for an internal symmetry is the invariance under global spin rotations, mathematically modeled by the non-abelian group $SU(2)$. Internal symmetries can be further distinguished by whether they are global, that is if the symmetry operation transforms the vector space of each site in the same way (e.g. spin-independent rotations) or local if it transforms the vector space of each lattice site in a different way (e.g. spin-dependent rotations). By performing a simulation only in a specific symmetry sector, the accessible Hilbert space is shrunk and the computational cost can often be significantly reduced, while improving accuracy by explicitly preserving the symmetry. Accordingly, symmetries play an important role in most numerical calculations.

These symmetries, of fundamental importance to computational physics, require a special treatment in the simulations. If these symmetries are not explicitly conserved at an algorithmic level, it is possible for accumulated numerical errors to destroy the symmetry, thereby destroying the validity of the simulation. In the case of MPS, symmetries have a long history of being used. Both abelian and non-abelian symmetries have been incorporated into MPS implementations to provide a boost for ground state and time-dependent calculations. When considering symmetries, it is important to note that the tensors constituting a MPS are trivalent, that is they have at most three indices. Since the Clebsch-Gordan coefficients of a symmetry group are also trivalent, the incorporation of arbitrary symmetries into MPS is conceptually particularly simple. In stark contrast are tensor networks, where an almost arbitrary number of indices can appear for a tensor, therefore requiring more care in the treatment of symmetries. But for abelian symmetries the implementation is still straightforward. Assuming a symmetry group G with quantum numbers g_1, g_2, g_3 , a tensor always has to fulfill the conservation of charge. That is: only those elements of $A_{g_1 g_2 g_3}$ are non-zero where $g_1 \circ g_2 = g_3$, with “ \circ ” being the group operation. This causes the tensors to factorize into a structural and a degeneracy part. While the structural part is solely determined by the symmetry group, the degeneracy tensor is acted on by the optimization procedure. In the case of abelian symmetries this can easily be implemented in the contraction prescriptions, as the symmetry constraints result in a block-diagonal structure tensor. Also, the addition of new abelian symmetries to an existing implementation is simple as only the group algebra is required to be known. The increased bookkeeping required to keep track of indices and quantum numbers is easily offset by the numerical speed-up. Instead of having to consider dense matrices of size $d\chi \times \chi$ in DMRG, even a simple symmetry like parity (i.e. Z_2) will reduce this to $\frac{d\chi}{2} \times \frac{\chi}{2}$ entries, thereby yielding a speed-up of about eight in the SVD step.

The same procedure can also be applied to tensor networks, where it is required to keep track of charge flux. This means that each index is considered to be either *incoming* or *outgoing* with the sign of the charge set accordingly. Then an arbitrary-rank tensor is again required to fulfill the laws of charge conservation: $A_{g_1 g_2 \dots g_R} = 0$ iff $g_1 \circ g_2 \circ \dots \circ g_R \neq 0$. This again reduces the cost of computations noticeably for the price of increasing the cost of tensor manipulations significantly.

Even more involved is the situation for non-abelian symmetries. While these symmetries are more powerful, they also require more book-keeping, as the more complicated group structure requires evaluating the Wigner-Eckart theorem for the coupling of charges. As an example we will consider the spin-rotation symmetry $SU(2)$ in the following. Again, we aim to work with only the degeneracy tensors of the symmetry, which in the case of general symmetries are known as reduced matrix elements. Let $T_q^{(k)}$ be a general irreducible tensor operator of rank k , then the reduced matrix elements are given by

$$\langle j' m' | T_q^{(k)} | j m \rangle = (j k m q | j' m') \langle j' | T^{(k)} | j \rangle \quad (2.50)$$

where the $(j k m q | j' m')$ are the Clebsch-Gordan coefficients that form the structure

tensors of the group. While the simplest case, the coupling of two spin-1/2 is a textbook application of the $SU(2)$, the problem becomes much more involved for arbitrary spins and higher number of spins. Once the reduced matrix elements have been obtained, the optimization procedure can again work on block matrices as it does for abelian symmetries. One of the first implementations of this symmetry was completed by Ian McCulloch [139] whose matrix-product toolkit was also used for the calculations of Chapter 3.

By now, the $SU(2)$ symmetry has also been implemented for tensor network algorithms, but there the increased bookkeeping does not appear to pay off yet [140–144]. For this thesis we also implemented abelian symmetries for arbitrary tensor networks. This implementation was used to perform the simulations described in Chapter 4.

2.5 Matrix Product Operators

Consider an operator \mathbf{O} acting on N sites. By writing it in the form

$$\hat{\mathbf{O}} = \sum_{\sigma, \sigma'} \mathbf{O}_{\sigma_1 \dots \sigma_N \sigma'_1 \dots \sigma'_N} |\sigma'_1\rangle \langle \sigma_1| \dots |\sigma'_N\rangle \langle \sigma_N| \quad (2.51)$$

we can again perform sequential singular value decompositions on the coefficients $\mathbf{O}_{\sigma_1 \dots \sigma_N \sigma'_1 \dots \sigma'_N}$, where the double indices (σ', σ) take the place of the single physical index σ in the construction of matrix product states, leading to a matrix product representation for operators

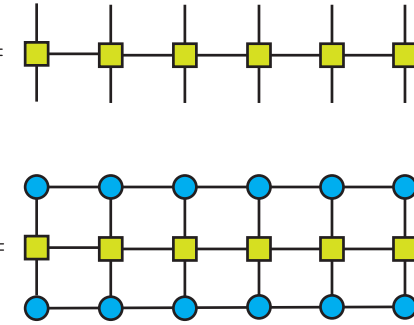
$$\hat{\mathbf{O}} = \sum_{\sigma, \sigma'} W_{\sigma'_1 \sigma_1} \dots W_{\sigma'_N \sigma_N} |\sigma'\rangle \langle \sigma| \quad (2.52)$$

where each $W_{\sigma'_\alpha \sigma_\alpha}$ is a rank four object with a graphical representation as shown in Figure 2.17. In analogy to MPS, this object is called a matrix product operator (MPO). While this construction is always possible, it is not obviously useful as the bond dimension of the MPO may be arbitrarily large.

As it turns out though, almost any physical few-body operator has an efficient representation as a MPO with a small bond dimension. This representation is extremely useful and lies at the heart of modern-day DMRG [48–50, 78]. For the construction of these MPOs I refer to the extensive literature, see e.g. refs. [48, 50] and references therein.

The key to this efficient representation is the realization that few-body interactions follow simple rules. MPOs can therefore be interpreted as cellular automata which interpret the rules to select the next operator to place in an expression [145, 146]. By writing the rules as matrix-products, we obtain the efficient form with low bond dimension we want.

In many ways MPOs can be treated analogously to MPS. The same algorithms apply for compressing, adding and multiplying MPOs. But the main operation is still the application of MPOs to MPS which can be easily performed by a simple site-wise contraction, enabling the efficient evaluation of expectation values. Furthermore, if

$$\hat{O} = \sum_{\vec{\sigma}, \vec{\sigma}'} W^{\sigma_1 \sigma'_1} \dots W^{\sigma_L \sigma'_L} |\vec{\sigma}\rangle \langle \vec{\sigma}'| =$$


$$\langle \psi | \hat{O} | \phi \rangle =$$

Figure 2.17: MPOs are represented diagrammatically in the same way as MPS (upper panel). The evaluation of a MPO reduces to the scalar product of the MPS over the operator, which is depicted in the lower panel.

we consider a MPS in its mixed canonical representation, the MPO formalism allows us to always write the Hamiltonian MPO in the correct basis for the center matrix, thereby enabling a quick and efficient computation of the energy.

2.6 Optimization Procedures

Over the past two decades DMRG has established itself as one of the leading numerical methods for the simulation of strongly correlated systems. DMRG is based on the matrix product state ansatz introduced earlier and employs a variational optimization scheme that we will introduce in the next section. While this variational scheme is one of the most successful schemes, there is also a scheme employing imaginary-time evolution to obtain the ground state. This scheme finds use e.g. in the (i)TEBD algorithm as well as most tensor network algorithms. Following the introduction of the different optimization schemes for one- or two-dimensional tensor networks we conclude this section with a description of the two DMRG algorithms in use today.

Let H be a Hamiltonian whose ground state we want to find. Assume we have some class of ansatz states, then we want to find the state $|\psi\rangle$ within this class that minimizes

$$E = \frac{\langle \psi | H | \psi \rangle}{\langle \psi | \psi \rangle}. \quad (2.53)$$

Usually the most efficient way of achieving this is a variational search in the ansatz space. A different approach is given by the imaginary-time evolution where a random initial state is slowly evolved to a good approximation of the ground state. Here we will start by describing the imaginary-time evolution, as it is the method of choice for most tensor networks and was also used to obtain the ground states in Chapter 4. This is followed by a description of the variational search algorithm as used e.g. in DMRG and to some extent in finite PEPS. Once the general principle is introduced,

we will give a detailed introduction to the single-site and two-site DMRG algorithms.

2.6.1 Imaginary-time evolution

Many tensor network algorithms employ a method known as imaginary-time evolution to compute the ground state. The imaginary-time evolution is based on the idea that a time evolution can not only be computed for real time t , but also for imaginary time, τ , where the non-unitary evolution in imaginary time is interpreted as coupling the system to a heat bath. By evolving the system information is transmitted to the bath, where it is irretrievably lost to the system. Since the bath can contain an arbitrary amount of information, its temperature is always lower than the system's temperature, putting it at $T = 0K$. The coupling of system and bath then corresponds to a cooling of the system. In the thermodynamic limit, i.e. after a time of $\tau \rightarrow \infty$ has passed, the system has the same temperature as the bath it is coupled to: it was cooled down to the ground state.

In a closed system with a given initial state $|\psi(t=0)\rangle$ the system's state at any point of time is known by

$$|\psi(t)\rangle = e^{-iHt}|\psi(0)\rangle, \quad (2.54)$$

where H is the Hamiltonian describing the considered system. If we substitute t by $t \mapsto -i\tau$ where $\tau \in \mathbb{R}$, we obtain the imaginary-time evolution:

$$|\psi(\tau)\rangle = \frac{e^{-H\tau}|\psi(0)\rangle}{\|e^{-H\tau}|\psi(0)\rangle\|}. \quad (2.55)$$

Since the evolution operator $U = e^{-H\tau}$ is not unitary, this is not the evolution of a closed system, but of an open system, necessitating the normalization. For $\tau \rightarrow \infty$ this evolution cools the initial state $|\psi(0)\rangle$ down to the system's ground state $|\psi_0\rangle$:

$$|\psi(\tau)\rangle = \frac{e^{-H\tau}|\psi(0)\rangle}{\|e^{-H\tau}|\psi(0)\rangle\|} \xrightarrow{\tau \rightarrow \infty} |\psi_0\rangle. \quad (2.56)$$

This can be shown by expanding the initial state $|\psi(0)\rangle$ in terms of the eigenstates $\{|\chi_k\rangle\}$ of the Hamiltonian with coefficients $\alpha_k \in \mathbb{C}$, resulting in

$$|\psi(0)\rangle = \sum_{k=1}^N \alpha_k |\chi_k\rangle. \quad (2.57)$$

The energy of state $|\chi_k\rangle$ is given by $H|\chi_k\rangle = \Lambda_k|\chi_k\rangle$ and the eigenstates are sorted according to their energies, such that we have $\Lambda_1 \leq \Lambda_2 \leq \dots \leq \Lambda_N$. The application of the time evolution operator then yields

$$e^{-H\tau}|\psi(0)\rangle = e^{-H\tau} \sum_{k=1}^N \alpha_k |\chi_k\rangle \quad (2.58)$$

$$= \sum_{k,k'=1}^N e^{-\Lambda_{k'}\tau} \alpha_k |\chi_{k'}\rangle \langle \chi_{k'} | \chi_k \rangle \quad (2.59)$$

$$= \sum_{k=1}^N e^{-\Lambda_k\tau} \alpha_k |\chi_k\rangle \quad (2.60)$$

$$= \alpha_1 e^{-\Lambda_1\tau} |\chi_1\rangle + \sum_{k=2}^N \alpha_k e^{-\Lambda_k\tau} |\chi_k\rangle. \quad (2.61)$$

As we have $\Lambda_1 \leq \Lambda_2$, all states other than the ground state are suppressed exponentially for $\tau \rightarrow \infty$ and only the ground state $|\psi_0\rangle$ remains. It is clear though, that numerically, due to the finite computational resources available, the ground state can not be exactly computed. Furthermore, our initial state has to have a finite overlap with the ground state: $\alpha_1 = \langle \psi_0 | \psi(0) \rangle \neq 0$. Otherwise, the eigenstate with the lowest energy will be reached. The speed of the convergence to the correct ground state is proportional to the energy gap above the ground state.

In general, the imaginary-time evolution is very stable and will converge to the correct ground state if the initial state had a finite overlap with the true ground state. But it is not a fast method as it does not contain a prescription to improve the state in a systematic way. This drawback is offset by its numerical stability, making it the method of choice for most tensor network algorithms.

Numerically this optimization scheme is usually implemented by making use of the Trotter-Suzuki decomposition to write the time evolution operator as a series of two-site gates. These operators increase the bond dimension between the sites they were applied to. The truncation of the bond dimension then leads to the time-evolving block-decimation (TEBD) algorithm in one dimension, which employs a well-defined truncation scheme. The same evolution scheme in higher dimensions works, but it is not clear that the correct states are truncated. It happens therefore on a regular basis that the ground state calculation via the imaginary-time evolution becomes stuck. This can be resolved by adding in 'pseudo-variational' update steps which change the site tensors.

2.6.2 Variational optimization

Variational optimization aims to minimize the energy $E = \langle \psi | H | \psi \rangle$ of the system while keeping the norm constant. Mathematically this can be modeled with a Lagrangian multiplier λ , thus arriving at the problem of minimizing

$$\langle \psi | H | \psi \rangle - \lambda \langle \psi | \psi \rangle. \quad (2.62)$$

Obtaining a solution directly is exponentially hard due to the product form of the problem making this a highly non-linear optimization problem. Since a direct solution is not feasible, an iterative procedure is a reasonable choice. A different way would be a stochastic optimization, leading to Monte Carlo methods which will not be discussed here.

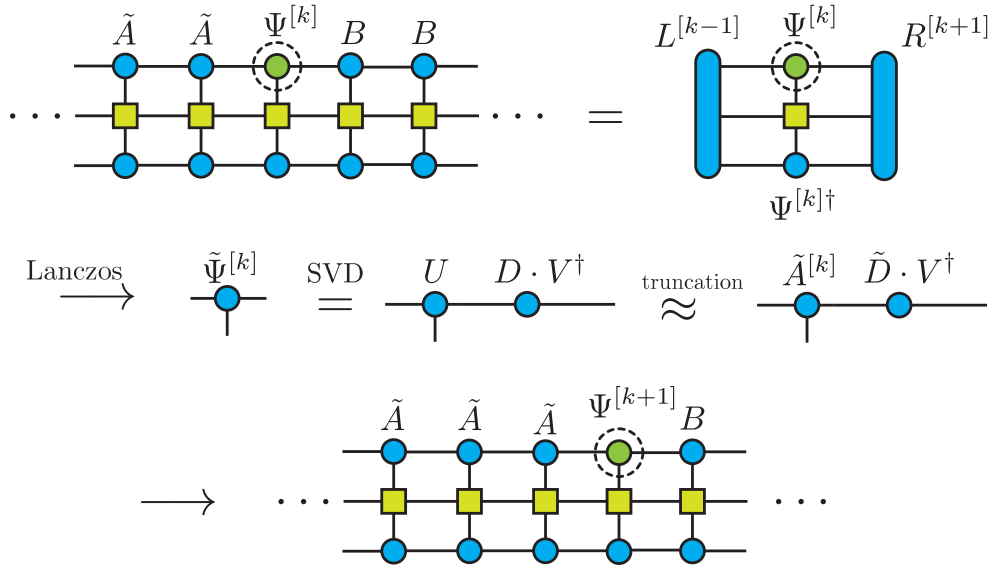


Figure 2.18: Sketch of the single-site update procedure as explained in the text.

The key to the iterative solution in terms of TPS or MPS is the realization that we can optimize the tensors site by site by varying one site tensor and keeping the remaining tensors constant. Under this condition the computation of the derivative of Eq. (2.62) with respect to a single site tensor yields a generalized eigenvalue problem

$$H\mathbf{v} - \lambda N\mathbf{v} = 0. \quad (2.63)$$

Here, N denotes the normalization matrix, i.e. the identity matrix for a properly orthonormalized state. Solving this equation for the lowest eigenvalue λ_0 yields a vector \mathbf{v}_0 which can be re-shaped into a new site tensor. Here, λ_0 is the current estimate of the ground state energy. In general, this problem is too hard for exact diagonalization, but since we are only interested in the lowest eigenvalue, there are efficient solvers available. On the downside, if the problem is badly conditioned (as happens when N is far from the identity) the numerical cost can become very high. For higher-dimensional tensor-product algorithms, where the orthonormality of the local basis can not be ensured this becomes a problem, making the more resilient imaginary-time evolution the method of choice. For matrix product states though, the mixed canonical form ensures correct orthonormalization at all times, reducing the problem to a normal eigenvalue problem which can be solved with algorithms such as the Lanczos or Davidson algorithms.

Note that we still have to compute both the normalization and the Hamiltonian matrices. In the case of canonical MPS the calculation of the normalization matrix is trivial, as it is the identity matrix by construction. The Hamiltonian matrix on the other hand has to be computed by explicit contraction, but this can be made much cheaper by employing an iterative contraction scheme that makes use of the MPO

structure. Of course we never actually compute the full Hamiltonian matrix in an optimized implementation of the DMRG algorithm. Instead the matrix elements are calculated on the fly to exploit the tensor-product structure of the Hamiltonian matrix. For tensor networks describing two-dimensional lattices on the other hand, one has to explicitly calculate both Hamiltonian matrix and normalization matrix. Since the contraction of a full tensor network is already a hard problem, the repeated contraction of the lattice for optimization schemes makes any tensor network algorithm much more costly numerically. Also, small numerical errors may accumulate and lead to a badly conditioned normalization matrix. This is actually a common problem, making the imaginary-time evolution the preferred optimization strategy for higher-dimensional tensor networks.

2.6.3 Single-site DMRG

Now that all the building blocks have been introduced, we can assemble the single-site serial DMRG algorithm [147]. A pictorial representation of the idea behind the single-site optimization is shown in Figure 2.18. The basic idea is to iteratively perform a variational optimization of each site, while keeping the orthonormal bases intact. Given an initial state $|\psi\rangle$, the algorithm then runs as follows (following the notation of Ref. [50]):

1. Bring $|\psi\rangle$ into right-canonical form by performing a sequence of SVDs starting from the right.
2. Compute the matrix elements of the Hamiltonian $R^{[j]}$ iteratively from the right, storing the the matrices $R^{[j]}$ for all positions.
3. Sweep right: Starting from site $k = 1$ through site $N - 1$, sweep through the system to the right as follows:
 - Solve the eigenvalue problem using a large sparse-matrix solver, yielding eigenvector $\tilde{\Psi}^{[k]}$.
 - Calculate the admixture to increase the size of the local Hilbert space:

$$\rho_{adm} = \alpha \sum_{b_i} \hat{H}_{b_i}^{A^\bullet} |\psi\rangle \langle \psi| H_{b_i}^{A^\bullet}, \quad (2.64)$$

where $H_{b_i}^{A^\bullet}$ denotes the contraction of the Hamiltonian with the left H matrix L and the newly constructed site tensor. This procedure is depicted again in Fig. 2.19.

- Diagonalize the density matrix via a SVD and truncate the states.
- Keep left-orthogonalized parts as new site tensor and multiply unused parts with right neighbor to obtain the new center matrix $\Psi^{[k+1]}$.
- Iteratively build up the left H matrices $L^{[k]}$ by absorbing the new site tensors $A^{[k]}$.

- Move to site $k + 1$ and repeat.
4. Sweep left following the analogous prescription. Starting from site $k = N$ through site 2, iterate through the chain to the left as follows:
- Solve the eigenvalue problem with an iterative large sparse matrix solver, using the current center matrix $\Psi^{[k]}$ as an initial guess to obtain the eigenvector $\tilde{\Psi}^{[k]}$ to the lowest eigenvalue.
 - Calculate the admixture

$$\rho_{adm} = \alpha \sum_{b_l} \hat{H}_{b_l}^{\bullet B} |\psi\rangle \langle \psi| H_{b_l}^{\bullet B}. \quad (2.65)$$

- Diagonalize the density matrix via a SVD and truncate the states according to their weight.
 - Keep right-orthogonalized parts as new site tensor and multiply remaining parts to the left to obtain the new center matrix $\tilde{\Psi}^{[k-1]}$.
 - Iteratively build up the right H matrices $R^{[k]}$ by including the new site tensor.
 - Move to site $k - 1$ and repeat.
5. Repeatedly sweep left and right until convergence is achieved.

Convergence can be defined in a variety of ways. While simply using the energy convergence as a criterion is the simplest case, best results are obtained by considering the variance, i.e. $(H - E)^2$, which should approach zero for a converged eigenstate.

Adding an admixture before orthonormalizing the new sites has the effect of increasing the vector space available for the optimization, which in turn allows the algorithm to re-shuffle the quantum numbers. This procedure goes back to White [147] and is explained in detail in Ref. [50].

A quite important consequence of the single-site algorithm is that the truncation error becomes linked to the mixing factor. By changing the mixing factor, one can tune the precision of the algorithm, thereby modifying the convergence behavior. Commonly a larger mixing factor is used in the beginning to enable the convergence to the right part of the phase space, where the mixing factor is then reduced to accommodate high precision calculations.

The advantage of the single-site scheme over the two-site scheme described in the next section is the reduced computational cost. By reducing the matrix dimension in the most expensive step (i.e. the Lanczos step), the single-site scheme becomes faster. The drawback of course is that we have to compute the admixture.

2.6.4 Two-site DMRG

The two-site algorithm for DMRG is the traditional variant of the algorithm. It is mostly identical to the single-site algorithm with one crucial difference: Instead of

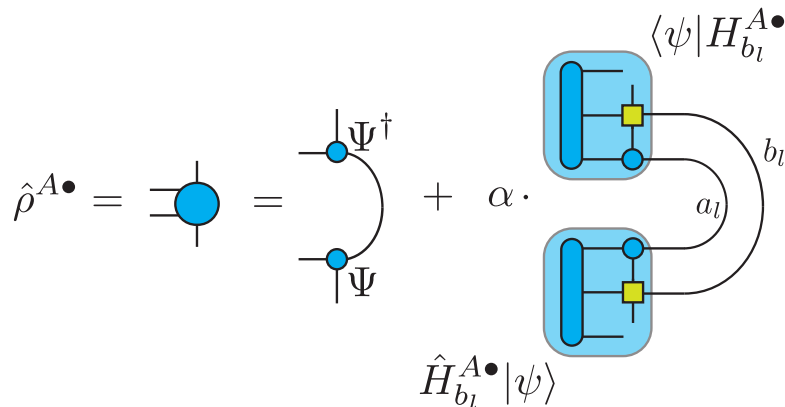


Figure 2.19: Sketch of the admixture procedure that is used to artificially increase the size of the vector space in which the truncation is performed. By considering the action of the Hamiltonian on the newly computed center site, we obtain a prediction for the new site tensor. This procedure significantly improves the single-site scheme, bringing it up to par with traditional two-site DMRG.

optimizing a single center site in the Lanczos step, one further site is incorporated into Ψ , leading to a two-site center matrix $\Psi^{\sigma_k \sigma_{k+1}} = \Psi^{\sigma_k} B^{\sigma_{k+1}}$ or $\Psi^{\sigma_{k-1} \sigma_k} = A^{\sigma_{k-1}} \Psi^{\sigma_k}$.

The main advantage of the two-site algorithm is that it optimizes directly in a larger space, removing the need for an artificial increase of the optimization space as done in the single site algorithm with the admixture. This has the consequence that the truncation error in two-site DMRG is a well-defined quantity. Also, the two-site algorithm is somewhat less prone to getting stuck, although this seems to be fixed by the admixture. In summary the single-site algorithm is conceptually more elegant and requires less resources, whereas the two-site algorithm is a bit better behaved but more costly.

2.7 Parallelization

Once symmetries have been implemented there are only a few avenues left that may improve the performance of general tensor network algorithms. While for two-dimensional methods there are still algorithmic improvements to explore, this is not the case for DMRG, which is already highly optimized. One such avenue is the usage of multiple processors, which we will discuss in two different variants. First we will introduce the concept of shared-memory parallelism, a technique already in widespread use, which aims to make use of multiple processors for a single update step. Then we will proceed to discuss a more recent development, the real-space parallelization [148]. This scheme was conceived to employ multiple processors for independent steps of the DMRG, possibly gaining a much larger speed-up than possible with only shared-memory parallelism.

2.7.1 Shared-Memory Parallelization

The numerical cost of most tensor network algorithms is dominated by linear algebra. In the case of DMRG the most expensive step is the solution of the eigenvalue problem which in the case of a Lanczos or Davidson solver boils down to matrix-vector multiplications.

These products are eminently parallelizable at a very elemental level. In fact, most modern implementations of the linear algebra package (LAPACK) such as the ACML¹ or MKL² already contain the option of employing multiple processors for these computations, as long as they are of the shared memory type. These can then be used simply by linking existing code against the shared-memory variants of LAPACK.

Shared-Memory parallelism is one of the two paradigms of parallel computing for general purpose computers. In the case of shared-memory computing all processors or cores have access to the same memory without explicit communication, effectively sharing the data contained therein. Therefore the communication of data between separate shared-memory threads is very efficient as only the addresses of memory segments have to be communicated.

On the downside, sharing of memory also requires sharing the memory bandwidth. Thus there is massive degradation in the speed-up for shared-memory parallelism (SMP) when a large number of cores is used. This scaling becomes better if the cores spend more computing cycles on actual computations instead of accessing data stored in memory as can be seen in Fig. 2.20, which in the case of DMRG requires very large bond dimensions to improve the scaling. So while shared memory has the lowest cost in implementation with acceptable payoff right away, it does not scale well for a large number of cores.

2.7.2 Real-Space Parallelization

Recently a new ansatz for the parallelization of DMRG has been proposed by M. Stoudenmire [148] which is akin to the paradigm of domain decomposition. Instead of trying to reduce the cost of the most expensive step it was suggested to do many expensive steps at once. The key to this idea is that the same canonical form does not have to be maintained at all points at once. Instead several processes can work at the same time in local canonical representations, even while the global state is not entirely orthonormal any more. This effectively transforms the MPS from a state with one orthonormalization center to one with multiple orthonormalization centers. This real-space parallelization scheme was originally presented for the two-site algorithm, but here we will adapt it for the single-site algorithm.

The key idea of this scheme is to assign separate processes to separated spatial regions. First, we divide the state into $n = (\text{Number of Processes})$ intervals of roughly equal length to avoid load imbalance, then we assign to each interval one process and let these processes sweep only the subsystems. By exchanging some information with

¹*AMD Core Math Library* i.e. the AMD implementation of LAPACK

²*Math Kernel Library* i.e. the Intel implementation of LAPACK

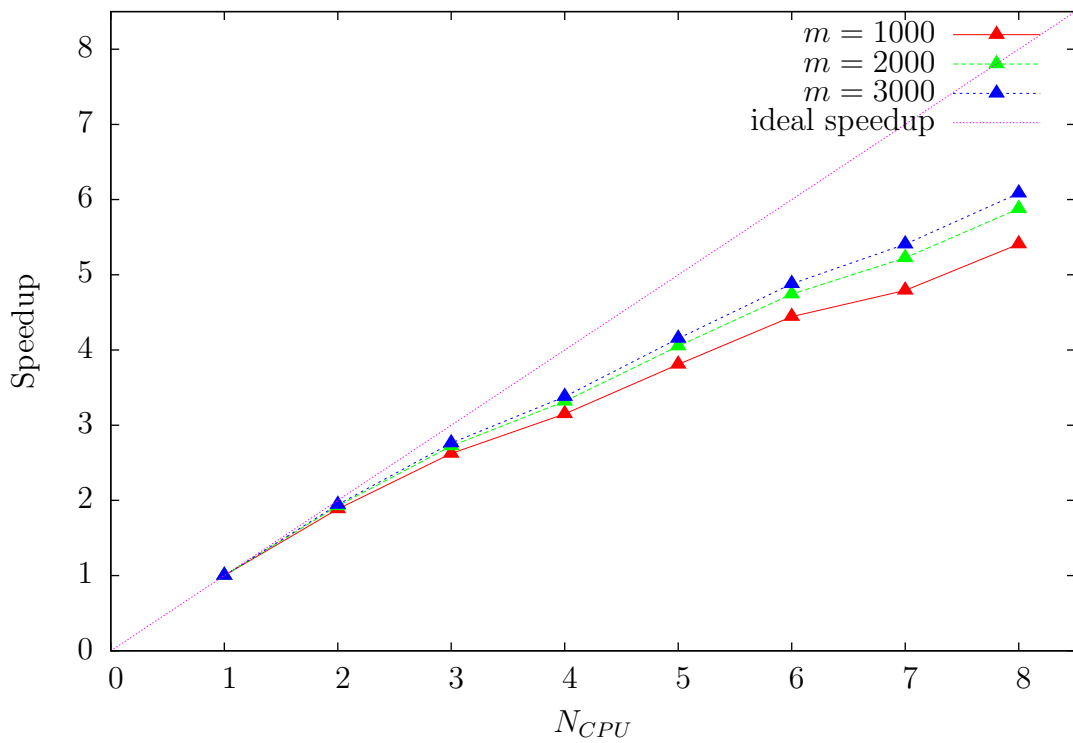


Figure 2.20: The scaling of the $SU(2)$ symmetric matrix product toolkit with shared-memory parallelization. Here N_{CPU} denotes the number of cores used for the computation and the pink line shows perfect scaling, where a speed up S corresponds to the calculation being S times faster when running on n cores. This plot was created using the $SU(2)$ symmetric Heisenberg model on a kagome cylinder with a circumference of 6 lattice spacings.

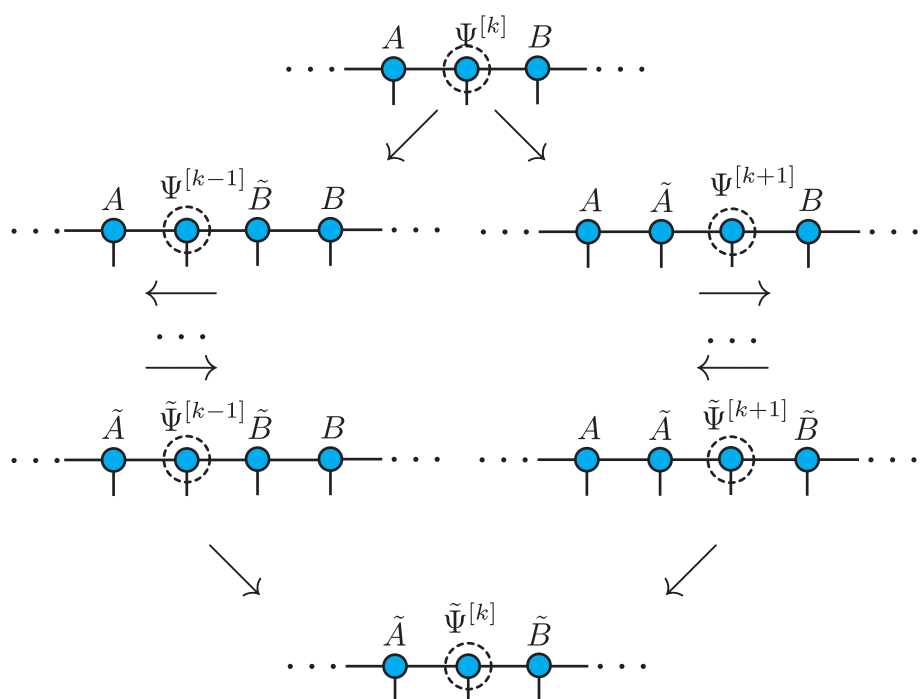


Figure 2.21: Sketch of the sweeping scheme for the parallelized DMRG. We begin by splitting the MPS with a SVD and then working on the two sides on different nodes. By introducing an inverted center matrix we can “glue” these separate parts back together after two half-sweeps, thereby closing the DMRG optimization loop.

their neighbors all processes always operate in a well-defined mixed canonical basis, while dealing only with their interval within the system. For concreteness, let us consider the case of two processors. To begin, we perform some serial sweeps of the system, then iterate to the middle of the state, i.e. our center matrix. In this form, our DMRG wave function can be written as

$$|\psi\rangle = \sum_{a_l, a_{l+1}, \sigma_l} \Psi_{a_l a_{l+1}}^{[l]\sigma_l} |a_l\rangle |\sigma_l\rangle |a_{l+1}\rangle. \quad (2.66)$$

Conventional serial DMRG would now continue by performing one SVD and iterating to the next site. but in the real-space parallelization scheme we actually perform two SVDs. A sketch of this sweeping scheme is shown in Fig. 2.21. First we perform a left-orthogonalization, resulting in a new left-canonical site tensor $A^{[l]}$. We then perform a right-orthogonalization resulting in a right-canonical site tensor $B^{[l]}$. Now we compute the new left Hamiltonian terms using $A^{[l]}$ and the new right Hamiltonian terms using $B^{[l]}$:

$$\begin{aligned} L^l &= \sum_{\sigma_l, \sigma'_l} A^{\sigma_l} * W^{[l]} A^{\sigma'_l} \\ R^l &= \sum_{\sigma_l, \sigma'_l} B^{\sigma_l} * W^{[l]} B^{\sigma'_l}. \end{aligned}$$

We then communicate R^l to the first process and L^l to the second process and let them start their left/right sweeps respectively. The details of the communication step are depicted in Fig. 2.22. Once the two processes have completed two half-sweeps of their intervals they arrive again at the center bond. There they exchange their respective L - and R -matrices to obtain an update for the other half-chain. At this point both processes are in a well-defined global basis. Ending the sweeping procedure now involves collecting all the updated site tensors and writing them to disk in a consistent way.

This parallelization scheme can be directly generalized to more than two nodes by spawning new processes multiple times at the SVD step. As a proof of principle the single-site parallelization scheme has been implemented for this thesis, using Ian McCulloch's MP Toolkit as the basis. The performance for this single-site update is shown in Fig. (2.23(a)), whereas the speed-up of the original two-site proposal is shown in Fig. (2.23(b)).

To test our implementation we applied it to a 96-site kagome cylinder with a circumference of 8 lattice spacings with a bond dimension of $m = 400$. As can be seen in the plots, the scaling of this trivial implementation is not yet as good as the original proposal. The bad scaling is caused on the one hand by the relatively small bond dimension for a sample with very long-range interactions. In this regime, the cost of the calculation is dominated by the serialized access to the wave function which has to be loaded by each separate process. This start-up overhead is increased by having to use a serial file system. Furthermore, with such a small bond dimension, the cost of using $SU(2)$ symmetry together with long-range interactions make the communication

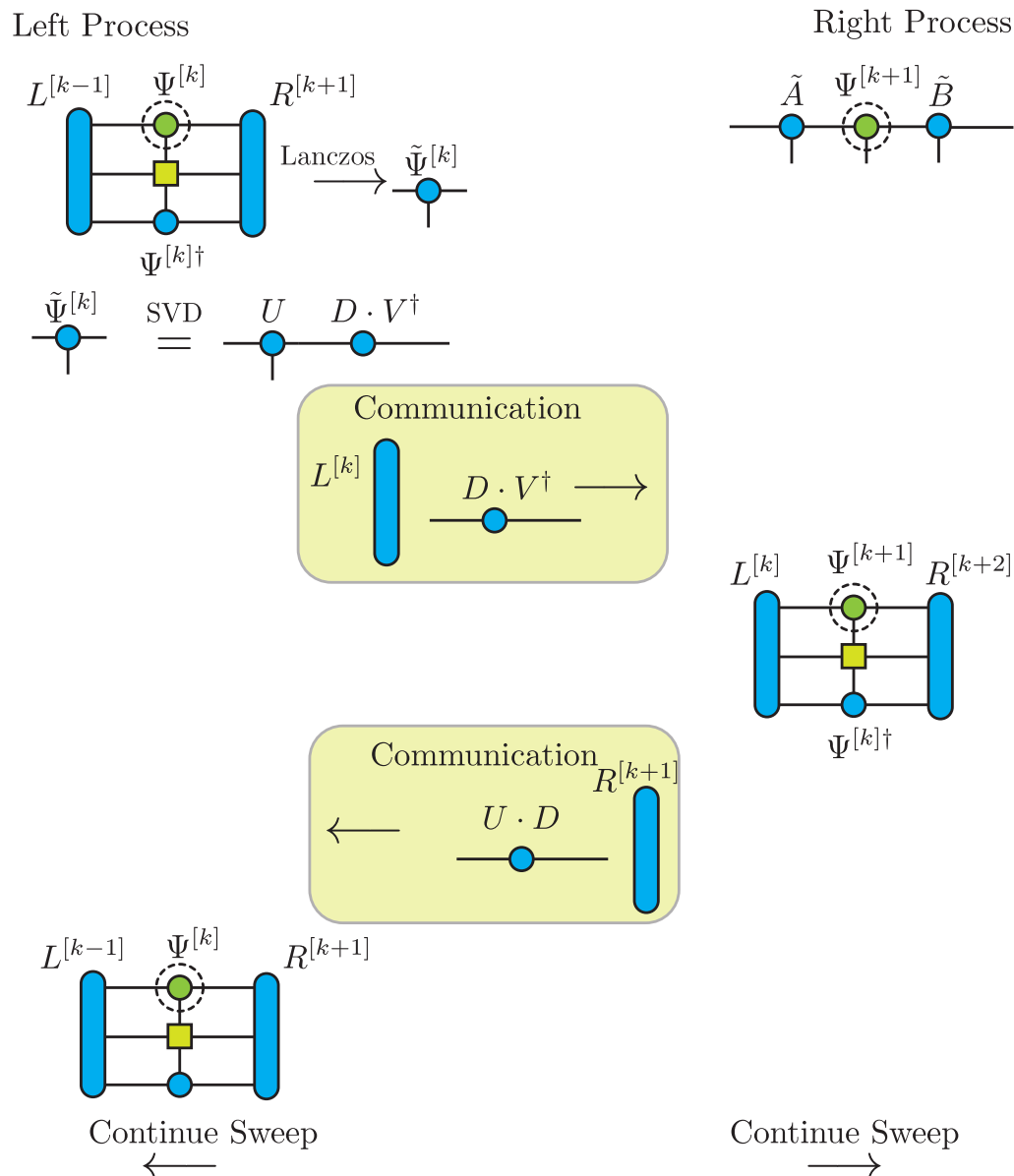
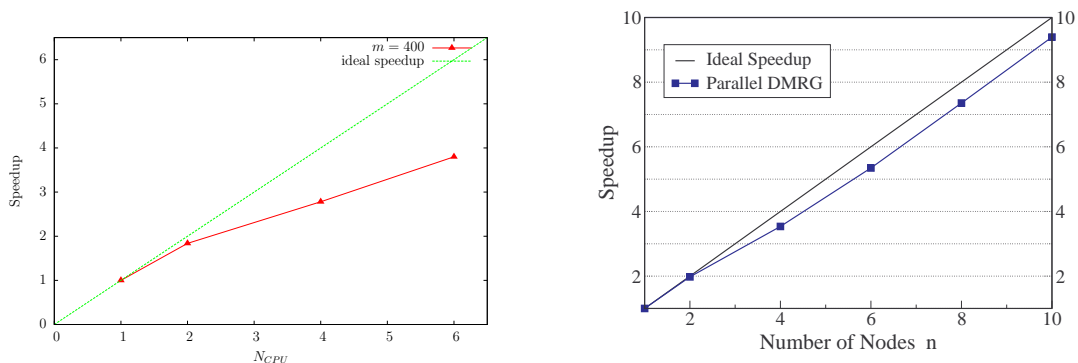


Figure 2.22: Sketch of the update procedure for the parallelized DMRG. We send the left Hamiltonian matrix and the left center matrix to the right-hand process, where we perform a single-site update with these tensors. We then communicate the new right-hand Hamiltonian matrix and right center matrix to the left process and start the serial sweeping procedure for both processes.



(a) Speedup of the single-site algorithm in parallel DMRG using a very simple proof-of-principle implementation that is not optimal. The implementation was tested for a 96-site kagome cylinder with bond dimension $m = 400$.

(b) Scaling of the original implementation in Ref. [96] as tested for the Heisenberg model on a 192-site square lattice cylinder with up to $m = 2000$ states. Used with permission from the author.

Figure 2.23: Scaling of the parallel DMRG algorithm in a one-site or two-site scheme.

of the Hamiltonian matrices L and R an expensive part. But the main bottleneck in this case was the implementation. We did not optimize the distribution of the intervals, but instead used intervals of equal lengths. This caused the edge processes to idle for long times, as their calculations are much faster than the calculations for the center processes.

But aside from this benchmark, we were able to demonstrate that the parallelized single-site update scheme described above actually works. With that in mind, we can now work on implementing a better variant, which especially takes into account the edge processes.

2.8 DMRG in Two Dimensions

While DMRG was originally conceived for one-dimensional systems it has long been used for two-dimensional simulations as well [93, 94, 96, 97, 101, 102] This is feasible due to the advantages of the slow scaling of DMRG with the bond dimension.

As mentioned above, the entanglement in gapped ground states follows an area law, which MPS fulfill exactly for one-dimensional systems. But in two dimensions the entanglement grows faster, so to describe these systems the bond dimension m of MPS has to grow exponentially as $m \propto e^S$. This exponential scaling severely limits the system sizes accessible to DMRG.

Exact diagonalization suffers from the same problem, but enables reliable extrapolations to large system sizes by using periodic boundary conditions and solving a system to a very high precision. While DMRG can determine the ground state of many systems very exactly the use of periodic boundary conditions is not advisable for DMRG simulations. Periodic boundary conditions (PBC) significantly increase

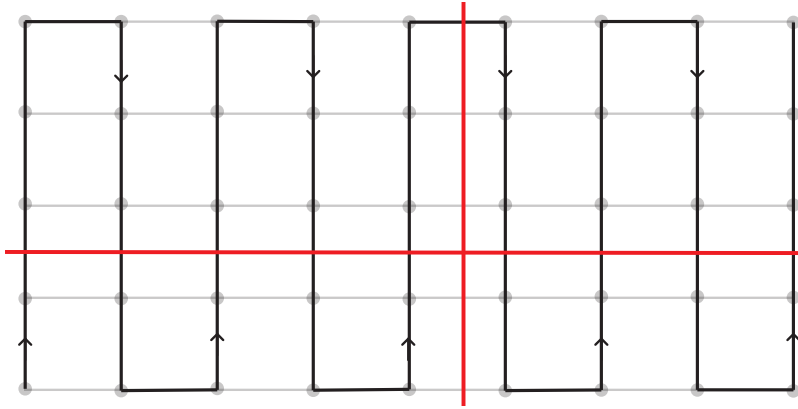


Figure 2.24: Sample mapping of a square lattice to a MPS. The black line denotes the MPS, while the red lines denote two different cuts of the system, as explained in the text. Note: this mapping introduces unnecessary long-range interactions into the Hamiltonian. A more optimal mapping is possible and was used for our calculations.

the entanglement in the system thereby causing MPS to fail even earlier. This problem can be partly negated by using cylindrical boundary conditions, i.e. PBC in one direction and OBC in the the other.

To see why this is the case, consider a system defined on the square lattice (see Fig. 2.24). To model this system we snake a path through the system, mapping the two-dimensional square lattice to a one-dimensional MPS. But this mapping introduces both long-range interactions and long-range entanglement into the 1D model. Whereas MPS can deal efficiently with short-range entanglement, long-range entanglement is much harder. If we now consider a cut parallel to the cylinder seam, i.e. in the x -direction in Fig. 2.24, then it becomes immediately obvious that increasing the system in the x -direction does not increase the entanglement per cut bond. An increase in the y -direction on the other hand will lead to more and more long-range entanglement being carried by single bonds, exponentially increasing the numerical cost and thus limiting the reachable system sizes.

Related to this is a sub-leading cost and that is the cost of the long-range interactions. While the bond dimension D_W of the MPOs only enters as a sub-leading contribution to the total numerical cost, it does become significant for very long-range interactions. This becomes even more significant when considering the memory requirements of DMRG.

Nevertheless, the low basic cost of DMRG enables us to treat even large systems with good precision using DMRG as will be described in the next chapter.

3 The Kagome Heisenberg Antiferromagnet

Following Landau's theory of phases, conventional phases can be identified by local order parameters. These local order parameters are associated with the breaking of symmetries, i.e. a broken symmetry will give rise to a local order parameter that can be used to identify the phase the system is in. The simple ingredients of symmetries and order parameters were enough to make Landau's theory of phase transitions, together with the Fermi-liquid theory for metals, the main building block of condensed matter theory for almost half a century.

This theory failed for the first time when fractional quantum Hall states were discovered. Subsequently, a plethora of phenomena beyond the reach of Landau's theory were found in a variety of theories and experimental systems. Among these states exciting new concepts appeared, such as quantum and topological order. As opposed to the Ginzburg-Landau paradigm, which is based on external symmetries such as lattice symmetries, the new ideas of order which were pioneered by X.-G. Wen are based on internal symmetries of the wave function [12, 19].

Topological states are also known as one of the exotic states of matter as their existence lies beyond the Landau theory that is able to explain so many observable phases. Exotic phases are strongly associated with quantum spin liquids (QSLs), a state of matter that does not break any symmetry, neither of the lattice nor the Hamiltonian [12, 19, 149–153]. In these phases there is no long-range order, instead there is long-range entanglement which is responsible for many of the strange phenomena one can find in these systems. Quantum spin liquids, as phases of strongly interacting spins that do not order even at absolute zero temperature, are linked to remarkable phenomena such as transmutation of statistics (*e.g.* fermions appearing in a purely bosonic model) [25, 154], fractional quantum numbers [21, 22, 155–157], and the enabling of otherwise impossible quantum phase transitions [158], to name just some of the exotic physics.

The theory of quantum spin liquids dates back to P.W. Anderson who observed in 1973 that states without magnetic long-range order were in principle viable ground state candidates for frustrated quantum antiferromagnets [157]. According to his idea, these systems could avoid all spontaneous symmetry breaking and therefore remain disordered down to absolute zero. The picture he proposed was that of the iconic resonating valence bond (RVB) wave function. The RVB state is a linear coherent superposition of singlet coverings of the lattice, making it a manifestly quantum state of matter (see Fig. 3).

Even though our understanding of frustrated quantum magnets has much advanced since the inception of the quantum spin liquid, the concept is still hard to grasp

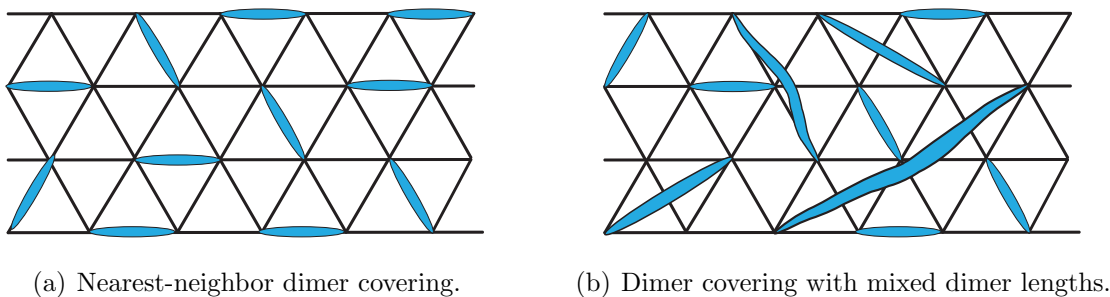


Figure 3.1: Two different valence bond coverings on the triangular lattice. On the left we have a short-range dimer covering with only nearest-neighbor valence bonds. On the right we have a dimer covering with longer-range valence bonds. A general RVB state is composed of a superposition of all such dimer coverings.

[12, 159]. First of all there is the obvious question of how to define a quantum spin liquid. Often a quantum spin liquid is defined by the absence of any symmetry breaking which is a purely negative definition and as such quite hard to show. A better definition also involves the absence of long-range n -spin correlations for any n and an even more restrictive, but also positive, definition requires QSLs to exhibit fractional excitations, such as spinons or visons. Here, we will adopt the second definition and require a quantum spin liquid to exhibit an absence of both long-range correlations and spontaneous symmetry breaking, as requiring fractional statistics is equivalent to requiring topological order.

While this definition is viable, it does not lend itself easily to the characterization and classification of general spin liquids. This task is performed instead by the framework of the projective symmetry groups (PSG), introduced by X.-G. Wen [12]. Within the PSG scheme one analyzes the breaking of gauge symmetries in a mean-field ansatz to classify the different QSL ansätze. This is to date the most powerful tool to study the properties of quantum spin liquids and we will describe it in more detail in the next section.

While the defining hallmark of all quantum spin liquids is the absence of any local order parameter [12, 159], the PSG classification of spin liquids resulted in the realization that spin liquids may be gapless or gapped. Although current experimental results found only gapless spin liquids [160–165], gapped spin liquids have been found in many numerical and analytical studies on the kagome, square, and honeycomb lattice [19, 27, 153, 162, 166–168]. As opposed to gapless spin liquids, which are quite involved and difficult to characterize, gapped spin liquids have the distinctive property that they are characterized by topological order, i.e. ground state degeneracy that only depends on the specific topology of the underlying space. We will treat this concept of order in more detail in the next section.

In the search for QSLs, two qualitatively different questions emerge immediately [150]:

- Considering a given Hamiltonian H , how do we know if it actually admits a QSL

as its ground state? If there is a QSL ground state can one further characterize the QSL?

- Given a ground state wavefunction in some form, how can one tell if this wavefunction really describes a QSL? If yes, how can this QSL be further characterized?

Obviously these two questions are related: if a numerical algorithm can procure the approximate ground state wavefunction of a particular model, then finding an answer to the second question immediately provides an answer to the first question as well. As it turns out there is a tool, the topological entanglement entropy, inspired by quantum information theory that enables us to partially answer these questions. The details of this calculation will be discussed in Sec. 3.2.3.

To establish the presence of any quantum spin liquid, gapped or gapless, we have to find a disordered state that is fully symmetric, so as to ensure the absence of any local order parameter. The key feature necessary to stabilize quantum spin liquids are therefore quantum fluctuations that suppress any ordering the system may attempt. Thus a system where low dimension, strong frustration, and low coordination number all work together to increase the classical degeneracy and subsequently also the quantum fluctuations will be a prime candidate for spin liquid physics [166]. The nearest-neighbor antiferromagnetic Heisenberg model on the kagome lattice displays all these properties and will be discussed in the next section [166, 169, 170].

A different picture emerges if we allow the state to spontaneously break the lattice symmetry while forcing it to keep the full symmetry of the Hamiltonian. Such states, with spin-rotation symmetry, but spontaneously broken lattice symmetry are known as valence bond solid (VBS) or valence bond crystal (VBC) states, where the difference between VBS and VBC lies in the regularity of the valence bond pattern. These states are known to occur in nature as they recently have been observed in nature in the organic compound $(\text{C}_2\text{H}_5)(\text{CH}_3)\text{P}[\text{Pd}(\text{dmit})_2]_2$ [171] and the kagome compound $\text{Zn}_x\text{Cu}_{4-x}(\text{OD})_6\text{Cl}_2$ [161]. Bond-centered modulations in the local density of states have also been observed in underdoped cuprates in scanning tunnelling microscopy experiments [172] and can immediately be interpreted in terms of doped VBS states [155]. While these states often do not break any apparent symmetry the VBS states can still be understood in terms of symmetry-breaking by considering “hidden” or “topological” symmetries. These states also appeared as candidate states for the ground state of the kagome Heisenberg antiferromagnet discussed below.

In the following we will first discuss the state of the current research in Sec. 3.1, then move on to elaborate on details of our simulations in Sec. 3.2 before finishing by presenting the published paper in Sec. 3.3.

3.1 Review of Published Results for the Kagome Heisenberg Antiferromagnet

Low-dimensional spin-1/2 Mott insulators in vertex-sharing regular two-dimensional lattices, have been studied extensively for many years as it is well-known that highly

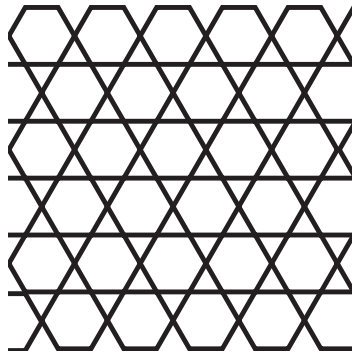


Figure 3.2: The kagome lattice of corner-sharing triangles.

frustrated 2D quantum antiferromagnets present a bewilderingly rich plethora of ground state phases. Many of the phases encountered in these systems do not have any classical counterparts and display exotic order, examples of which include various valence-bond crystal and quantum spin-liquid phases. The phases one can observe in such systems are determined not only by the dimensionality and structure (e.g. the coordination number) of the lattice on whose sites the spins are situated but also by the spin quantum number S , as well as the type and range of the magnetic interactions between these spins that often compete for different forms of order, thus leading to frustrated magnets. It is also known that the quantum versions of classical models with massively degenerate ground states are prime candidates for systems with novel ground states, even more so are those model systems with a non-zero ground state entropy [166, 169, 170].

A special niche among all such candidate spin systems is occupied by those lattices with periodic arrays of corner-sharing structures, where each corner-sharing structure (e.g. triangles for nearest-neighbor interactions) in itself is magnetically frustrated [173]. Within this niche one finds the Heisenberg model on the three-dimensional pyrochlore lattice of corner-sharing tetrahedra as well as on the two-dimensional kagome lattice of vertex-sharing triangles. Of these, especially the spin-1/2 Heisenberg antiferromagnet (HAF) on the 2D kagome lattice has been the subject of a profusion of studies in recent years [35, 36, 56, 100, 156, 165, 166, 174–243]. A sketch of the kagome lattice is shown in Fig. 3.2. The Hamiltonian for this model is given by

$$H = \sum_{\langle i,j \rangle} \mathcal{S}_i \cdot \mathcal{S}_j, \quad (3.1)$$

where the brackets $\langle \cdot, \cdot \rangle$ denote nearest neighbors. This model first appeared as a description for Helium on a graphite substrate in the late eighties [244]. Soon it was realized that this model's ground state was lacking magnetic long-range order while displaying strong frustration and a low coordination number [245–248]. But even after several decades of research the exact nature of the ground state of the spin-1/2 Heisenberg antiferromagnet on the kagome lattice has remained unclear. There exist several proposed candidate ground states, ranging from states with magnetic order to valence-bond crystals or quantum spin liquids of different types [27, 156, 167]. In

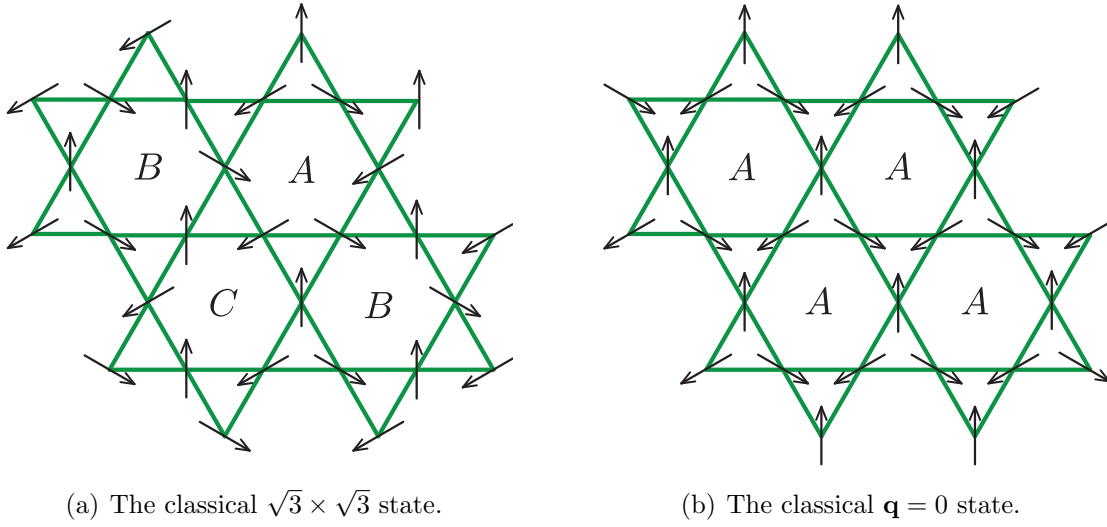


Figure 3.3: The two different classical ground states for the kagome lattice Heisenberg antiferromagnet, where the arrows denote classical spin orientations. The $\sqrt{3} \times \sqrt{3}$ state on the left breaks translational invariance and requires a larger unit cell. The $\mathbf{q} = 0$ state (right) on the other hand does not break the elemental translational symmetry of the kagome lattice.

the remaining parts of this section we will endeavor to explain the different ideas and candidates for the ground state of this system, leading up to a discussion of the methods we employed in a large-scale DMRG study to determine the ground state.

3.1.1 Classical ground state

The kagome lattice is based on the triangular Bravais lattice. Its classical ground state is similar to the triangular lattice in that it obeys the so-called ice-rules, i.e. neighboring spins have a relative angle of 120° to each other, resulting in a non-trivial infinite classical degeneracy. From this degeneracy set, by the mechanism of *order by disorder*, two different ground states can be selected [249]. These states are usually known as the $\mathbf{q} = 0$ and $\sqrt{3} \times \sqrt{3}$ states respectively and are shown in Fig. 3.3. It has long been debated whether the remnants of the classical orderings would survive the onset of quantum fluctuations at zero temperature, as e.g. semi-classical approaches such as large- S calculations plead in favor of the $\sqrt{3} \times \sqrt{3}$ state as the ground state [250, 251]. Exact diagonalization results [188, 215, 252, 253] also show this state to be stabilized on addition of a ferromagnetic J_2 interaction [166].

3.1.2 Valence bond crystals

When considering RVB-like dimer coverings of the kagome lattice, one realizes that any dimer covering must leave some bonds empty. Indeed it was shown early on that one-fourth of all triangles in the kagome lattice remain empty in any dimer covering. These triangles are the source of quantum fluctuations in the system. It is therefore

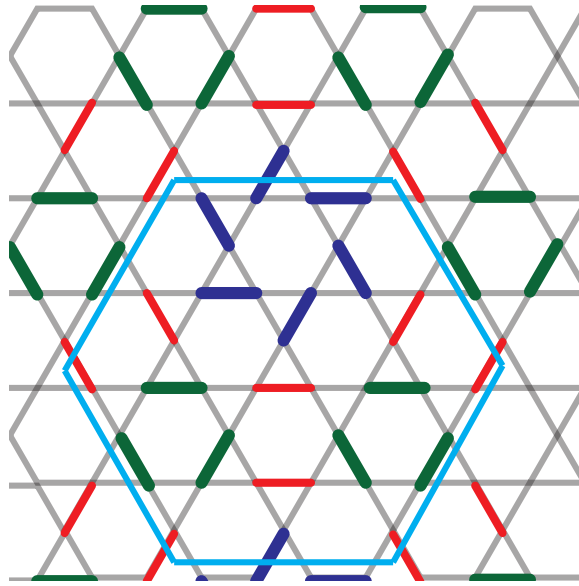


Figure 3.4: The unit cell for the 36-site hexagonal valence bond crystal. Here the broad lines represent valence bond, with blue bonds forming the pinwheel structure, green bonds forming a perfect hexagon, and red bonds connecting them. The light blue line is an outline of a possible choice of unit cell.

instructive to consider different tilings of these empty triangles and to compute the energy of these coverings.

Calculations with various methods resulted in VBC proposals with 6-, 12-, 18-, and 36-site unit cells [167, 185, 187, 201]. Using series expansion the lowest energy of these proposals was computed for the 36-site unit cell [185, 187] which is sketched in Fig. 3.4. The construction of this unit cell is based on the idea that the perfect hexagons minimize the energy and should be as closely packed as possible. From this goal results the ansatz with the large unit cell, which was later shown to occur naturally in the vicinity of the ground state [56, 100, 254].

3.1.3 Quantum spin liquids

Many of the competing proposals for the ground state of the kagome lattice Heisenberg antiferromagnet were formulated within the framework of the slave-particle ansatz and classified using projective symmetry groups [12, 159, 205, 255]. The slave-particle technique is a flavor of mean-field theory, where each spin-1/2 operator is re-written in terms of creation and annihilation operators. By using different statistics for these operators two different variants of slave-particle theory can be identified. Here we will concentrate on slave-boson theory, but slave-fermion theory is equally valid for this problem. It is important to point out that both slave-boson and slave-fermion theory can create the same low-energy theories. Since both theories operate on virtual spaces, the creation of valid low-energy theories requires gauging

the mean-field theory down to a physical theory, making the differences between the two slave-particle approaches purely technical [164, 256].

In slave-boson (Schwinger-fermion) theory, each spin-1/2 operator is decomposed at every site in terms of a bilinear

$$\mathcal{S}_i = \frac{1}{2} f_{i\alpha}^\dagger \sigma_{\alpha\beta} f_{i\beta}, \quad (3.2)$$

where $\alpha, \beta = \uparrow, \downarrow$, and σ is the vector composed of the Pauli matrices [12, 159]. The f -operators obey fermionic statistics and are known as *spinon* creation and annihilation operators. These spinons carry spin and form the low-energy quasi-particles whose excitation spectrum mainly characterizes the effective low-energy theory of a mean-field ansatz. Spinons can in principle obey both fermionic or bosonic statistics, but only fermionic spinons can create both gapped and gapless quantum spin liquids. Common to both fermionic and bosonic approaches is the gauge redundancy introduced by the slave-particle representation, causing the spinons to be coupled to an emergent gauge field. The symmetry of the invariant gauge group derived from this gauge field then serves to classify the quantum spin liquid.

To obtain a physical state from the mean-field theory one has to project the enlarged spinon space down to the physical space with the constraint

$$\sum_{\alpha} f_{i\alpha}^\dagger f_{i\alpha} = 1 \quad (3.3)$$

where the sum runs over all spin flavors. Note that within this mean field theory picture the interactions between spinons appear only beyond the mean field level and are mediated by fluctuating gauge fields. By re-writing in terms of spinon operators the spin-spin interaction terms give rise to quartic spinon interactions. These interactions can be decoupled in two channels, divided into spinon hopping (particle-hole) and pairing (particle-particle) channels. Together these constitute an ansatz for a QSL, where different mean field ansätze are distinguished by their different structure. The redundancy in the choice of gauge field however shows the mean-field states to be only projective representations of physical states. Hence, the same physical state may be represented by many *gauge equivalent* mean-field ansätze forming a set. Different projective representations of the lattice and time-reversal symmetries of the Hamiltonian are formed by different mean-field spin liquid ansätze. A systematic understanding of distinct quantum spin liquids therefore requires a careful analysis of the projective symmetry group which is beyond the scope of this work.

When both spinon hopping and pairing terms are present, the calculations of the spinon ground state can be re-written in the form of a BCS type Hamiltonian for the spinons, enabling the solution via a Bogoliubov transformation. If the Hamiltonian is symmetric under spin-rotations, the hopping and pairing channels can be separated completely into a singlet part which is spin independent and a triplet part with spin dependency. In a model with spin-rotation invariant exchange the singlet ansatz already gives rise to stable quantum spin liquid mean field solutions, making the triplet channels obsolete. Following this one obtains symmetric QSLs that do not

spontaneously break spin-rotation symmetry. A PSG analysis of the singlet ansätze on the kagome lattice has been done both for slave-fermion and for slave-boson theories, revealing QSL states which can serve as parent states for physical spin liquids. Although mean-field theory is in general a rather poor approximation of strongly correlated systems, it can be shown that a mean-field ansatz can be stable in the presence of some perturbations. Since we lack another method to classify quantum order at the moment, we have to deal with this kind of approach.

From these theories emerged numerous different proposals for the kagome Heisenberg antiferromagnet. Derived from mean-field theory there are also various theories for a so-called *algebraic* or gapless $U(1)$ spin liquid [161, 162, 164, 165, 211, 257, 258]. Based on these proposals Iqbal *et al.* performed Gutzwiller-projected Monte Carlo studies, finding the energy of the candidate states to be competitive [223–226]. The distinctive feature of these ansatz states is the absence of a gap, which can not be discounted by exact diagonalization [170, 188, 246, 247, 252] and is actually supported by experimental findings [162, 235]. By adding mass-fields or symmetry-breaking gauge fields to the mean-field theories, these parent states can be broken down to a lower symmetry, giving rise to gapped quantum spin liquids. Gapped spin liquids are also known as topological spin liquids as they exhibit fractionalized excitations, one of the key properties of topological order [6, 8, 9, 11, 12, 173, 206, 259–261].

Topological order

Gapless quantum spin liquids form extremely interesting ground states considering their ground state is protected by their projective symmetry groups [159]. A different mechanism for protecting a certain ground state occurs in spin liquids that are gapped or where the gapless sector is decoupled [12]. These spin liquids sustain a kind of hidden order called *topological order* [13, 14]. In these topological spin liquids there exist fractional excitations which interact with each other through emerging gauge fields [155, 158, 261, 262].

Topological order is not related to any symmetries of the system and therefore is not described by any local order parameters. Since this kind of order is determined by global properties, it is also robust against all local perturbations. Topological order is characterized either by global properties such as ground state degeneracy, by fractional excitations, and/or by non-abelian exchange statistics. Progress from quantum information theory has suggested the topological entanglement entropy [263, 264] as a probe [152, 265–267], a technique we will illuminate later on.

The concept of topological order and quantum order are central to the understanding of quantum spin liquids. A detailed exposition of these ideas would go beyond the scope of this work, we therefore refer the interested reader to the seminal works by Wen and co-workers [12, 17, 20, 150, 264, 268, 269].

In this context it is sufficient to understand the significance of the low-energy theories appearing in the PSG. Usually, these low-energy theories correspond to general quantum order as is the case for a spin liquid with a continuous invariant gauge group such as the algebraic spin liquid. But if the symmetry is broken, then the bulk can be gapped, leading to fractionalized excitations and thereby to topological order. A

possible mechanism for this is known as *string-net condensation* has been proposed by Levin and Wen [270, 271].

The emerging spin liquids are then classified according to their invariant gauge groups. The most prominent examples of which are discussed in the following.

Quantum spin liquid proposals

Based on various mean-field theories there are many proposals for spin liquid ground states on the kagome lattice. These ansätze have been classified using PSG leading to many different proposals with many symmetries. Here, we will concentrate on the main difference, i.e. the presence or absence of topological order. The key competitors for the ground state are the following:

- An **algebraic spin liquid**, also known as gapless or $U(1)$ spin liquid depending on the underlying low-energy theory [161, 162, 164, 165, 272]. This spin liquid's mean field ansatz is given by uniform hopping amplitudes, making it a fully symmetric spin liquid. While this spin liquid does not exhibit topological order, it can be identified by considering the long-range spin-spin or dimer-dimer correlation functions which are conjectured to decay with a power-law [165]. Based on this ansatz there were many projected wave function studies [161, 165, 223–226], examining the ground state properties, allowing a close comparison between unbiased data and the gapless spin liquid. Depending on the method used, these gapless spin liquids emerge as stable low-energy theories [223–226].
- A **chiral spin liquid**, which breaks time-reversal symmetry [27, 205, 207, 235, 237] due to massive fermions in the mean-field theory, making it a gapped ground state. While exact diagonalization studies failed to find conclusive evidence for a chiral theory [252], a chiral theory may be able to explain some of the features observed in numerical studies [207]. Since these theories possess an energy gap to the lowest excitations, they exhibit topological order [14, 205, 273].
- A variety of Z_2 **spin liquids**, all of which are gapped [155, 156, 180, 181, 229, 230, 255]. These theories are derived either from classical states such as the $\mathbf{q} = 0$ state [156] or various mean-field theories [161, 181, 257, 258]. The classification of the different proposals showed there were a number of spin liquids that were compatible with the system, while breaking some of the lattice symmetries. As gapped spin liquids on the kagome lattice, all Z_2 spin liquids exhibit topological order, which can be detected via the topological entanglement entropy, even though the underlying topological quantum field theory remains unknown.

3.1.4 Numerical results

Since analytical theories were not able to conclusively determine the ground state phase of the kagome lattice Heisenberg antiferromagnet, numerical studies tried to

explore the problem early on. But the exact structure of the KHAFM is very hard to determine precisely as very small energy differences may lead to very significant changes in the ground state structure.

This is exemplified by exact diagonalization (ED) studies which computed the ground state and the excitation spectrum for various system sizes without finding a conclusive answer [166, 169, 170, 188, 202, 215, 237, 252, 253]. While the classical $\sqrt{3} \times \sqrt{3}$ order was shown to be unstable early on [253], the fate of the energy gap remained entirely unclear, as ED studies found a continuum of singlet states in the spin gap. This failure of exact diagonalization opened the field wide to approximate methods such as Gutzwiller-projected quantum Monte Carlo, DMRG, PEPS, series expansion, contractor renormalization (CORE), and multi-scale entanglement renormalization ansatz (MERA). The results can be loosely grouped according to the different proposals:

- **Valence Bond Crystals:** After the failure of semi-classical approaches, valence bond crystals were shown to exhibit a very low energy [167, 185, 187, 216] as computed via series expansion by Singh and Huse. Earlier, a different VBC proposal was found to have a competitive energy by exact diagonalization of a reduced basis [274]. This finding was later independently confirmed by a MERA study that also found the 36-site VBC structure [56] although the validity of the MERA results was questioned, as the ansatz chosen was biased towards this ground state. Irrespective of these problems, a study employing quantum dimer models [191, 275] found a ground state resonating around a certain diamond VBC to be energetically competitive. Recently a quantum Monte Carlo study investigated the ground state phase diagram of Zn-paratacamite, a compound with a distorted kagome lattice, finding evidence for a VBC ground state [254].

The presence of a VBC ground state was disputed by a Gutzwiller-projected QMC study performed by Iqbal and coworkers [223, 224], where they investigated the stability of the gapless $U(1)$ Dirac spin liquid against dimerization into a VBC. While they found the $U(1)$ spin liquid to be stable against dimerization, the ground state energy computed within this ansatz was higher than the energy computed for the valence bond crystal, raising some questions about the validity of the $U(1)$ ansatz. But the biggest blow to this 36-site VBC proposal came by the large-scale DMRG study performed by Yan *et al* [100], who found a lower-energy ground state after destabilizing the valence bond crystal. Since in this study the authors deliberately biased their ansatz towards the VBC state, but still found a spin liquid using the essentially unbiased DMRG, the VBC was concluded to be unlikely. These findings were independently confirmed by our own results shown in the last section of this chapter.

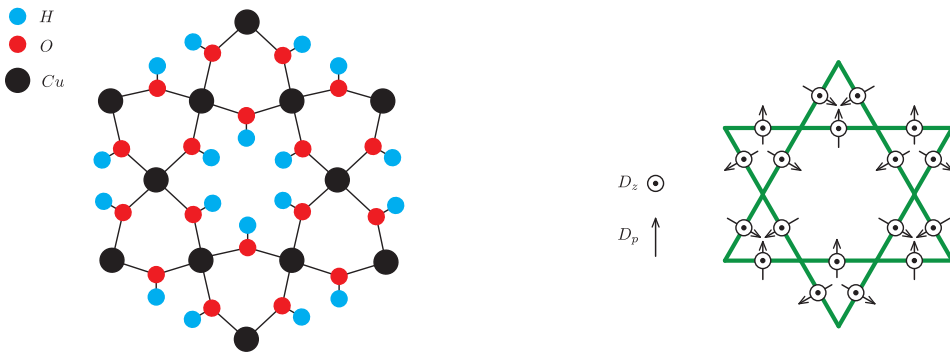
- **Gapless Spin Liquids:** Some of the most promising candidates for the ground state of the kagome lattice Heisenberg antiferromagnet are gapless quantum spin liquids, which exist in various flavors, among them the algebraic QSL, the $U(1)$ Dirac QSL, and the uniform RVB QSL [161, 164, 165, 194]. All of these states have the full symmetry of the Hamiltonian and appear naturally

as solutions in many slave-particle approaches. The gapless spin liquid has repeatedly been found to form a stable ground state phase within the framework of projected wave function studies [161, 165, 223–226]. In these publications, the gapless spin liquid was found to be stable against dimerization into a VBC [223, 224], stable against symmetry breaking into a gapped spin liquid [225, 226], and also energetically competitive. But apart from these Gutzwiller-projected QMC works, there is no data supporting the gapless spin liquid. In fact, there now exist various independent DMRG studies which find evidence against the gapless QSL, such as our own work.

- **Chiral Spin Liquids:** A projected wave function study found the chiral quantum spin liquid to be stable at mean-field level [27], but unstable upon inclusion of quantum fluctuations [225]. A different ansatz for a chiral quantum spin liquid known as the *cuboc1* phase was studied using mean-field theory without addition of quantum fluctuations. While this ansatz is able to reproduce and explain some of the features observed in exact diagonalization, this ansatz is contradicted by our data and the absence of significant chiral correlations in ED data [252]. The same is true for a recent contractor renormalization (CORE) study [276], which proposed the so-called *p6* chiral order. As for the *cuboc1* order proposed in Ref. [207], their data is incompatible with both our structure factors and the topological entanglement entropy [152].
- **Gapped Z_2 Spin Liquids:** A gapped Z_2 QSL was among the first proposals for the ground state of this system [156]. This proposal has now found support from many DMRG studies, which all find a spin gap [100, 220]. Additionally, there is some evidence for the gapped QSL phase to extend beyond the isotropic Heisenberg point [183, 277]. Our own work binds all this together, where by specifically looking for the type of the quantum spin liquid, we were able to show the presence of the gapped Z_2 spin liquid.

3.1.5 Experimental realizations

Theoretical interest in the spin-1/2 kagome HAF lessened for a while before increasing again in the last few years with computational advances and the discovery of several candidate materials that promised to realize the model experimentally [162, 278]. Chronologically, the first of these promising candidates was herbertsmithite $\text{ZnCu}_3(\text{OH})_6\text{Cl}_2$ [190, 200, 208, 238, 279–283]. For this mineral it has been shown that the spin-1/2 Cu^{2+} ions are antiferromagnetically coupled and lie on the corners of well separated and structurally undistorted kagome lattice planes, as sketched in Fig. 3.5(a). Even though the structure of the underlying kagome planes constituting this mineral appears to be perfect, the model is perturbed by a significant amount of disorder. This is likely caused by the mixing of the diamagnetic zinc ions and the spin-1/2 copper ions between the two types of sites. The effect of the disorder is the introduction of effectively three-dimensional coupling, i.e. it introduces a coupling between neighboring kagome planes. This interaction acts to destroy the



(a) The structure of the kagome planes in Herbertsmithite where the kagome planes are separated by zinc ions (not shown).

(b) The Dzyaloshinski-Moryia vector pattern of out-of-plane D_z and in-plane D_p components in Herbertsmithite.

Figure 3.5: Experimental realization of the kagome lattice Heisenberg antiferromagnet. On the left the structure of Herbertsmithite is sketched which suffers from Dzyaloshinski-Moryia interactions with a structure as shown on the right.

local two-dimensional nature of the system, giving rise to additional terms in the Hamiltonian in form of a Dzyaloshinskii-Moryia interaction [210, 284], as shown in Fig. 3.5(b). While herbertsmithite may be structurally perfect, the impurities together with the spin-orbit coupling have the effect of complicating the comparison of the unperturbed Heisenberg model with experiments on herbertsmithite. Following this realization, herbertsmithite lost part of its initial allure of being an almost perfect spin-1/2 kagome Heisenberg antiferromagnet.

More recently a new candidate for the role of the experimental realization of the isotropic kagome HAF was discovered. Kapellasite $\alpha\text{-Cu}_3\text{Zn}(\text{OH})_6\text{Cl}_2$ is another member of the atacamite family and a polymorph of herbertsmithite [221, 235, 242]. Even though both herbertsmithite and kapellasite share the same chemical composition, the kagome lattice structure is created in a different way in the two minerals. Caused by a different crystallographic structure, the kagome lattice in kapellasite is obtained by doping. In kapellasite, the spin-1/2 Cu^{2+} ions form a regular triangular sublattice, which by doping with diamagnetic Zn^{2+} ions can be diluted to form a kagome lattice, as opposed to herbertsmithite, where a three-dimensional pyrochlore lattice has to be doped to form a kagome lattice. The difference in doping is conjectured to reduce the interlayer coupling, as the mixing of copper and zinc sites will only lead to intralayer disorder.

But while kapellasite may feature less or no spin-orbit coupling, a recent theoretical electronic study employing density functional theory within the local density approximation revealed appreciable non-nearest-neighbor exchange coupling both for kapellasite and its relative haydeite, $\text{Cu}_3\text{Mg}(\text{OH})_6\text{Cl}_2$ [285, 286]. This is shown to introduce further-neighbor coupling, especially across the diagonals of the hexagons on the kagome lattice. Also, a recent high-temperature series expansion considered kapellasite and performed fits to the DC magnetic susceptibility $\chi_{DC}(T)$ measured

in experiment. These fits agree best with a ferromagnetic nearest-neighbor exchange interaction on the kagome planes (i.e. $J_1 < 0$), while the overall antiferromagnetic behavior of the mineral is explained by large antiferromagnetic couplings to farther neighbors. [235, 242].

Apart from spatially isotropic kagome lattices, there are some materials with anisotropic versions of the kagome lattice where the spin-1/2 HAF has been suggested to occur [34, 287, 288]. Prominent among those are the minerals vorborthite, $\text{Cu}_3\text{V}_2\text{O}_7(\text{OH})_2 \cdot 2\text{H}_2\text{O}$ and vesignieite [175, 178, 196, 289], $\text{BaCu}_3(\text{VO}_4)_2(\text{OH})_2$. Small differences in the bond lengths between the three copper ions forming triangles result in inequivalent Cu sites. This in turn leads to the splitting of the interaction J into two different interactions J and J' , making the description of the system harder.

The identification of the ground state phase is further hampered by the different ground states being extremely close together in energy [290]. Even small perturbations can therefore cause huge difference in ground state structure. These problems can be caused by Dzialoshinski-Moriya interactions or impurities in experimental samples, destroying the order known from numerical and analytical studies.

3.2 Methodology

Employing the DMRG, an essentially one-dimensional method, to perform a ground state search for a two-dimensional system is plagued by many problems. Some of the issues arising when using DMRG in two dimensions have been covered in Chap. 2.8. Here we will address the details of simulating large kagome cylinders within the framework of the $SU(2)$ -symmetric DMRG.

3.2.1 Mapping the lattice

In order to obtain the ground state of any system with DMRG we first have to model the system. While this is straightforward for one-dimensional systems, there are some points to consider in higher dimensions (see also Chap. 2.8). Here we employed a variety of different mappings to ensure the results were independent of the specific mapping chosen. For the kagome lattice, there are two main mappings, depending on the lattice axis we chose to align to, dubbed XC and YC respectively [100]. A further mapping was used to simulate torus systems. All of these paths are displayed in Fig. 3.6. The paths were chosen in such a way that the resulting lattice was symmetric under reflection at the center. Furthermore the lattices were constructed with edges of a form that was smooth and reconcilable with many of the valence bond crystal proposals.

3.2.2 Simulation details

The simulations themselves were performed as for any other DMRG calculations, that is we started with an ansatz state with a small bond dimension m and then started

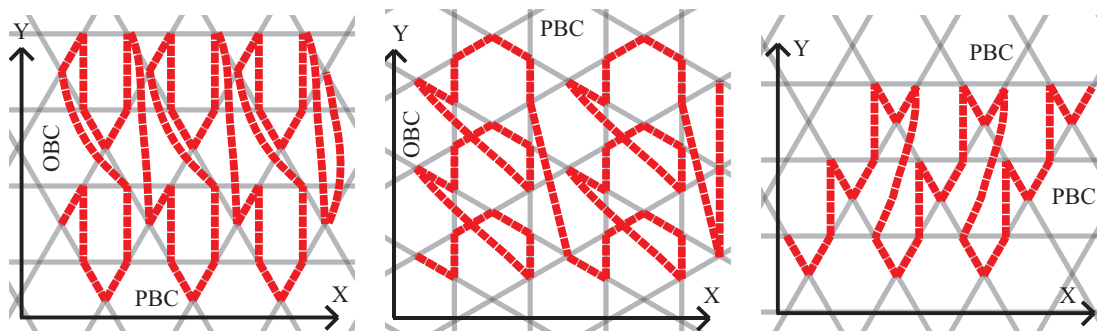


Figure 3.6: Sketches of the mappings of the two-dimensional kagome lattices to one-dimensional chains. We mapped the cylinders using two different mappings, one for aligning the lattice to the X-axis (a) and one for aligning it to the Y-axis (b) with periodic (open) boundary conditions in the vertical (horizontal) direction. A different path was chosen for a torus (c), where we used periodic boundary conditions in both directions. The red broad line represents the one-dimensional chain.

increasing the bond dimension iteratively while sweeping the system. Whereas conventional implementations have to resort to pinning fields to ensure smooth convergence, the $SU(2)$ symmetry significantly eases this calculation by not having to employ any tricks, special sweeping schemes, or pinning fields. While sweeping it is important to keep track of the truncation error and the change in energy as well as the mixing factor α (see also Chap. 2.8). In the beginning, a small mixing factor serves to keep the single-site algorithm from getting stuck, but at some point it has to be decreased to improve the accuracy of the simulation. One major advantage of the $SU(2)$ -symmetric implementation employed for this simulation is the ability to directly target specific sectors of the total spin, thus enabling us to perform the simulations in both the spin $S = 0$ and the spin $S = 1$ sector enabling us to compute the spin gap later on. Once the simulations had reached the limit of the computational capabilities available to us, the raw data served as the basis for extrapolations. A standard DMRG technique is the extrapolation of the energy in the truncation error with a linear fit. But for the single-site algorithm the truncation error directly depends on the choice of mixing factor. Therefore α has to be kept constant for the last few sweeps to make the extrapolation well defined and controlled.

The extrapolation in the truncation error yields an estimate for the ground state energy of a specific cylinder with a specific aspect ratio. To obtain an estimate for the bulk energy of an infinite cylinder, we used the subtraction method detailed in Ref. [96]. The subtraction method is based on the assumption that boundary effects are identical for short and for long cylinders, therefore enabling us to remove them by subtracting a small cylinder from a large cylinder. If the assumption holds, we thus obtain the bulk energy.

3.2.3 Entanglement entropy

How can you identify something if you only know what it is not? As quantum spin liquids are defined by the absence of any local order parameter they are extremely hard to characterize. Topological order can not be detected by simple local measurements, but for two-dimensional quantum spin liquids, the degeneracy of the ground state of the system is linked to the topological genus of the surface on which the QSL lives [11, 28, 291]. Of particular usefulness has been the influx of new ideas from quantum information theory to the physics of strongly correlated systems, namely the entanglement entropy [149–152, 265, 292–294]. This usefulness is based on the long-range entanglement that causes topological order, as opposed to the short-range entanglement associated with conventional order [14]. The heuristic picture of a long-range entangled phase is that it cannot be written as a direct product state, albeit this is possible for most conventionally ordered phases [18, 295–299]. From this follows that gapless phases, such as a superfluid or Fermi liquid that exhibit algebraic decay of correlations will imply long-range entanglement in real space. The converse does not hold though, as even phases with short-range correlations, such as gapped spin liquids, can still support long-range entanglement.

Formally, this can be shown using the entanglement entropy, defined as

$$\mathcal{S}_A = -\text{Tr}_B \rho_A \log \rho_A \quad (3.4)$$

i.e. the von Neumann entropy \mathcal{S}_A obtained by tracing out the subsystem B . As mentioned in Chap. 2, the entanglement entropy of gapped systems has been shown to obey an area law, but in recent years, Levin and Wen [264] and Kitaev and Preskill [263] showed in their seminal papers that the entanglement entropy of a topologically ordered phase such as a gapped spin liquid contains a universal sub-leading correction:

$$\mathcal{S}(L) = cL - \gamma + \mathcal{O}\left(\frac{1}{L}\right). \quad (3.5)$$

This universal correction γ is known as the *topological entanglement entropy* $\mathcal{S}_{\text{topo}}$. The topological entanglement entropy is non-zero if and only if the system has topological order. Furthermore, γ serves to partially characterize the topological order as it is related to the total quantum dimension of the underlying topological field theory via $\mathcal{S}_{\text{topo}} = -\log(D)$. Here, D is the total quantum dimension associated with the phase of matter and given by $D = \sqrt{\sum_i d_i^2}$ where d_i is the individual quantum dimension of the i -th quasi-particle.

While $\mathcal{S}_{\text{topo}}$ can serve as a positive identification of topological order, two complications arise:

1. Is it a unique characterization of the topological state?
2. Does this hold for any of the degenerate topological ground states of the Hamiltonian?

The first question has to be negated, as there may be more than one topological theory with the same total quantum dimension. For example, for Kitaev’s toric code

model, there are four quasi-particles, each with the individual quantum dimension one, yielding a total quantum dimension of $D = \sqrt{4} = 2$. The same quantum dimension results from a doubled semionic theory though or an Ising-type theory where there are only three types of quasi-particles. A more detailed characterization can be achieved by computing the braiding and exchange statistics for the topological excitations, which has recently been demonstrated in the context of iDMRG [300].

The second question is more subtle. It has been shown that equation 3.5 holds for the minimally entangled basis states of the system, but there still remains the question of how to obtain those minimally entangled states (MES), as any linear combination of two degenerate eigenstates is still an eigenstate. Here, a built-in bias of DMRG towards minimum-entropy states serves to eliminate this complication as DMRG will always try to minimize the entanglement carried by the wave function.

DMRG now gives us direct access to the topological entanglement entropy, because at every optimization step the system is bipartitioned into two subsystems. By evaluating only those splittings of the wave function that are also bipartitions of the cylinders we can compute $\mathcal{S}(L)$ for various cylinder circumferences L . While this is possible, a better scheme involves a generalization of the von Neumann entropy, namely the Renyi entropies, defined as

$$S_n = \frac{1}{1-n} \log(\text{Tr}_B \rho_A^n). \quad (3.6)$$

It has been shown that the same topological entanglement entropy results from the Renyi entropies as from the von Neumann entropy [301]. The advantage of the Renyi entropies lies in the fact that numerical errors tend to be suppressed in the Renyi entropies. While DMRG is very good at calculating the largest eigenvalues of the reduced density matrix, its precision for the smallest eigenvalues is limited both by numerical rounding errors and by the convergence of the wave function. Therefore it would be advantageous to give more weight to the large eigenvalues and less weight to the smaller eigenvalues, which is exactly what the Renyi entropies do. In our numerical simulations we have observed a much improved convergence behavior already for Renyi indices $n \simeq 3$.

3.3 Nature of the Spin Liquid Ground State of the $S = 1/2$ Kagome Heisenberg Model

In the previous sections we have presented the antiferromagnetic Heisenberg model on the kagome lattice and introduced a way to use DMRG to study the problem. We have shown the model to be of much current interest, both because of the many exotic proposals for its ground state and because the model, even after more than 20 years of research being still unsolved. In this section we present our work on this model system. We employed the DMRG to obtain the ground state for cylinders of an unprecedented size both in the spin $S = 0$ and $S = 1$ sectors. This computation of the spin gap was followed by a thorough and complete investigation of the ground state properties, finding no sign of a local order parameter. Meanwhile we found short-ranged correlation functions for spin-spin, dimer-dimer, and chiral-chiral correlations as well as a diffuse static structure factor. With this characterization of the ground state we continued to employ a new and untested tool, the analysis of the entanglement entropy, to gain further understanding of the ground state. We find all of these results to be compatible with only one particular proposal for the ground state, namely the gapped topological Z_2 spin liquid.

Our study is therefore an independent confirmation of earlier DMRG results for tori [220] and cylinders [100], which arrived at the same conclusion. At the same time it improves on their results by yielding better energy estimates while also considering larger systems. By making use of the $SU(2)$ symmetry it was also possible for us to obtain wave functions with a significantly higher precision, enabling us to evaluate new observables, making our study the logical extension of the earlier DMRG studies. These results agree well with data from state-of-the-art exact diagonalization [214], but fail to rule out certain other proposals. On the one hand, there are proposals for chiral spin liquids [207, 276], which may escape us due to symmetry constraints. On the other hand, there is some evidence for $U(1)$ gapless spin liquids being very close in energy [223–226]. Nevertheless our study provides a very complete picture of this problem, arriving at a Z_2 quantum spin liquid.

Nature of the Spin-Liquid Ground State of the $S = 1/2$ Heisenberg Model on the Kagome Lattice

Stefan Depenbrock,^{1,*} Ian P. McCulloch,² and Ulrich Schollwöck¹

¹*Department of Physics and Arnold Sommerfeld Center for Theoretical Physics,
Ludwig-Maximilians-Universität München, 80333 München, Germany*

²*Centre for Engineered Quantum Systems, School of Mathematics and Physics, The University of Queensland,
St. Lucia, Queensland 4072, Australia*

(Received 22 May 2012; published 7 August 2012)

We perform a density-matrix renormalization group (DMRG) study of the $S = 1/2$ Heisenberg antiferromagnet on the kagome lattice to identify the conjectured spin liquid ground state. Exploiting SU(2) spin symmetry, which allows us to keep up to 16 000 DMRG states, we consider cylinders with circumferences up to 17 lattice spacings and find a spin liquid ground state with an estimated per site energy of $-0.4386(5)$, a spin gap of $0.13(1)$, very short—range decay in spin, dimer and chiral correlation functions, and finite topological entanglement γ consistent with $\gamma = \log_2 2$, ruling out gapless, chiral, or nontopological spin liquids in favor of a topological spin liquid of quantum dimension 2, with strong evidence for a gapped topological \mathbb{Z}_2 spin liquid.

DOI: 10.1103/PhysRevLett.109.067201

PACS numbers: 75.10.Jm, 75.40.Mg

A pervasive feature of physics is the presence of symmetries and their breaking at low energies and temperatures. It would be an unusual system in which at $T = 0$ (quantum) fluctuations are so strong that all symmetries remain unbroken in the ground state. In magnetic systems, such a state is dubbed a quantum spin liquid (QSL)[1] and is most likely to occur if fluctuations are maximized by low-dimension, low-spin, and strong geometrical frustration; the search for a QSL has thus focused on frustrated $S = 1/2$ quantum magnets in two dimensions. The Heisenberg antiferromagnet on the kagome lattice [2] (KAFM) is a key candidate, described by the $S = 1/2$ model

$$\mathcal{H} = \sum_{\langle i,j \rangle} \vec{S}_i \cdot \vec{S}_j, \quad (1)$$

with $\langle i, j \rangle$ nearest neighbors.

Experimentally, the focus is on the herbertsmithite $\text{ZnCu}_3(\text{OH})_6\text{Cl}_2$, modeled by Eq. (1) on a kagome lattice with additional Dzyaloshinskii-Moriya interactions [3]. It is thought that the ground-state is a spin liquid [4–10], with no onsite magnetization [6,11] and no spin gap [11–14] within very tight experimental bounds.

On the theoretical side, the kagome model of Eq. (1) remains a formidable challenge. While all proposed ground states show no magnetic ordering, they can be classified by whether they break translational invariance or not. The former type of ground state, a valence bond crystal (VBC), was pioneered by Marston [15]. The emerging proposal was that of a “honeycomb VBC” (HVBC) with a hexagonal unit cell of 36 spins [16–20] sharing in dimer-covered hexagons and a sixfold “pin wheel” at the center. On the other hand, a multitude of QSL states were proposed [21–32]. Proposals for a QSL ground state include a chiral topological spin liquid [21,22,33,34], a

gapless spin liquid [23–26], and various \mathbb{Z}_2 spin liquids [27–30] with topological ground-state degeneracy.

In the past, numerical methods failed to resolve the issue conclusively. Quantum Monte Carlo calculations face the sign problem. Sizes accessible by exact diagonalization [2,35–48] are currently limited to 48. Other approaches diagonalized the valence bond basis or applied the contractor renormalization group (CORE) method, or the coupled cluster method (CCM) [49–55]. The multiscale entanglement renormalization ansatz (MERA) [56] found the VBC state lower in energy than the QSL state reported in an earlier density-matrix renormalization group (DMRG) study of tori up to 120 sites [31].

Recently, strong evidence for a QSL was found in a large-scale DMRG study [57] considering long cylinders of circumference up to 12 lattice spacings. Ground-state energies were substantially lower than those of the VBC state, and an upper energy bound substantially below the VBC-state energy was found; the ground state, having the hallmarks of a QSL, was not susceptible to attempts to enforce a VBC state. As to the type of QSL, Ref. [57] did not provide direct evidence for a \mathbb{Z}_2 topological QSL. This has sparked a series of papers trying to identify the QSL [21,24,32,54,58], where again chiral spin liquids and gapless U(1) spin liquids were advocated and a classification of \mathbb{Z}_2 spin liquids achieved. At the moment, the issue is not conclusive.

Here we study the KAFM using DMRG [59–61], in the spirit of Ref. [57]. DMRG is a variational method in the ansatz space spanned by matrix product states, which allows it to find the ground state of one-dimensional (1D) systems efficiently even for large system sizes. It can also be applied successfully to two-dimensional (2D) lattices by mapping the short-ranged 2D Hamiltonian exactly to a long-ranged 1D Hamiltonian [57,62–66]. DMRG cost

scales roughly exponentially with entanglement entropy, such that area laws limit system sizes, and DMRG favors open boundary conditions (OBCs) over preferable periodic boundary conditions (PBCs). The conventional compromise [57], taken also by us, is to consider cylinders, i.e., PBCs along the short direction (circumference c) and OBCs along the long direction (length L), where boundary effects are less important. Cost is dominated exponentially by circumference c . We use two different 1D mappings (labeled as XC and YC plus cylinder size) (see Supplemental Material [67]) to check for undesired mapping dependencies of the DMRG results. Instead of earlier Abelian U(1) DMRG with up to 8000 ansatz states, we employ non-Abelian SU(2) DMRG [68,69] based on irreducible representations corresponding to 16 000 ansatz states in a U(1) approach. This has crucial advantages: available results can be verified with much higher accuracy. The circumference of the cylinders can be increased by almost 50% from 12 to 17.3 lattice sites (up to 726 sites in total), strongly reducing finite size effects; we also consider tori of up to 108 sites. We can eliminate the spin degeneracy that necessitates pinning fields in U(1)-symmetric simulations and avoid artificial constraints in gap calculations, making them more accurate and reliable. We also present results on spin, dimer, and chiral correlation functions, the structure factor, and topological entanglement entropy. All data agree with a gapped nonchiral \mathbb{Z}_2 spin liquid; other QSL proposals for the KAFM are inconsistent with at least one of the numerical results.

Energies.—Energies for cylinders of fixed c and L are extrapolated in the truncation error of single-site DMRG [70]; bulk energies per site are extracted by a subtraction technique [66] and extrapolated to $L \rightarrow \infty$. Results for various 1D mappings and c are displayed in Table I. We also show the spin (triplet) gap to the $S = 1$ spin sector. We confirm and extend earlier results [57]. At 16 000 states, DMRG is highly accurate; negligible changes in energy for

TABLE I. Ground-state energy per site (E/N) and gaps for $L = \infty$ cylinders (circumference c). Errors are from extrapolation; comparisons are with Ref. [57] except for the tori.

c	E/N	gap Δ_E	E_{earlier}	$\Delta_{E,\text{earlier}}$	
YC4	4	-0.446 77	0.2189	-0.4467	
YC6	6	-0.439 15(5)	0.1396(6)	-0.439 14	0.142(1)
YC8	8	-0.438 38(5)	0.135(3)	-0.438 36(2)	0.156(2)
YC10	10	-0.4378(2)		-0.4378(2)	0.070(15)
YC12	12	-0.4386(4)		-0.4379(3)	
XC8	6.9	-0.438 26(4)	0.13899(1)	-0.438 24(2)	0.1540(6)
XC12	10.4	-0.438 29(7)	0.134(4)	-0.4380(3)	0.125(9)
XC16	13.9	-0.4391(3)	0.130(7)		
XC20	17.3	-0.4388(8)			
Torus	3	-0.436 278	0.2687	-0.436 278	0.2687 [47]
Torus	4	-0.4383(2)	0.151	-0.435 91	0.140 [31]
Torus	6	-0.4383(3)	0.1148(1)	-0.431 11	0.105 [31]

substantially larger c confirm that the thermodynamic limit energy is found, which we place at $-0.4386(5)$ (Fig. 1). Similar to Ref. [57], we find the energy to be significantly below that of VBC states and no trace of a VBC in the correlation patterns. Except for the edges, bond energies are fully translationally invariant. All results are consistent with strict variational upper bounds obtained without extrapolations from independent DMRG calculations for infinitely long cylinders using the iDMRG variant [71], which are below the VBC energies.

On the issue of a spin (triplet) gap [45,72], Yan *et al.* [57] argue in favor of a small but finite spin gap. SU(2) DMRG computes the $S = 1$ state directly and more efficiently; boundary excitations are excluded by examining local bond energies. We find the spin gap (Table I and Fig. 2) to remain finite also for cylinders of large c . Whereas the results for small c agree with the $S = 1$ state energies and gaps reported in Ref. [57], they display significant differences for larger c , perhaps due to the more complex earlier calculation scheme. SU(2)-invariant results evolve more smoothly with c , allowing a tentative extrapolation to a spin gap $\Delta_E = 0.13(1)$ in the thermodynamic limit. Size dependence is small, in line with very short correlation lengths. The finite spin gap contradicts conjectures of a U(1) or other gapless spin liquids. For the calculation of the singlet gap found to be finite in Ref. [57], SU(2) DMRG does not offer a significant advantage to be reported here.

Correlation functions.—For all cylinders, we find an antiferromagnetic spin-spin correlation function $\langle \vec{S}_i \cdot \vec{S}_j \rangle$ along different lattice axes with almost no directional dependence. Exponential fits with a very short correlation length of $\xi \simeq 1$ [Fig. 4(a)] were consistently better than power law fits, in agreement with a spin gap. This is not consistent with an algebraic spin liquid [23], where the correlations are predicted to decay according to a power law $\sim \frac{1}{x^4}$.

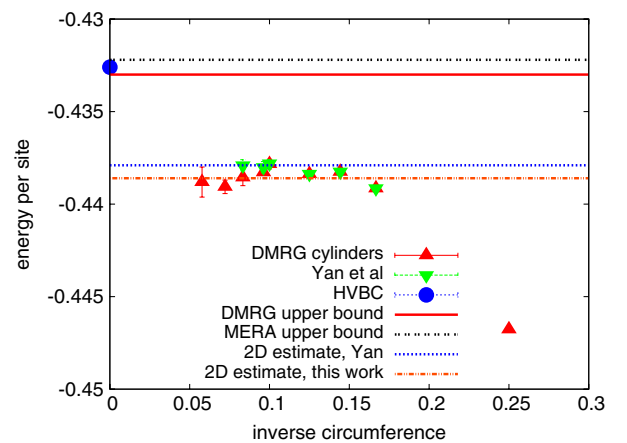


FIG. 1 (color online). Bulk energies per site. Lengths are in units of lattice spacings. The HVBC result [18,19] and the upper bounds of MERA [56] and DMRG [57] apply directly to the thermodynamic limit; 2D estimates are extrapolations.

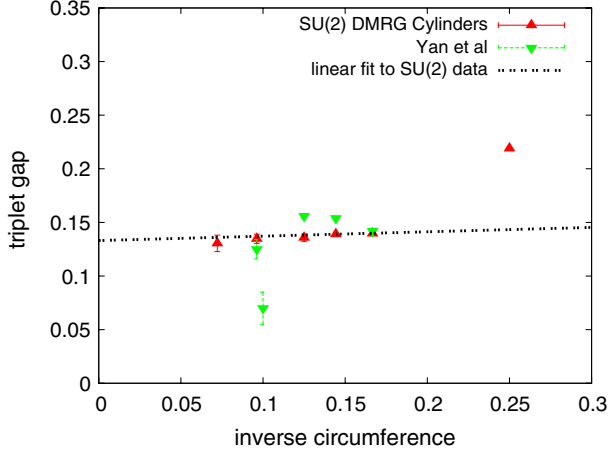


FIG. 2 (color online). Plot of the bulk triplet gap for infinitely long cylinders versus the inverse circumference c in units of inverse lattice spacings with an empirical linear fit to the largest cylinders, leading to a spin gap estimate of $0.13(1)$.

We also consider the static spin structure factor $S(\vec{q}) = \frac{1}{N} \sum_{ij} e^{i\vec{q} \cdot (\vec{r}_i - \vec{r}_j)} \langle \vec{S}_i \cdot \vec{S}_j \rangle$, \vec{q} in units of basis vectors (\vec{b}_1, \vec{b}_2) of the reciprocal lattice. The spectral weight is concentrated evenly around the edge of the extended Brillouin zone, with not very pronounced maxima on the corners of the hexagon (Fig. 3). Results for large cylinders agree well with ED results for tori up to 36 sites [44]. All our $S(\vec{q})$ are in accordance with the prediction for a \mathbb{Z}_2 QSL [27].

We also find antiferromagnetically decaying, almost direction-independent dimer-dimer correlations, for which, again, an exponential fit is favored [Fig. 4(b)], in agreement with a singlet gap. Our data do not support the algebraic decay predicted [23] for an algebraic QSL.

Chiral correlation functions [40] $\langle C_{ijk} C_{lmn} \rangle = \langle \vec{S}_i \cdot (\vec{S}_j \times \vec{S}_k) \cdot \vec{S}_l \cdot (\vec{S}_m \times \vec{S}_n) \rangle$, where the loops considered are elementary triangles, did not show significant correlations for any distance or direction and decay exponentially (Fig. 5), faster than the spin-spin correlations. Expectation values of single loop operators C_{ijk} vanish, as expected for finite size lattices. Chiral correlators for other loop types and sizes decay even faster. Our findings do not support chiral spin liquid proposals [21,22,34].

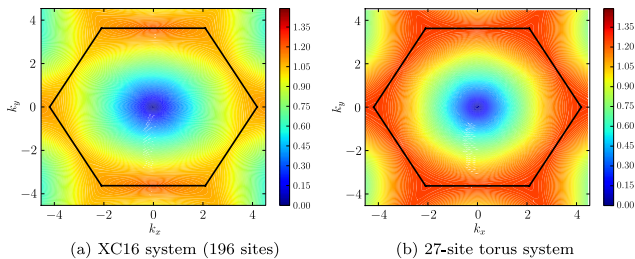


FIG. 3 (color online). Two static structure factors $S(\vec{q})$; k_x, k_y in units of reciprocal lattice basis vectors. Results are independent of the choice of 1D mapping (not shown).

Topological entanglement entropy.—To obtain direct evidence regarding a topological state, we consider the topological entanglement entropy [73–75]. For the ground states of gapped, short-ranged Hamiltonians in 2D, entanglement entropy scales as $\mathcal{S} \simeq c$, if we cut cylinders into two, with corrections in the case of topological ground states [76]. We examine Renyi entropies $\mathcal{S}_\alpha = (1 - \alpha)^{-1} \log_2 \text{tr} \rho^\alpha$, $0 \leq \alpha < \infty$, where ρ is a subsystem density matrix. Scaling is expected as $\mathcal{S}_\alpha \simeq \eta c - \gamma$, where η is an α -dependent constant. γ , the topological entanglement entropy, is independent of α [77–79] and depends only on the total quantum dimension D as $\gamma = \log_2(D)$ [73,74]. In our mappings, DMRG gives direct access to density matrices of cylinder slices. We calculate \mathcal{S}_α for cylinders of fixed c and extrapolate in L^{-1} to $L \rightarrow \infty$; a linear extrapolation in $c \rightarrow 0$ yields γ . Results are 1D mapping independent. We show intermediate values of α (Fig. 6), which all show a clearly finite value of γ , with a value very consistent with $\gamma = 1$; large- α results agree. Small- α results are unreliable, as DMRG does not capture the tail

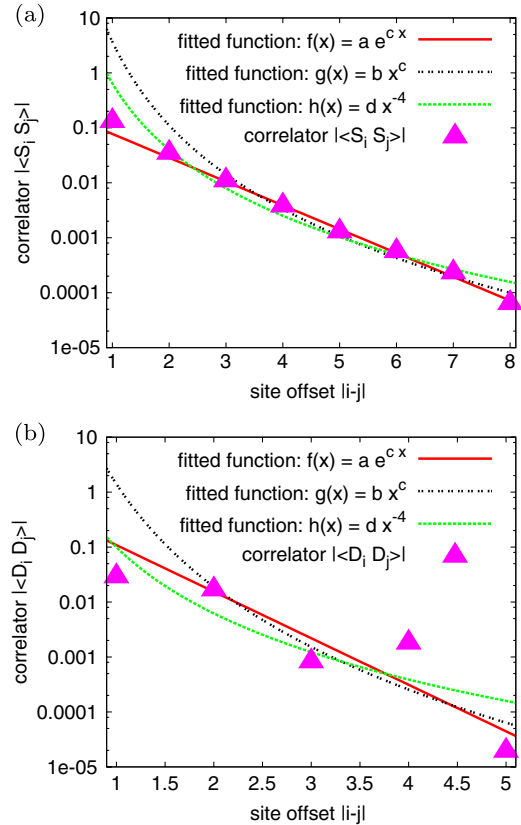


FIG. 4 (color online). Log-linear plots of the absolute value of the Fig. 4(a) spin-spin and Fig. 4(b) dimer-dimer correlation functions versus the distance $x = |i - j|$ for a XC12 [Fig. 4(a)] and a YC8 [Fig. 4(b)] sample along one lattice axis with exponential and power law fits. An x^{-4} line is shown as a guide to the eye.

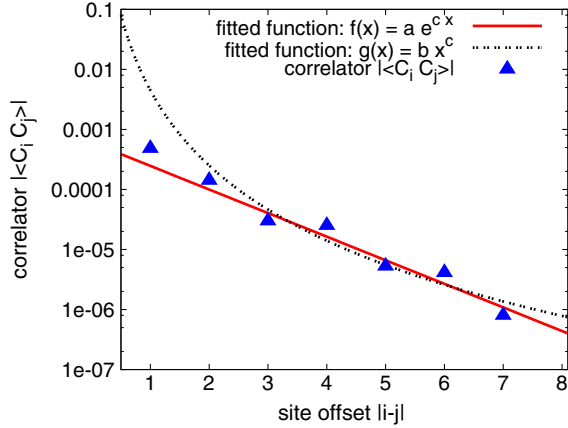


FIG. 5 (color online). Log-linear plot of the absolute value of the chiral correlation function $\langle C_0, C_x \rangle = \langle S_{i_0} \cdot (S_{j_0} \times S_{k_0}) \cdot S_{i_x} \cdot (S_{j_x} \times S_{k_x}) \rangle$ versus the distance $x = |\Delta_0 - \Delta_x|$ along a lattice axis for a 196-site YC8 sample with exponential and power law fits.

of the spectrum of ρ properly, but also point to a finite value of γ , and hence a topological ground state. The quantum dimension is $D = 2$, excluding chiral spin liquids ($\gamma = 1/2$ or $D = \sqrt{2}$ [77]). Rigorously, DMRG only provides a lower bound on D [80], but the bound is essentially exact as DMRG is a method with low entanglement bias [81].

Conclusion.—Through a combination of a large number of DMRG states, large samples with small finite size effect, and the use of the SU(2) symmetry of the kagome model, we have been able to corroborate earlier evidence for a QSL as opposed to a VBC, due to energetic considerations and complete absence of breaking of space group invariance, although DMRG should be biased towards VBC due to its low-entanglement nature and the use of OBC. On the basis of the numerical evidence (spin gap, structure factor, spin, dimer and chiral correlations, topological entanglement entropy) numerous QSL proposals can be ruled out for the kagome system. On the system sizes reached, the spin gap is

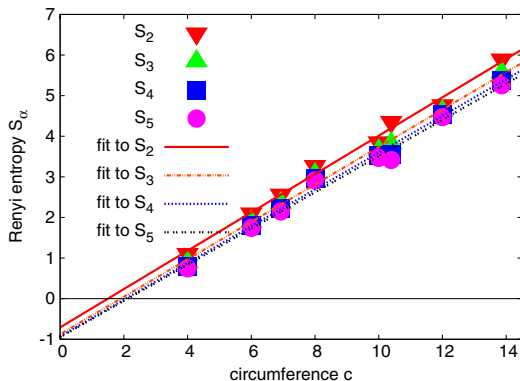


FIG. 6 (color online). Renyi entropies S_α of infinitely long cylinders for various α versus circumference c , extrapolated to $c = 0$. The negative intercept is the topological entanglement entropy γ .

very robust and essentially size independent, ruling out all proposals for gapless spin liquids, consistent with the exponential decay of correlators. Individual gapless QSL proposals make other predictions not supported by numerical data, e.g., the static spin structure factor [23]. Another strong observation is the very rapid decay of chiral correlations, ruling out proposals related to chiral QSL. The third strong observation is finite topological entanglement, which implies a topologically degenerate ground state for the kagome system. For quantum dimension 2, as found here, we have in principle, for a time-reversal invariant ground state, a choice between a \mathbb{Z}_2 phase and a double-semion phase [82,83]. A \mathbb{Z}_2 QSL emerges straightforwardly in effective field theories of the kagome model as a mean-field phase stable under quantum fluctuations, breaking a U(1) gauge symmetry down to \mathbb{Z}_2 due to a Higgs mechanism [84], and, microscopically, a resonating valence bond state formed from nearest-neighbor Rokhsar-Kivelson dimer coverings of the kagome lattice directly leads to a \mathbb{Z}_2 QSL [85,86] albeit for a variational energy far from the ground-state energy. The concentration of weight of the structure factor at the hexagonal Brillouin zone edge with shallow maxima at the corners would also point to the \mathbb{Z}_2 QSL as proposed by Sachdev [27], and a \mathbb{Z}_2 QSL is also consistent with all other numerical findings. All this provides strong evidence for the \mathbb{Z}_2 QSL, whereas to our knowledge, no plausible scenario for the emergence of a double-semion phase in the KAFM has been discovered so far, making it implausible, but of course not impossible. An analysis of the degenerate ground-state manifold as proposed in Ref. [80], not possible with our data, would settle the issue. Even if the answer provided final evidence for a \mathbb{Z}_2 QSL, many questions regarding the detailed microscopic structure of the ground-state wave functions and the precise nature of the \mathbb{Z}_2 QSL would remain for future research.

S. D. and U. S. thank F. Essler, A. Läuchli, C. Lhuillier, D. Poilblanc, S. Sachdev, R. Thomale, and S. R. White for discussions. S. D. and U. S. acknowledge support by DFG. U. S. thanks the GGI, Florence, for its hospitality. I. P. M. acknowledges support from the Australian Research Council Centre of Excellence for Engineered Quantum Systems and the Discovery Projects funding scheme (Project No. DP1092513).

Note added.—Recently, we became aware of Ref. [81], which calculates topological entanglement entropy from von Neumann entropy for a next-nearest neighbor modification of the KAFM, perfectly consistent with our results of $D = 2$ for the KAFM itself.

*stefan.depenbrock@lmu.de

- [1] L. Balents, *Nature (London)* **464**, 199 (2010).
- [2] V. Elser, *Phys. Rev. Lett.* **62**, 2405 (1989).
- [3] K. Matan *et al.*, *Phys. Rev. B* **83**, 214406 (2011).

- [4] A. Olariu, P. Mendels, F. Bert, F. Duc, J. C. Trombe, M. A. de Vries, and A. Harrison, *Phys. Rev. Lett.* **100**, 087202 (2008).
- [5] F. Bert, S. Nakamae, F. Ladieu, D. L'Hôte, P. Bonville, F. Duc, J.-C. Trombe, and P. Mendels, *Phys. Rev. B* **76**, 132411 (2007).
- [6] P. Mendels, F. Bert, M. A. de Vries, A. Olariu, A. Harrison, F. Duc, J. C. Trombe, J. S. Lord, A. Amato, and C. Baines, *Phys. Rev. Lett.* **98**, 077204 (2007).
- [7] T. Imai, E. A. Nytko, B. M. Bartlett, M. P. Shores, and D. G. Nocera, *Phys. Rev. Lett.* **100**, 077203 (2008).
- [8] S.-H. Lee, H. Kikuchi, Y. Qiu, B. Lake, Q. Huang, K. Habicht, and K. Kiefer, *Nature Mater.* **6**, 853 (2007).
- [9] M. A. de Vries, K. V. Kamanev, W. A. Kockelmann, J. Sanchez-Benitez, and A. Harrison, *Phys. Rev. Lett.* **100**, 157205 (2008).
- [10] P. Mendels and F. Bert, *J. Phys. Conf. Ser.* **320**, 012004 (2011).
- [11] J. S. Helton *et al.*, *Phys. Rev. Lett.* **98**, 107204 (2007).
- [12] T. Imai, M. Fu, T. H. Han, and Y. S. Lee, *Phys. Rev. B* **84**, 020411 (2011).
- [13] M. Jeong, F. Bert, P. Mendels, F. Duc, J. C. Trombe, M. A. de Vries, and A. Harrison, *Phys. Rev. Lett.* **107**, 237201 (2011).
- [14] D. Wulferding, P. Lemmens, P. Scheib, J. Röder, P. Mendels, S. Chu, T. Han, and Y. S. Lee, *Phys. Rev. B* **82**, 144412 (2010).
- [15] J. B. Marston and C. Zeng, *J. Appl. Phys.* **69**, 5962 (1991).
- [16] M. B. Hastings, *Phys. Rev. B* **63**, 014413 (2000).
- [17] P. Nikolic and T. Senthil, *Phys. Rev. B* **68**, 214415 (2003).
- [18] R. R. P. Singh and D. A. Huse, *Phys. Rev. B* **76**, 180407 (2007).
- [19] R. R. P. Singh and D. A. Huse, *Phys. Rev. B* **77**, 144415 (2008).
- [20] Y. Iqbal, F. Becca, and D. Poilblanc, *Phys. Rev. B* **83**, 100404 (2011).
- [21] L. Messio, B. Bernu, and C. Lhuillier, *Phys. Rev. Lett.* **108**, 207204 (2012).
- [22] K. Yang, L. K. Warman, and S. M. Girvin, *Phys. Rev. Lett.* **70**, 2641 (1993).
- [23] M. Hermele, Y. Ran, P. A. Lee, and X. G. Wen, *Phys. Rev. B* **77**, 224413 (2008).
- [24] Y. Iqbal, F. Becca, and D. Poilblanc, *Phys. Rev. B* **84**, 020407 (2011).
- [25] Y. Ran, M. Hermele, P. A. Lee, and X. G. Wen, *Phys. Rev. Lett.* **98**, 117205 (2007).
- [26] S. Ryu, O. I. Motrunich, J. Alicea, and M. P. A. Fisher, *Phys. Rev. B* **75**, 184406 (2007).
- [27] S. Sachdev, *Phys. Rev. B* **45**, 12377 (1992).
- [28] F. Wang and A. Vishwanath, *Phys. Rev. B* **74**, 174423 (2006).
- [29] Y. M. Lu, Y. Ran, and P. A. Lee, *Phys. Rev. B* **83**, 224413 (2011).
- [30] G. Misguich, D. Serban, and V. Pasquier, *Phys. Rev. Lett.* **89**, 137202 (2002).
- [31] H. C. Jiang, Z. Y. Weng, and D. N. Sheng, *Phys. Rev. Lett.* **101**, 117203 (2008).
- [32] Y. Huh, M. Punk, and S. Sachdev, *Phys. Rev. B* **84**, 094419 (2011).
- [33] V. Kalmeyer and R. B. Laughlin, *Phys. Rev. B* **39**, 11879 (1989).
- [34] X. G. Wen, F. Wilczek, and A. Zee, *Phys. Rev. B* **39**, 11413 (1989).
- [35] C. Zeng and V. Elser, *Phys. Rev. B* **42**, 8436 (1990).
- [36] J. T. Chalker and J. F. G. Eastmond, *Phys. Rev. B* **46**, 14201 (1992).
- [37] P. W. Leung and V. Elser, *Phys. Rev. B* **47**, 5459 (1993).
- [38] N. Elstner and A. P. Young, *Phys. Rev. B* **50**, 6871 (1994).
- [39] P. Lecheminant, B. Bernu, C. Lhuillier, L. Pierre, and P. Sindzingre, *Phys. Rev. B* **56**, 2521 (1997).
- [40] C. Waldtmann, H.-U. Everts, B. Bernu, C. Lhuillier, P. Sindzingre, P. Lecheminant, and L. Pierre, *Eur. Phys. J. B* **2**, 501 (1998).
- [41] P. Sindzingre, G. Misguich, C. Lhuillier, B. Bernu, L. Pierre, Ch. Waldtmann, H.-U. Everts, *Phys. Rev. Lett.* **84**, 2953 (2000).
- [42] C. Waldtmann, H. Kreutzmann, U. Schollwöck, K. Maisinger, and H. U. Everts, *Phys. Rev. B* **62**, 9472 (2000).
- [43] J. Richter, J. Schulenburg, and A. Honecker, *Lect. Notes Phys.* **645**, 85 (2004).
- [44] A. Läuchli and C. Lhuillier, [arXiv:0901.1065](https://arxiv.org/abs/0901.1065).
- [45] P. Sindzingre and C. Lhuillier, *Europhys. Lett.* **88**, 27009 (2009).
- [46] E. S. Sørensen, M. J. Lawler, and Y. B. Kim, *Phys. Rev. B* **79**, 174403 (2009).
- [47] A. M. Läuchli, J. Sudan, and E. S. Sørensen, *Phys. Rev. B* **83**, 212401 (2011).
- [48] H. Nakano and T. Sakai, *J. Phys. Soc. Jpn.* **80**, 053704 (2011).
- [49] C. Zeng and V. Elser, *Phys. Rev. B* **51**, 8318 (1995).
- [50] M. Mambrini and F. Mila, *Eur. Phys. J. B* **17**, 651 (2000).
- [51] R. Budnik and A. Auerbach, *Phys. Rev. Lett.* **93**, 187205 (2004).
- [52] S. Capponi, A. Läuchli, and M. Mambrini, *Phys. Rev. B* **70**, 104424 (2004).
- [53] D. Poilblanc, M. Mambrini, and D. Schwandt, *Phys. Rev. B* **81**, 180402 (2010).
- [54] D. Schwandt, M. Mambrini, and D. Poilblanc, *Phys. Rev. B* **81**, 214413 (2010).
- [55] O. Götze, D. J. J. Farnell, R. F. Bishop, P. H. Y. Li, and J. Richter, *Phys. Rev. B* **84**, 224428 (2011).
- [56] G. Evenbly and G. Vidal, *Phys. Rev. Lett.* **104**, 187203 (2010).
- [57] S. Yan, D. A. Huse, and S. R. White, *Science* **332**, 1173 (2011).
- [58] D. Poilblanc and G. Misguich, *Phys. Rev. B* **84**, 214401 (2011).
- [59] S. R. White, *Phys. Rev. Lett.* **69**, 2863 (1992).
- [60] U. Schollwöck, *Rev. Mod. Phys.* **77**, 259 (2005).
- [61] U. Schollwöck, *Ann. Phys. (N.Y.)* **326**, 96 (2011).
- [62] S. R. White, *Phys. Rev. Lett.* **77**, 3633 (1996).
- [63] S. R. White and D. J. Scalapino, *Phys. Rev. Lett.* **80**, 1272 (1998).
- [64] S. R. White and D. J. Scalapino, *Phys. Rev. Lett.* **81**, 3227 (1998).
- [65] S. R. White and A. L. Chernyshev, *Phys. Rev. Lett.* **99**, 127004 (2007).
- [66] E. M. Stoudenmire and S. R. White, *Annu. Rev. Condens. Matter Phys.* **3**, 111 (2012).
- [67] See Supplemental Material at <http://link.aps.org/supplemental/10.1103/PhysRevLett.109.067201> for

- DMRG mappings and more information on ground and first excited state.
- [68] I. P. McCulloch, *J. Stat. Mech.* (2007) P10014.
- [69] I. P. McCulloch and M. Gulácsi, *Europhys. Lett.* **57**, 852 (2002).
- [70] S. R. White, *Phys. Rev. B* **72**, 180403 (2005).
- [71] I. P. McCulloch, [arXiv:0804.2509](https://arxiv.org/abs/0804.2509).
- [72] P. Sindzingre, C. Lhuillier, and J. B. Fouet, [arXiv:cond-mat/0110283](https://arxiv.org/abs/cond-mat/0110283).
- [73] M. Levin and X.-G. Wen, *Phys. Rev. Lett.* **96**, 110405 (2006).
- [74] A. Kitaev and J. Preskill, *Phys. Rev. Lett.* **96**, 110404 (2006).
- [75] H. C. Jiang, H. Yao, and L. Balents, *Phys. Rev. B* **86**, 024424 (2012).
- [76] X. G. Wen, *Phys. Rev. B* **44**, 2664 (1991).
- [77] Y. Zhang, T. Grover, and A. Vishwanath, *Phys. Rev. B* **84**, 075128 (2011).
- [78] S. T. Flammia, A. Hamma, T. L. Hughes, and X. G. Wen, *Phys. Rev. Lett.* **103**, 261601 (2009).
- [79] Y. Zhang, T. Grover, and A. Vishwanath, *Phys. Rev. Lett.* **107**, 067202 (2011).
- [80] Y. Zhang, T. Grover, A. Turner, M. Oshikawa, and A. Vishwanath, *Phys. Rev. B* **85**, 235151 (2012).
- [81] H.-C. Jiang, Z. Wang, and L. Balents, [arXiv:1205.4289](https://arxiv.org/abs/1205.4289).
- [82] M. A. Levin and X.-G. Wen, *Phys. Rev. B* **71**, 045110 (2005).
- [83] Z.-C. Gu, M. Levin, B. Swingle, and X. G. Wen, *Phys. Rev. B* **79**, 085118 (2009).
- [84] S. Sachdev, *Nature Phys.* **4**, 173 (2008).
- [85] D. Poilblanc *et al.*, [arXiv:1202.0947](https://arxiv.org/abs/1202.0947).
- [86] N. Schuch *et al.*, [arXiv:1203.4816](https://arxiv.org/abs/1203.4816).

Electronic physics auxiliary publication service for: Nature of the Spin Liquid Ground State of the $S = 1/2$ Heisenberg Model on the Kagome Lattice

Stefan Depenbrock,¹ Ian P. McCulloch,² and Ulrich Schollwöck¹

¹Department of Physics, Universität München, 80333 München, Germany

²Centre for Engineered Quantum Systems, School of Mathematics and Physics,
The University of Queensland, St Lucia QLD 4072, Australia

(Dated: June 22, 2012)

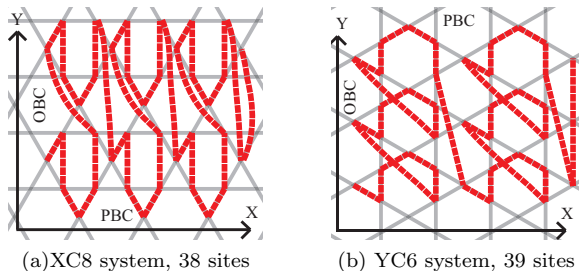


FIG. 1. (Color online) We map the two-dimensional system to a one-dimensional chain using two different mappings, one for aligning the lattice to the X-axis (a) and one for aligning it to the Y-axis (b) with periodic (open) boundary conditions in the vertical (horizontal) direction. The red broad line represents the one-dimensional chain.

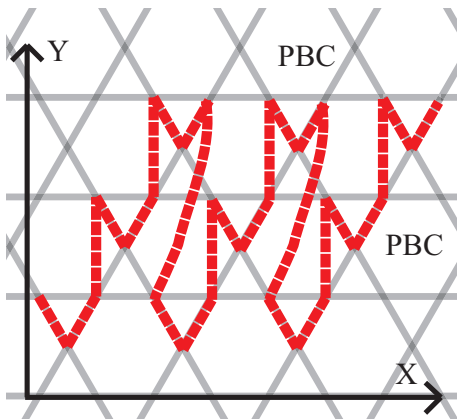


FIG. 2. (Color online) Path for a torus in DMRG

Mapping two-dimensional kagome lattices to one-dimensional chains for DMRG treatment. As DMRG is a one-dimensional method, the two-dimensional kagome lattice on cylinders and tori has to be mapped to a one-dimensional chain with long-ranged interactions. There are multiple (in fact, combinatorially many) ways to map cylinders and tori to one-dimensional systems, however, ideally they keep interactions as short-ranged and the resulting path as regular as possible. Out of a large variety we tested we choose the two ways to map the kagome lattice to chains (Fig. 1) that show the fastest convergence of energy in DMRG runs and label these either as X-cylinders (XC) or Y-cylinders (YC) depending on the

lattice axes' alignment. In this notation, YC6 denotes a cylindrical system where one of the three lattice axes is aligned with the y -axis and a circumference c of six lattice spacings. For XC systems (alignment of one of the lattice axes with the x -axis) the circumference is measured instead in units of $\sqrt{3}/2$ times the lattice spacing, so that e.g. the XC12 has a circumference of $c = 6\sqrt{3} \approx 10.4$ lattice spacings. In the case of tori, which we considered mainly for reference purposes, only a single path was retained (Fig. 2). It is worthwhile to point out the path independence of results: where we consider the same cylinders as [1], results do agree although they used yet another mapping.

Identification of bulk vs. boundary excitations. To rule out boundary excitations in the lowest $S = 1$ state, we examine the difference in bond energies for the lowest lying states in the two spin sectors $S = 0$ and $S = 1$, finding no significant difference at the boundaries but a visible change in the bulk (Fig. 3).

Supplementary information on ground state properties. In order to exclude a valence bond crystal more rigorously, we consider the bond energies (nearest-neighbor correlators) where a valence bond crystal would exhibit a frozen pattern of different bond energies. We do not observe this for any of our ground states (see Fig. 3(a)). Interestingly, it turns out that we can see this frozen pattern in *unconverged* wave functions (Fig. 4(a)). A further increase of the number of kept DMRG states and continued sweeping makes these patterns vanish in the bulk (Fig. 4(b)). The presence of these frozen bond patterns hence is a distinguishing feature of an insufficiently converged wave function as it disappears upon lowering the energy and approaching the true ground state, where the bond energies only show deviations from the average at the cylinder's edges (Fig. 3). DMRG – similar to other tensor network methods such as PEPS and MERA – has a low-entanglement bias, because the underlying matrix product states structure can only capture entanglement up to a strength roughly logarithmic in the number of DMRG states: for an insufficient number of ansatz states, DMRG will therefore among states of similar energy prefer those of low entanglement, in our case valence bond crystals compared to quantum spin liquids.

To elicit additional information on the spin liquid state, we strengthen selectively the interaction on various patterns on some bonds, namely on a hexagon and on a

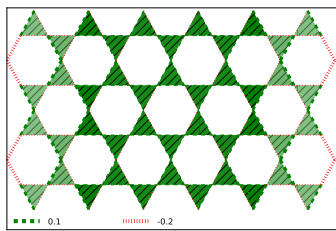
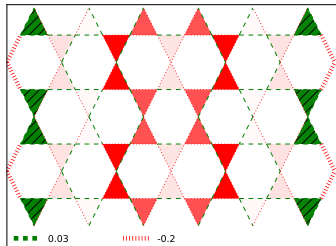
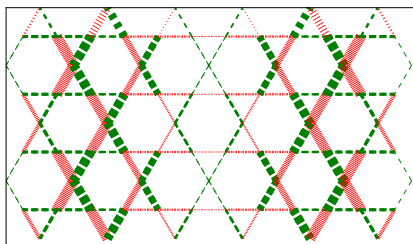
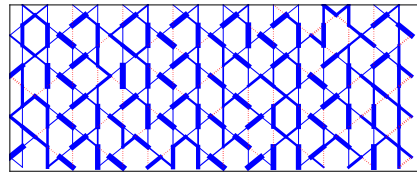
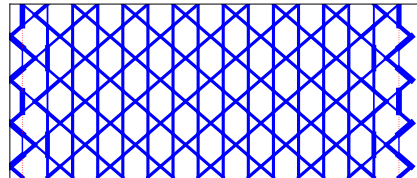
(a) Ground state for $S = 0$.(b) Ground state for $S = 1$.(c) Difference in bond energies between the $S = 0$ and the $S = 1$ samples.

FIG. 3. (Color online) Bond and triangle energies for the ground state and lowest triplet excitation of a 74-site XC8 sample. In panels (a) and (b), the line width is proportional to $|\langle \vec{S}_i \cdot \vec{S}_j \rangle - e_0|$ where e_0 is the mean bulk energy. Green bonds denote $\langle \vec{S}_i \cdot \vec{S}_j \rangle < e_0$, red (dotted) bonds denote $\langle \vec{S}_i \cdot \vec{S}_j \rangle > e_0$. The triangle color (pattern) and intensity correspond to the deviation of the sum of the bond energies on the three triangle bonds from the mean $3e_0$, where the green (hatched) triangles denote a lower value, i.e. $\sum e_i < 3e_0$. In panel (c), bond energies of the lowest $S = 0$ state are subtracted from those of the lowest $S = 1$ state. The line width is proportional to the absolute value of the energy difference, green (hatched) lines correspond to positive and red (dotted) lines to negative energy differences.

diamond pattern and check whether this is taken up by the ground state structure (Fig. 5(a) and (b)). In agreement with the U(1) DMRG calculation of [1], we find in the SU(2) DMRG calculation that strengthening the interactions on the diamond pattern elicits the strongest response in the bond energies. Agreement is also obtained for modulating a pattern of every second vertical



(a) This snapshot of a not yet converged calculation (insufficient number of DMRG states) shows bond energy patterns that break the translational invariance.



(b) This snapshot of a well converged calculation (sufficient number of DMRG states and sweeps) shows no pattern in the bond energies except for edge effects. In the bulk, a spin liquid state without breaking of translational invariance emerges.

FIG. 4. Visualization of the energy per bond for two snapshots in an iterative DMRG ground state calculation. The bond line width corresponds to the absolute value of the bond energy; the sign is negative (antiferromagnetic) for blue bonds, positive (ferromagnetic) for all red bonds, of which there are a few towards the edge.

bond (Fig. 5 (c)), which finds an even stronger response; this was considered in [1] as evidence that the ground state of the kagome model arises from melting a valence bond state exhibiting a similar bond pattern.

As an additional check for preferred orderings, we also consider spin-spin correlations in real space (Fig. 6) where lattice symmetry breaking orderings would show up as stronger correlations in certain directions. While we do not observe any signs for a valence bond crystal in the ground state, we see the band-like structure of the spin-spin correlations that was reported by Läuchli *et al.*[2] for tori. These pronounced staggered correlations along selected loops wrapping around the sample are artifacts of the periodic boundary conditions and disappear for large circumferences. In agreement with expectations for a topological \mathbb{Z}_2 QSL we also observe the forming of band-like structures in the bond energies for cylinders with an odd number of sites (not shown).

[1] S. Yan, D. A. Huse, and S. R. White, *Science* **332**, 1173 (2011)

[2] A. M. Läuchli, J. Sudan, and E. S. Sørensen, *Phys. Rev. B* **83**, 212401 (2011)

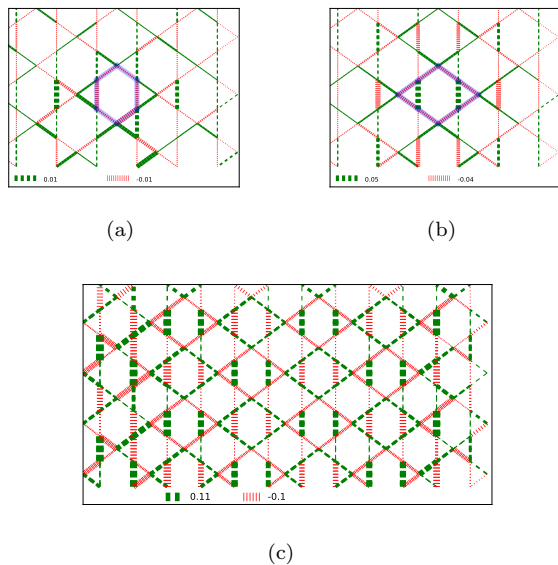


FIG. 5. (Color online) Snapshots of the resonance pattern for a 150-site YC8 sample, using the same nomenclature as Fig. 3. Line widths correspond to the deviation of the bond energy from the mean bulk energy e_0 ; triangle color and intensity show the deviation of the sum of the three triangle bond energies from the bulk average $3e_0$. In each case, interactions on certain bonds (highlighted by color) have been enhanced, in 5(a) a six-site hexagon, in 5(b) an eight-site diamond by 0.001 each. In 5(c), the interaction strength of every second vertical bond was alternatingly changed by $\pm 0.5\%$, i.e. every fourth bond was strengthened. The surrounding dimers arose in response to these changes, with the response increasing from 5(a) to 5(b) to 5(c).

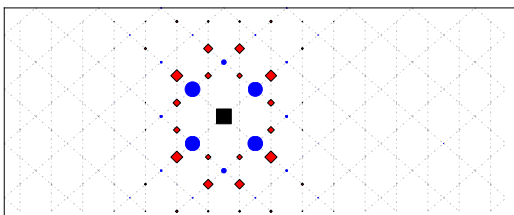


FIG. 6. (Color online) Spin-spin correlations in the ground state of a 196-site YC8 sample system. The diameter of the circles (diamonds) is proportional to the absolute value of the spin-spin correlation with the central reference site (black square). Blue circles (red diamonds) denote positive (negative) correlations. Nearest-neighbor correlations have been left out for clarity. The lattice is drawn as a guide for the eyes.

4 Symmetry-Protected Topological Phases and the Bethe Lattice

As we have seen in the last chapter, there are phases of matter which are not characterized by a broken symmetry but rather by an underlying hidden structure. These phases are usually known as topological phases which can again be divided into two general classes, according to their stability under perturbations.

The first class is known as intrinsic topological order. The Z_2 quantum spin liquid discussed in the previous chapter belongs to this class. Its discriminating feature is its stability against local perturbations: these systems do not reduce to topologically trivial phases, no matter what kind of perturbation is added.

Intrinsic topological order is characterized by long-range entanglement, implying that the ground state can not be mapped to a simple product state using linear unitary transformations [18, 295–299]. As discussed in the previous chapter, systems with intrinsic topological order have been found to exhibit topology-dependent ground state degeneracy, fractional bulk excitations, and non-trivial topological entanglement entropy.

The second class of topological order is called *symmetry-protected* topological (SPT) order and is sometimes also called symmetry-protected trivial order. As is the case for intrinsic topological order, the states in SPT phases do not break the system's symmetries. Systems with SPT order are instead usually characterized by non-degenerate ground states on closed manifolds and non-trivial edge degrees of freedom if the system does have a boundary. These phenomena are caused by a non-trivial entanglement structure in their ground states, i.e. the states can not be continuously connected to a topologically trivial state.

The key difference to intrinsic topological order lies in the SPT order's robustness with respect to perturbations. If arbitrary perturbations are allowed, one can show the ground state to belong to the same phase as a topologically trivial state. The ground state can therefore be mapped to a product state with local unitary transformations, implying it to be only short-range entangled [20]. If however, certain symmetries are enforced, i.e. only perturbations with certain symmetries are allowed, systems in this class are in a different phase from the trivial phase. The topological order in these systems is therefore protected by these symmetries. Accordingly, such phases are known as symmetry-protected (SPT) topological phases.

Historically the first system with known SPT order was the spin-1 Haldane chain [302, 303] which we will study in two dimensions later on. In more than one dimension on the other hand, a general theory is still missing, even though many efforts have been made to obtain a more complete understanding of SPT order. Most SPT phases in two and higher dimensions have only been identified in non-interacting

fermion systems. Common examples of this type of symmetry-protected order are topological insulators, i.e. non-interacting systems with a gapped bulk and gapless edge modes. The non-interacting nature of free fermions in these system allowed a classification of SPT order in topological insulators [304]. For interacting systems a different scheme of classifying and identifying SPT phases based on symmetry groups has been generalized by X.-G. Wen and co-workers [12, 18, 295, 297–299, 305, 306], who derived a complete classification procedure for one-dimensional gapped systems based on projective representations and group cohomology. But the question of stability and existence of SPT phases in the presence of strong interactions has so far not been answered conclusively.

After discussing intrinsic topological order in the context of the kagome lattice Heisenberg antiferromagnet, we will now focus on symmetry-protected topological order in this chapter. First we will introduce the notion of the Haldane phase, followed by a numerical study on the Bethe lattice we performed where we establish the presence of a Haldane-like phase for a strongly interacting model.

4.1 Haldane Phase and Haldane Conjecture

The prime example for a symmetry-protected topological phase is the so-called *Haldane* phase in quantum spin chains. The Haldane phase was predicted by Haldane for the anti-ferromagnetic Heisenberg chain with the Hamiltonian

$$\mathcal{H} = J \sum_i \mathbf{S}_i \cdot \mathbf{S}_{i+1} \quad (4.1)$$

with integer spin S . This phase was conjectured to exhibit a non-zero excitation gap and exponentially decaying correlations [302, 307]. The same model on the other hand was conjectured to be gapless with power-law correlations in the case of half-integer spins.

Following this prediction, Affleck, Kennedy, Lieb, and Tasaki found a related model Hamiltonian for which the ground state could be computed exactly [303, 308, 309]. Since one can show this modified Hamiltonian to be in the same phase as the Heisenberg antiferromagnetic chain, the so-called AKLT Hamiltonian provided a tractable testing ground for the Haldane conjecture. Later on it was realized that the AKLT state is actually a SPT phase, as it was found to exhibit many of the hallmarks of a SPT phase, such as edge states and non-local string order. The AKLT model was also one of the first SPT model systems where edge states could be experimentally observed [310]. Today, more than twenty years after its inception, the AKLT model is one of the canonical spin models and has been covered extensively in the literature.

In one dimension the Haldane phase has been the subject of intensive study, resulting in a clear picture of the phase. Already in the original papers it was shown that parity (inversion) symmetry suffices to protect the stability of the Haldane phase for $S = 1$. In recent years Pollmann and co-workers [259, 311–313] showed the Haldane phase to exist only for odd integer spins and in the presence of preserved time-reversal, link-centered inversion or global dihedral rotation symmetry. As long as

these symmetries are preserved, the system exhibits non-local string order and edge spins. This picture changes dramatically in higher dimensions, where many classification schemes fail. Furthermore it is not immediately obvious whether the AKLT phase exists only at a single point or in an extended region of the phase diagram of this interacting model. By using tensor product states we were able to answer some of these questions. [314]

4.2 Phase Diagram of the Isotropic Spin-3/2 Model on the $z = 3$ Bethe Lattice

Here we present a numerical study we performed of a higher-dimensional generalization of the AKLT model on the Bethe lattice. The Hamiltonian we studied is the bilinear-biquadratic-bicubic Heisenberg Hamiltonian given by

$$\mathcal{H} = \sum_i \alpha \mathbf{S}_i \cdot \mathbf{S}_{i+1} + \beta (\mathbf{S}_i \cdot \mathbf{S}_{i+1})^2 + \gamma (\mathbf{S}_i \cdot \mathbf{S}_{i+1})^3 \quad (4.2)$$

with spin $S = 3/2$. This model can be shown to exhibit an AKLT-like phase which we show to be a symmetry-protected topological phase using an adaptation of the tensor product state algorithms to infinite trees. Similar to intrinsically topologically ordered phases, SPT phases do not break any symmetries and can not be characterized by a local order parameter, making them hard to identify. The problem is even more difficult in this case, as the topological order in SPT phases is trivial, i.e. there is no ground state degeneracy, the topological entanglement entropy is trivial, and there are no fractional excitations present. Here we were able to identify the SPT phase by studying the entanglement spectrum across a cut of the system, the presence of finite edge spins, and the absence of conventional order. We contrast this with the identification of the conventional symmetry-breaking order also present in the phase diagram [315].

Recently, a similar approach has been put forward [314], where the tensor renormalization algorithm was modified to protect SPT order in the model. The key difference to our study is that we studied the model on the Bethe lattice where Huang *et al* studied it on the honeycomb lattice. Further differences lie in the scope of the work, i.e. we employed a basically unbiased algorithm, enabling us to investigate the full phase diagram without prejudice, where they only studied the AKLT phase.

Both ref. [314] and our work mark a new stage in the study of SPT order. Despite many years of trying to develop a theoretical perspective on topological order it is unclear how either symmetry-protected or intrinsic topological order can be realized in real materials. As most of the exactly solvable higher-dimensional model Hamiltonians involve rather unrealistic interactions, it is highly interesting to identify the presence of SPT order in more realistic models. In our study we demonstrated that tensor network algorithms, which so far have mainly been employed to study conventional order, are capable of finding and describing non-trivial SPT order, while simultaneously capturing conventional symmetry-breaking order.

Phase diagram of the isotropic spin-3/2 model on the $z = 3$ Bethe lattice

Stefan Depenbrock*

*Department of Physics and Arnold Sommerfeld Center for Theoretical Physics,
Ludwig-Maximilians-Universität München, 80333 München, Germany*

Frank Pollmann†

Max-Planck-Institut für Physik komplexer Systeme, 01187 Dresden, Germany

We study an $SU(2)$ symmetric spin-3/2 model on the $z = 3$ Bethe lattice using the infinite Time Evolving Block Decimation (iTEBD) method. This model is shown to exhibit a rich phase diagram. We compute the expectation values of several order parameters which allow us to identify a ferromagnetic, a ferrimagnetic, a anti-ferromagnetic as well as a dimerized phase. We calculate the entanglement spectra from which we conclude the existence of a symmetry protected topological phase that is characterized by $S = 1/2$ edge spins. Details of the iTEBD algorithm used for the simulations are included.

I. INTRODUCTION

Quantum antiferromagnets are a challenging and interesting topic in condensed matter physics. The interplay between strong correlations, quantum fluctuations, and frustration can yield very exciting new phases with often unexpected properties. One dimensional quantum spin chains have been proven to be very useful to understand many of these interesting phases. For these systems, very powerful analytical and numerical methods exist. A major advance on the numerical side was the introduction of the Density-Matrix-Renormalization Group (DMRG) method which allows for the efficient simulation of one-dimensional systems.¹ One of the first successes of the then new DMRG method was its use to prove the famous Haldane conjecture for integer spin chains numerically. The Haldane conjecture states that the Heisenberg antiferromagnetic (HAF) chain with integer spin S has a nonzero excitation gap and exponentially decaying spin correlation functions (while spin chains with half-integer spin are gapless).^{2,3} For odd integer spins, the Haldane phase is an example of a so-called *symmetry protected topological phase* (SPTP) which is characterized by $S = 1/2$ edge spins. This kind of phase cannot be characterized by symmetry breaking but instead by using cohomology theory.⁴⁻⁹

In this paper we make use of an extension of the DMRG algorithm to the Bethe lattice and study the phase diagram of a general $SU(2)$ symmetric $S = 3/2$ spin model on a Bethe lattice with coordination number $z = 3$. This model has a special point in this phase diagram, the so-called Affleck-Kennedy-Lieb-Tasaki (AKLT) point, at which the ground state is known exactly.¹⁰ The AKLT wave function for this model is a quantum paramagnet with exponentially decaying correlation functions.¹⁰⁻¹³ We argue that the AKLT point extends to a phase which is similar to the Haldane phase in one-dimensional spin chains in that it is characterized by a fractionalized edge spin (the precise meaning of an edge spin in this context is explained Sec. IV). Beside the Haldane phase, the model is shown to exhibit different magnetic phases

as well as a dimerized phase. Even though there exist experimental systems, such as dendrimers that realize the tree structure¹⁴ related to the Bethe lattice considered in this work, we are mainly interested in this system because of its theoretical nature. The $S = 3/2$ model has already been shown to exhibit a very complex phase diagram on the mean field level and in one-dimensional systems.¹⁵⁻¹⁷ The main goal is to present a conclusive phase diagram of the model utilizing recently introduced algorithms which allow an efficient simulation of quantum spin systems on Bethe lattices. We use a descendant of Vidal's infinite time-evolving block decimation algorithm (iTEBD)¹⁸ adapted to the tree like structure. The iTEBD method as well as the DMRG have already successfully been applied to reproduce, e.g., the phase diagram of the transverse field Ising model and the spin 1/2 XXZ model on the $z = 3$ Bethe lattice.¹⁹⁻²³ We include details of the algorithm in this paper and discuss a number of improvement that make it more stable.

This paper is organized as follows: in Sec. II we introduce the model and discuss some of its basic properties leading up to section Sec. III where we describe the method we used to obtain the results. In Sec. IV we first take a closer look at symmetry protected topological phases before we present the results in Sec. V. The key points of this paper are summarized again in Sec. VI.

II. MODEL

Throughout this paper we consider the following nearest-neighbor spin-3/2 model Hamiltonian

$$H = \sum_i \alpha \vec{S}_i \cdot \vec{S}_{i+1} + \beta \left(\vec{S}_i \cdot \vec{S}_{i+1} \right)^2 + \gamma \left(\vec{S}_i \cdot \vec{S}_{i+1} \right)^3 \quad (1)$$

where a different parametrization of the Hamiltonian is given by

$$\alpha = \cos \varphi \cos \theta \quad (2)$$

$$\beta = \sin \varphi \cos \theta \quad (3)$$

$$\gamma = \sin \theta \quad (4)$$

with $\varphi \in [-\pi, \pi]$ and $\theta \in [-\frac{\pi}{2}, \frac{\pi}{2}]$. The symmetries of this model include translation, spatial inversion, $SU(2)$, and time reversal (TR). This model is known to exhibit an AKLT-like wavefunction at the point $\alpha = 1.0$, $\beta = \frac{116}{243}$, $\gamma = \frac{16}{243}$ when placed on a $z = 3$ Bethe lattice. The AKLT state has symmetry protected $S = 1/2$ edge spins which are discussed in detail in Sec. IV. Furthermore this model exhibits a $SU(4)$ symmetry at four points in the phase diagram connected by a $SO(5)$ symmetric line which is given by^{15,16} $\alpha = -\frac{1}{96}(31J_0 + 23J_2)$, $\beta = \frac{1}{72}(5J_0 + 17J_2)$, and $\gamma = \frac{1}{18}(J_0 + J_2)$ with $J_0, J_2 > 0$. We place this Hamiltonian on the Bethe lattice with coordination number $z = 3$. The Bethe lattice and its finite counterpart, the Cayley tree, has first been used in statistical mechanics.^{24–26} More recently it has also proved to be a highly instructive testing ground for tensor network methods as it is loop-free thus removing one of the major sources of entanglement. Additionally, the Bethe lattice is self-similar, enabling the application of efficient infinite-system methods. This lattice is infinite by definition and thus there are no surface effects.²⁷ Note that the thermodynamic limit of the Cayley tree and the Bethe lattice are not equivalent. This inequivalence is rooted in the large number of surface sites contained in any Cayley tree.²⁸ Whereas in most systems the ratio of boundary to bulk sites reduces to zero for large systems, it remains finite for the Cayley tree. The finite tree is thus dominated by the boundary conditions, making it unsuitable to study the model's properties in the thermodynamic limit.

III. TENSOR PRODUCT STATE BASED SIMULATIONS ON A TREE LATTICE

A. Definitions

For our simulations we use the infinite tree tensor network state (iT_{TTN})^{20,23,29–31} representation of the ground state wave function. The iT_{TTN} states are the natural choice of ansatz state for our model system, since they model the tree's geometry. We thus employ this representation to compute the ground state properties numerically, using the infinite time-evolving block decimation (iTEBD) method^{18,32,33} adapted to infinite trees. The iTEBD method is a descendant of the density matrix renormalization group (DMRG) method^{1,34,35} based on matrix product states (MPS)¹¹ which can be generalized to trees. For the sake of completeness, we now review some of the properties of MPS's, followed by an introduction to TTN states.

A translationally invariant MPS for a chain of length L can formally be written in the following form

$$|\psi\rangle = \sum_{\{m_j\}} \text{tr} [\Gamma_{m_1} \Lambda \dots \Gamma_{m_L} \Lambda] |m_1 \dots m_L\rangle. \quad (5)$$

Here, Γ_m are $\chi \times \chi$ matrices with χ being the dimension of the matrices used in the MPS. The index $m = -S, \dots, S$

is the ‘‘physical’’ index, e.g., enumerating the spin states on each site, and Λ is a $\chi \times \chi$, real, diagonal matrix. Ground states of one dimensional gapped systems can be efficiently approximated by matrix-product states^{36–38}, in the sense that the value of χ needed to approximate the ground state wavefunction to a given accuracy converges to a finite value as $N \rightarrow \infty$. We therefore think of χ as being a finite (but arbitrarily large) number, which can be used to control the simulation's precision.

The matrices Γ, Λ can be chosen such that they satisfy the canonical conditions for an infinite MPS^{33,39}

$$\sum_m \Gamma_m \Lambda^2 \Gamma_m^\dagger = \sum_m \Gamma_m^\dagger \Lambda^2 \Gamma_m = \mathbf{1}. \quad (6)$$

These equations can be interpreted as stating that the transfer matrix

$$T_{\alpha\alpha';\beta\beta'} = \sum_m \Gamma_{m\beta}^\alpha \left(\Gamma_{m\beta'}^{\alpha'} \right)^* \Lambda_\beta \Lambda_{\beta'} \quad (7)$$

has a right eigenvector $\delta_{\beta\beta'}$ with eigenvalue $\lambda = 1$. (* denotes complex conjugation.) Similarly, $\tilde{T}_{\alpha\alpha';\beta\beta'} = \sum_m \left(\Gamma_{m\beta'}^{\alpha'} \right)^* \Gamma_{m\beta}^\alpha \Lambda_\alpha \Lambda_{\alpha'}$ has a left eigenvector $\delta_{\alpha\alpha'}$ with $\lambda = 1$. We further require that $\delta_{\alpha\alpha'}$ is the *only* eigenvector with eigenvalue $|\lambda| \geq 1$ (which is equivalent to the requirement that $|\psi\rangle$ is a pure state⁴⁰).

The considerations given here become most intuitive when one considers, formally, an infinite chain. We form a partition of the chain by cutting a bond which results in two half-chains. The wavefunction can then be Schmidt decomposed⁴¹ in the form

$$|\psi\rangle = \sum_\alpha \lambda_\alpha |\alpha L\rangle |\alpha R\rangle, \quad (8)$$

where $|\alpha L\rangle$ and $|\alpha R\rangle$ ($\alpha = 1, \dots, \chi$) are orthonormal basis vectors of the left and right partition, respectively. In the limit of an infinite chain, and under the canonical conditions (6), the Schmidt values λ_α are simply the entries of the Λ matrix, $\Lambda_{\alpha\alpha}$. The λ_α^2 are the eigenvalues of the reduced density matrix of either of the two partitions, and are referred to as the *entanglement spectrum*. The entanglement entropy is $S = -\sum_\alpha \lambda_\alpha^2 \ln \lambda_\alpha^2$. This is the von Neumann entropy of the reduced density matrix. The states $|\alpha L\rangle$ and $|\alpha R\rangle$ can be obtained by multiplying together all the matrices to the left and right of the bond, e.g., if the broken bond is between sites 0 and 1, $|\alpha L\rangle = \sum_{\{m_j\}, j \leq 0} \left[\prod_{k \leq 0} \Lambda \Gamma_{m_k} \right]_{\gamma_\alpha} | \dots m_{-2} m_{-1} m_0 \rangle$. Here, γ is the index of the row of the matrix; when the chain is infinitely long, the value of γ affects only an overall factor in the wavefunction. Reviews of MPS's as well as the canonical form can be found in Refs. 33 and 42.

B. Tree Tensors Networks

While MPS are the natural choice of ansatz state for one-dimensional systems, they are eminently unsuitable

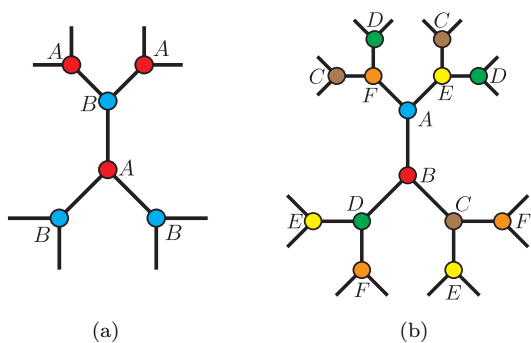


FIG. 1. The two different tilings for the infinite Bethe lattice that were employed in the simulations.

for large higher-dimensional systems. For these systems the ideas behind MPS can be generalized to create a new class of states known as tensor product (TPS) or projected entangled pair-states (PEPS).^{43,44} The construction of these states is based on the bipartite nature of trees, allowing them to be split into two subsystems via the Schmidt decomposition, analogous to one-dimensional chains. Thus the generalization of the one-dimensional construction to trees is straightforward but in order to introduce our ansatz and the notation, we will cover it here as well.

To describe a tree of coordination number z (i.e. each vertex has z nearest neighbors), we place tensors $\Gamma^{[i]}$ of order $z + 1$ on the vertices and vectors Λ^k on the edges of the tree graph in Fig. 1. We then connect the tensor's indices in a way that mimics the model's underlying lattice structure. A state $|\psi\rangle$ on the $z = 3$ Bethe lattice can in this representation be written as

$$|\psi\rangle = \left(\prod_{k \in \text{bonds}} \sum_{a_k < \chi} \Lambda_{a_k}^k \right) \times \left(\prod_{i \in \text{sites}} \sum_{s_i < d} \Gamma_{a_l a_m a_n}^{[i] s_i} | \dots \rangle | s_i \rangle | \dots \rangle \right).$$

While the dimension d of the physical indices s_i is dictated by the model, the dimension χ of the virtual indices a_k can be chosen arbitrarily and is only limited by computational resources. This ansatz can easily be extended to lattices with a higher coordination number but in this publication we will only cover the case of $z = 3$. Analogous to MPS, the tensors in a tree tensor network can be chosen such that they satisfy the conditions for a canonical tensor network:

$$\sum_{a_k} \Lambda_{a_k}^2 = 1 \quad (9)$$

$$\sum_{s_i} \sum_{a_k a_l} \Gamma_{a_k a_l a_m}^{s_i} \Lambda_{a_k}^2 \Lambda_{a_l}^2 \left(\Gamma_{a_k a_l a'_m}^{s_i} \right)^* = \delta_{a_m a'_m}. \quad (10)$$

The advantages of the canonical form of TPS are the same as for MPS, i.e. the canonical form provides a well-defined basis for evaluations of observables and the imaginary-time evolution.

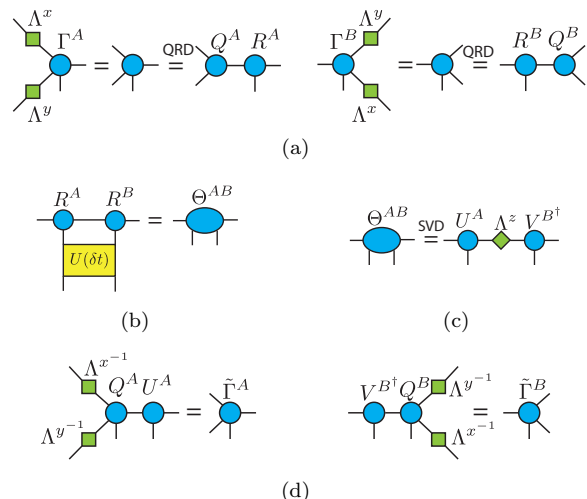


FIG. 2. The simple update procedure for a single two-site unit cell. By repeating this procedure for every tensor combination one full update step is completed. Details on the procedure are provided in the text.

C. Imaginary-time evolution

In order to obtain the model's ground state within this class of iTTN we evolve an initial state $|\psi\rangle$ in imaginary time. Since the Hamiltonian is given by the sum over nearest neighbors of products of commuting operators, we can implement the imaginary-time evolution as a product of local unitary operators using the second-order Suzuki-Trotter decomposition of the evolution operator: $e^{-Ht} = \lim_{n \rightarrow \infty} (e^{-H\delta t})^n$. This decomposition incurs a systematic non-accumulating error of $\mathcal{O}(\delta t^2)$ which can be neglected if the time step δt is sufficiently small (in our simulations we use $\delta t = 10^{-6}$ as the final time step). While in principle each site tensor $\Gamma^{[i]}$ and bond tensor Λ^k can be different for different sites and bonds we will calculate the ground state within the translation-invariant sector of iTTN. In this picture, let us consider the effects of the imaginary-time evolution of the tree tensor network by a translationally invariant Hamiltonian. If given a translation-invariant state, the symmetry of the Hamiltonian guarantees it to never be broken in time, thus enabling us to describe the full state by examining only a small number of sites. However, if the system is in a phase in which the translational symmetry is spontaneously broken, it turns out to be advantageous to allow for a larger unit cell and to guide the wave function into a symmetry broken state.

Since the infinite Bethe lattice is self-similar, a translation-invariant ansatz state is the natural choice. For numerical reasons it is advantageous to slightly break that translational invariance by adopting a larger unit cell. Canonically a two-site unit cell is used, but here we will extend this scheme and for some calculations employ a six-site unit cell (see Fig. 1), which enables us to also

capture more involved states such as a dimerized state. In accordance with the canonical iTEBD algorithm, the two-site unit cell consists of two site tensors A and B and three bond vectors Λ^x , Λ^y , and Λ^z , whereas the six-site cell uses six site tensors and nine bond tensors.

We now have all the ingredients necessary to compute the ground state. By repeatedly applying the near-unitary operators $U(\delta t) = e^{-H\delta t}$ to an initial state $|\psi\rangle$ and then truncating the entanglement spectrum we can obtain the ground state. The operator's near-unitary nature allows us to perform the truncation in a well-defined basis, yielding a stable algorithm to find the ground state on the Bethe lattice. This procedure was introduced in the context of MPS as iTEBD¹⁸ and later on generalized the Bethe lattice.^{20,21,23} The same algorithm is also used to find an approximate TPS representation on higher-dimensional lattices in the so-called *simple update*.⁴⁵ However, as the update algorithm ignores the loops present in a two-dimensional lattice, the TPS found is not optimal to represent the 2D ground state.

The update procedure for the imaginary-time evolution of a tree tensor network consisting of an infinitely repeated two-site unit cell is now given by the following steps (Fig. 2):

(1) Contract the site tensors with the adjacent bond vectors, leaving one bond open.

(2) Compute the QR decomposition of the resulting tensors relative to the open bond. This modification was recently introduced by Wang⁴⁶ to reduce the scaling of the update with the bond dimension and to stabilize the update procedure.

(3) Contract the evolution operator with the R tensors resulting from the QR decomposition and calculate the singular value decomposition of the resulting 4-index tensor.

(4) Truncate the entanglement spectrum to χ entries and absorb the unitary matrices in the Q tensors.

(5) Contract the tensors with the inverse bond vectors to obtain the updated site tensors.

By repeating this procedure for every bond, one full update step is completed, i.e., the full lattice is updated. Repeatedly applying the update to the system while decreasing the time step brings the initial wave function increasingly closer to the true ground state wave function.

For a general Bethe lattice with coordination number z the computational cost of this algorithm scales as $\mathcal{O}(\chi^{3z-3}) + \mathcal{O}(d^2\chi^{z+1})$ and is dominated by the cost of the SVD step. The high cost of the SVD limits our algorithm to values of $\chi \approx 40$ on a desktop machine when no additional symmetries are used.

D. Symmetries

The algorithm's performance can be improved by exploiting the model's symmetries, which enable a de-

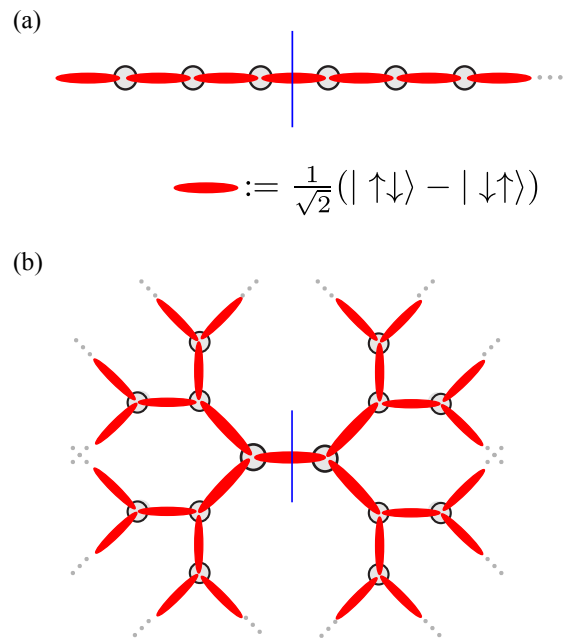


FIG. 3. Diagrammatic representation of the AKLT wave function on a chain (a) and a $z = 3$ Bethe lattice (b). The red ovals are representing $S = 1/2$ singlets. A Schmidt decomposition at the blue line cuts in both cases one singlet, leaving behind localized $S = 1/2$ edge spins.

composition of the matrices into block-diagonal matrices, hence reducing the cost of the numerical operations. Here, we made use of the models $U(1)$ symmetry in the S_z sector. By implementing this symmetry the computational cost can be significantly reduced, allowing a larger cut-off dimension of $\chi \approx 80$. Details of how to implement this symmetry can be found in e.g. Refs. 47 and 48.

IV. SYMMETRY PROTECTED TOPOLOGICAL PHASES

Symmetry protected topological phases (SPTP) are gapped phases which cannot be characterized by any local order parameters and are distinct from trivial phases (i.e., product states) only in the presence of certain symmetries. In a series of works it had been shown that these phases can be completely characterized using projective representations of the symmetries present.^{7-9,49-53} In spin systems this means physically that the spin fractionalizes and the projective representation is due to localized spin-half degrees at the edge of a cut. We briefly review SPTP for one-dimensional systems and show that the concept directly generalizes to the Bethe lattice.

We start from a state $|\psi\rangle$ on an infinite chain that is invariant under an *internal symmetry*. The internal symmetry is represented in the spin basis by a unitary matrix

Σ acting on each site so that $|\psi\rangle \rightarrow [\bigotimes_i \Sigma(i)] |\psi\rangle$. We perform a Schmidt decomposition of the system into two subsystems (see Fig. 3a) by cutting one bond. We now only consider the *important* Schmidt states which correspond to Schmidt values $\Lambda_\alpha > \epsilon$ for a given $\epsilon > 0$. These Schmidt states transform under a symmetry transformation as (modulo an overall phase):

$$\left[\bigotimes_i \Sigma(i) \right] |\alpha R\rangle = \sum_{\alpha'} U_{\alpha\alpha'} |\alpha' R\rangle, \quad (11)$$

where U is a unitary matrix which commutes with the Λ matrices.^{8,40} Similarly, the left Schmidt states $|\alpha L\rangle$ transform by the conjugate matrix. As the symmetry element g is varied over the whole group, a set of matrices U_g results. The matrices U_g form a χ -dimensional (projective) representation of the symmetry group. A projective representation is like an ordinary regular representation up to phase factors; i.e., if $\Sigma^g \Sigma^h = \Sigma^{gh}$, then

$$U_g U_h = e^{i\rho(g,h)} U_{gh}. \quad (12)$$

The phases $\rho(g,h)$ can be used to classify different topological phases.^{5,7-9}

As a concrete example, we now consider the Haldane phase around the AKLT state in the presence of a $\mathbb{Z}_2 \times \mathbb{Z}_2$ symmetry. The generators of the symmetry group are the spin rotations $\mathcal{R}_x = \exp(i\pi S^x)$ and $\mathcal{R}_z = \exp(i\pi S^z)$. The phases for each spin rotation individually (e.g., $U_x^2 = e^{i\alpha} \mathbb{1}$) can be removed by redefining the phase of the corresponding U -matrix. However, the representations of $\mathcal{R}_x \mathcal{R}_z$ and $\mathcal{R}_z \mathcal{R}_x$ can also differ by a phase, which it turns out must be ± 1 :

$$U_x U_z = \pm U_z U_x. \quad (13)$$

I.e., the matrices either commute or anti-commute. This resulting phase cannot be gauged away because the phases of U_x and U_z enter both sides of the equation in the same way. Thus we have two different classes of projective representations. If the phase is -1 , then the spectrum of Λ is doubly degenerate, since Λ commutes with the two unitary matrices U_x, U_z which anti-commute among themselves. For the AKLT state considered here, the Schmidt states have half-integer edge spins (see Fig. 3). Thus we find $U_x = \sigma_x$ and $U_z = \sigma_z$, therefore $U_x U_z = -U_z U_x$, and the Haldane phase is protected if the system is symmetric under both \mathcal{R}_x and \mathcal{R}_z . An analogous argument can be made for inversion symmetry (i.e., spatial inversion of the system at a bond) and time reversal symmetry.^{5,8}

Using the above arguments, we can now characterize the $S = 3/2$ AKLT state on the $z = 3$ lattice. As illustrated in Fig. 3b, a single cut through a bond separates the Bethe lattice into two disconnected subsystems. In the AKLT state, any of the bonds has a $S = 1/2$ singlet and thus the Schmidt states have localized half-integer spins at the edges. Thus the transformation of the Schmidt states under a symmetry operation yields

a (projective) representation U of the symmetry group which characterizes the phase. Note that there are in fact different kinds of SPTP that can be realized on the Bethe lattice depending on the fractionalization of the spin. For example, in an $S = 1$ model on a $z = 3$ lattice with strong dimerization (two strong bonds and one weak bond), we would obtain a network of $S = 1$ Haldane chains.

V. NUMERICAL RESULTS

We employ our variant of the iTEBD algorithm to study the bilinear-biquadratic-bicubic Heisenberg model defined in Eq. (1) over the full parameter range of $\varphi = -\pi \dots \pi$, $\theta = -\frac{\pi}{2} \dots \frac{\pi}{2}$. To ensure unbiased results we use different iTEBD implementations, one with a two-site unit cell and one with a six-site unit cell (see Fig. 1). The simulations were conducted both with and without explicitly conserving the model's $U(1)$ symmetry and were started from different initial wavefunctions ranging from completely random to fully polarized initial states. Furthermore, we also studied the dependence on the evolution scheme by starting the imaginary-time evolution with a slightly modified evolution operator (e.g. by adding a small ferromagnetic or symmetry-breaking interaction term to the Hamiltonian) and only later in the calculation using the actual Hamiltonian to converge the trial wavefunction to the groundstate.

The simulations were started with a large time step of $\delta t = 0.1$ which was then in several steps decreased to $\delta t = 10^{-6}$, reducing the Trotter error to insignificance. These checks are commonly accepted best practice for any imaginary-time evolution, as the overlap of the initial state and the true groundstate has to be finite in order for the algorithm to be able to evolve the trial wavefunction to the groundstate. Hence we have to ascertain the result's independence of the procedure and the initial states. As expected we find the strongest dependence on the initial tensors in the ferromagnetic (anti-ferromagnetic) phase when starting with an anti-ferromagnetic (ferromagnetic) initial state, but no significant correlation otherwise. To establish that our findings are not dependent on the unit cell, i.e., the constraint of a two-site unit cell, we also implemented a variant of the iTEBD algorithm that operates on a six-site unit cell, see Fig. 1(a). This implementation enables us to also describe a dimerized phase which would otherwise be able to escape characterization as it is not commensurate with a two-site unit cell.

Special attention was paid to the four $SU(4)$ symmetric points shown in the phase diagram Fig. 4 where we ran a variety of simulations to ascertain the model's behavior. With the exception of the multi-critical point at $\varphi = 2.93$, $\theta = 0.17$ we were not able to observe any behavior diverging from the encompassing phase.

Our results for the phase diagram of the bilinear-biquadratic-bicubic Heisenberg model are shown in

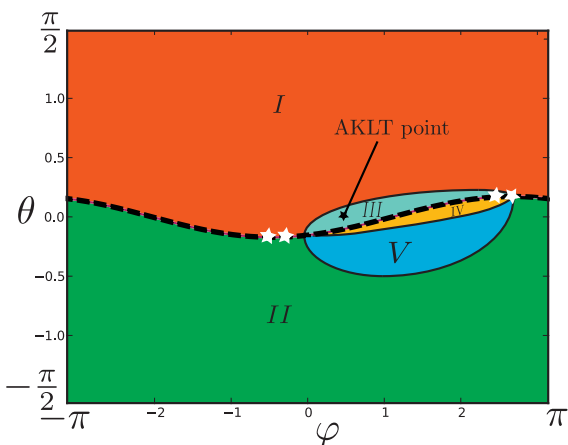


FIG. 4. The phase diagram as determined by the tree network iTEBD method. We established the presence of an anti-ferromagnetic phase (*I*), a ferromagnetic phase (*II*), the Haldane phase (*III*), a dimerized phase (*IV*), and a ferrimagnetic phase (*V*). For reference purposes the phase diagram also includes the AKLT point denoted by a black star and the $SO(5)$ symmetric line denoted by the dotted line between phases *I* and *II*. The $SU(4)$ symmetric points are marked by white stars and lie on the $SO(5)$ line.

Fig. 4. We find five different phases: a Néel phase, a ferromagnetic polarized phase, the Haldane phase, a dimerized phase, and a ferrimagnetic phase.

A. (Anti-)Ferromagnetic phases

We start our analysis of the phase diagram with the straightforward phases, i.e. the AFM and FM phases. First we consider the staggered magnetization m_z^s and the uniform magnetization m_z . The polarized phases can easily be identified by observing the two different order parameter's behavior shown in Fig. 5. In the ferromagnetic region $\theta < -\frac{\pi}{3}$ the staggered magnetization m_z^s disappears, while the magnetization per site m_z is maximal in this region. The opposite holds for the anti-ferromagnetic part of the phase diagram, where only the staggered magnetization remains non-zero. Inspired by the (anti-) nematic order found in mean-field studies¹⁶ we also calculate the octupolar order parameter in the vicinity of the $SO(5)$ line. Again we observe the absence of different order, except for some small contributions in the ferromagnetic region at negative φ . This might be due to remnants of the classical order persisting to zero temperature.

B. Dimerized phase

We determine a dimerized phase to be present in the region denoted by *IV* in the phase diagram (Fig. 4). This

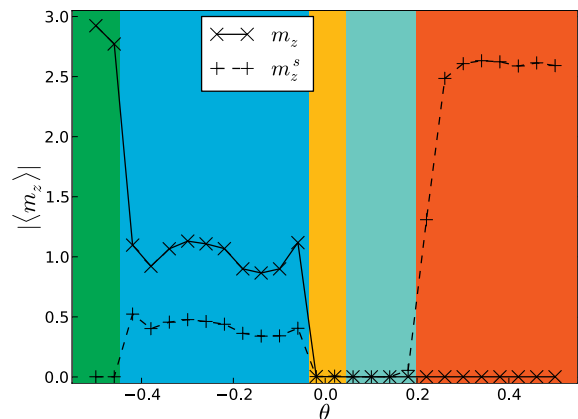


FIG. 5. The (staggered) magnetization for various of values of θ and $\varphi = 0.9$ with $\chi = 24$. The ferromagnetic phase can be identified as the region with maximal uniform magnetization per site, whereas the anti-ferromagnetic phase is distinguished by the finite staggered magnetization and vanishing uniform magnetization per site. Inbetween those two phases are the dimerized and the Haldane phases, where both the staggered (m_z^s) and uniform magnetization (m_z) vanish. In the ferrimagnetic phase they take intermediate values. The colors correspond to the phases introduced in Fig. 4.

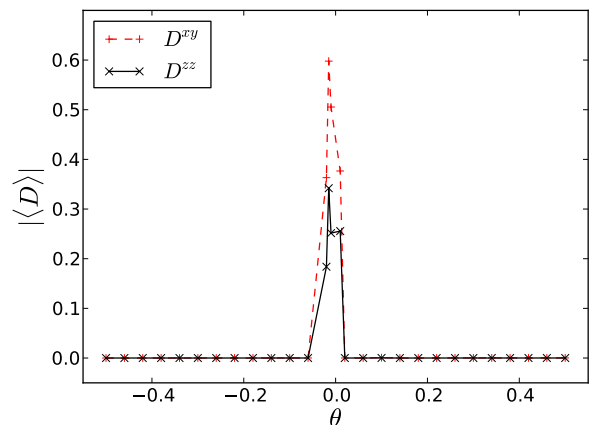


FIG. 6. Behavior of the dimer order parameters defined in Eq. 14 for a cut through the phase diagram at $\varphi = 0.9$ with $\chi = 24$. The increase of the dimer order parameters occurs at the boundary between the Haldane and the ferrimagnetic phase.

phase is hard to characterize due to its diminutive size and vanishing magnetization, however, careful calculations strongly indicate its existence. To determine the properties of this elusive plains we calculate the xy and z components of the dimer order parameters D^{xy} and D^{zz} defined via

$$D_{i,j,k}^{xy} = \langle (S_i^x S_j^y + S_i^y S_j^x) \rangle \quad (14)$$

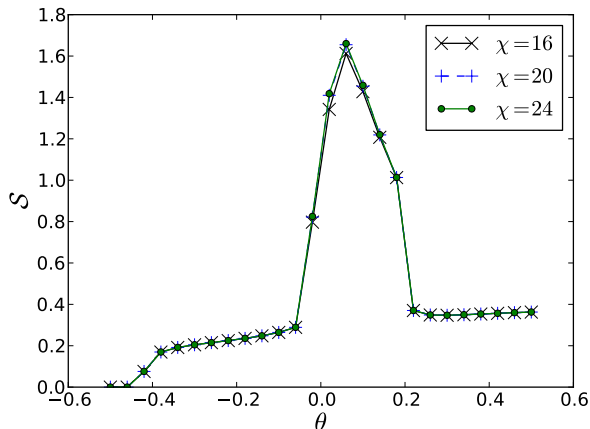


FIG. 7. The entropy for a cut in θ direction through the phase diagram at $\varphi = 0.9$ for various values of χ showing the entropy to be clearly converged when increasing the bond dimension.

$$- (S_j^x S_k^y + S_j^y S_k^x) \quad (15)$$

$$D_{i,j,k}^z = \langle S_i^z S_j^z - S_j^z S_k^z \rangle, \quad (16)$$

where i , j , and k label consecutive lattice sites residing on different shells (e.g. sites A , B , and C in Fig. 1 (b)). Calculation of these order parameter components reveals them to vanish for the magnetically ordered phases, as well as in the Haldane phase. Only in the dimer phase do they assume finite values. The hypothesis of a dimer phase is further corroborated by the vanishing magnetization. As opposed to the Haldane phase we also fail to observe finite edge spins in this phase. Together these observations indicate the existence of a narrow dimerized phase close to the $SO(5)$ symmetric line.

C. Ferrimagnetic phase

We found a ferrimagnetic phase that exists between the dimer phase and the ferromagnetic phase. This phase shows both a finite staggered magnetization as well as a finite magnetization per site, but displays vanishing dimer order parameters. As a test for this phase we try adding a small (staggered) field in the z direction to the Hamiltonian. Performing the simulation with this modified Hamiltonian results in strong polarization which could be both anti-ferromagnetic or ferromagnetic depending on the applied field.

D. Haldane phase

The last phase is a phase with exponentially decaying correlations and no broken symmetries (i.e., no local order parameter exists) which is identified as a SPTP. In this phase, the entanglement spectrum always displays

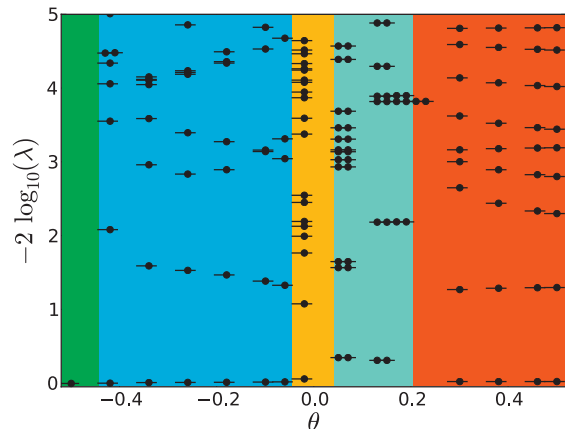


FIG. 8. Entanglement spectrum throughout a cut in the phase diagram at $\varphi = 0.9$ with $\chi = 24$ for various values of θ . Clearly visible is the doubling of the levels in the Haldane phase.

an even degeneracy in the entire phase, which is clearly visible in the iTEBD calculations. The identification of this phase rests on the presence of a finite $S = 1/2$ edge spin and its characteristic degeneracies in the entanglement spectrum shown in Fig. 8. As a direct evidence, we also calculated the edge spin of the Schmidt states directly and find a localized spin-1/2. In our simulations we are also able to observe the AKLT point where the ansatz state reduces to an exact tensor network with bond dimension $\chi = 2$. By adding small perturbations which destroy all the necessary symmetries to protect the phase, it is possible to drive the system out of the Haldane phase without a phase transition (i.e., the degeneracies in the spectrum are lifted for an arbitrarily small perturbation). We also checked numerically that the phase is robust against small perturbations which do not break the symmetries needed to protect it. All of these observations can be explained by the presence of a SPT phase as discussed in section IV.

VI. SUMMARY

In this work, we have studied a general $SU(2)$ symmetric spin-3/2 model on the $z = 3$ Bethe lattice using the infinite Time Evolving Block Decimation (iTEBD) method. We found that the model exhibits a rich phase diagram containing several magnetic phases, a dimerized phase as well as a symmetry protected topological phase (SPTP). The magnetic phases were identified by calculating the uniform and the staggered magnetization. We found a polarized ferromagnetic phase, an anti-ferromagnetic as well as a ferrimagnetic phase with finite (staggered) magnetization. Our simulations suggest the presence of a dimerized phase with vanishing magnetization and finite dimer order parameters. We

also identified a symmetry protected topological phase which shows all the key features of the Haldane phase. This phase is characterized by spin-1/2 edge spins and degeneracies in the entanglement spectrum.

ACKNOWLEDGMENT

We thank Erez Berg, Alexei Kolezhuk, Karlo Penc, Stephan Rachel, and Ari Turner for stimulating discus-

sions. SD would like to thank the Max Planck Institute for the Physics of Complex Systems for the generous access to their computing facilities.

-
- * stefan.depenbrock@lmu.de
† frankp@pks.mpg.de
- ¹ S. R. White, Phys. Rev. Lett. **69**, 2863 (1992).
 - ² F. D. M. Haldane, Phys. Rev. Lett. **50**, 1153 (1983).
 - ³ F. D. M. Haldane, Phys. Rev. Lett. **93A**, 464 (1983).
 - ⁴ Z.-C. Gu and X.-G. Wen, Phys. Rev. B **80**, 155131 (2009).
 - ⁵ X. Chen, Z. Gu, and X. Wen, Physical Review B **83**, 035107 (2011).
 - ⁶ X. Chen, Z. Gu, and X. Wen, arXiv:1103.3323 .
 - ⁷ F. Pollmann, E. Berg, A. M. Turner, and M. Oshikawa, Phys. Rev. B **85**, 075125 (2012).
 - ⁸ F. Pollmann, A. M. Turner, E. Berg, and M. Oshikawa, Phys. Rev. B **81**, 064439 (2010).
 - ⁹ N. Schuch, D. Pérez-García, and I. Cirac, Phys. Rev. B **84**, 165139 (2011).
 - ¹⁰ I. Affleck, T. Kennedy, E. H. Lieb, and H. Tasaki, Phys. Rev. Lett. **59**, 799 (1987).
 - ¹¹ M. Fannes, B. Nachtergaele, and R. W. Werner, Commun. Math. Phys. **144**, 443 (1992).
 - ¹² H. Niggemann and J. Zittartz, Euro. Phys. J. B **10**, 731 (1999).
 - ¹³ C. R. Laumann, S. A. Parameswaran, S. L. Sondhi, and F. Zamponi, Phys. Rev. B **81**, 174204 (2010).
 - ¹⁴ D. A. Tomalia and P. R. Dvornic, Nature **372**, 617 (1994).
 - ¹⁵ C. Wu, Modern Physics Letters B **20**, 1707 (2006).
 - ¹⁶ Y. A. Fridman, O. A. Kosmachev, A. K. Kolezhuk, and B. A. Ivanov, Phys. Rev. Lett. **106**, 097202 (2011).
 - ¹⁷ S. Rachel and A. M. Läuchli, Manuscript in preparation (2013).
 - ¹⁸ G. Vidal, Phys. Rev. Lett. **98**, 070201 (2007).
 - ¹⁹ M. A. Martín-Delgado, J. Rodríguez-Laguna, and G. Sierra, Phys. Rev. B **65**, 155116 (2002).
 - ²⁰ D. Nagaj, E. Farhi, J. Goldstone, P. Shor, and I. Sylvester, Phys. Rev. B **77**, 214431 (2008).
 - ²¹ A. Nagy, Annals of Physics **327**, 542 (2012).
 - ²² M. Kumar, S. Ramasesha, and Z. G. Soos, Phys. Rev. B **85**, 134415 (2012).
 - ²³ W. Li, J. von Delft, and T. Xiang, Phys. Rev. B **86**, 195137 (2012).
 - ²⁴ H. Falk, Phys. Rev. B **12**, 5184 (1975).
 - ²⁵ K. Chakraborty, Zeitschrift für Physik B Condensed Matter **55**, 231 (1984).
 - ²⁶ D. J. Thouless, Phys. Rev. Lett. **56**, 1082 (1986).
 - ²⁷ M. Ostilli, Physica A **391**, 3417 (2012).
 - ²⁸ H. J. Changlani, S. Ghosh, C. L. Henley, and A. M. Läuchli, Phys. Rev. B **87**, 085107 (2013).
 - ²⁹ Y.-Y. Shi, L.-M. Duan, and G. Vidal, Physical Review A **74**, 022320 (2006).
 - ³⁰ L. Tagliacozzo, G. Evenbly, and G. Vidal, Physical Review B **80**, 235127 (2009).
 - ³¹ V. Murg, F. Verstraete, Legeza, and R. M. Noack, Physical Review B **82**, 205105 (2010).
 - ³² G. Vidal, J. I. Latorre, E. Rico, and A. Kitaev, Phys. Rev. Lett. **90**, 227902 (2003).
 - ³³ R. Orús and G. Vidal, Phys. Rev. B **78**, 155117 (2008).
 - ³⁴ U. Schollwöck, Reviews of Modern Physics **77**, 259 (2005).
 - ³⁵ U. Schollwöck, Annals of Physics **326**, 96 (2011).
 - ³⁶ M. B. Hastings, J. Stat. Mech. **2007**, P08024 (2007).
 - ³⁷ D. Gottesman and M. B. Hastings, arXiv:0901.1108 .
 - ³⁸ N. Schuch, M. M. Wolf, F. Verstraete, and J. I. Cirac, Phys. Rev. Lett. **100**, 030504 (2008).
 - ³⁹ G. Vidal, Phys. Rev. Lett. **91**, 147902 (2003).
 - ⁴⁰ D. Pérez-García, M. Wolf, M. Sanz, F. Verstraete, and J. Cirac, Phys. Rev. Lett. **100**, 167202 (2008).
 - ⁴¹ E. Schmidt, Math. Annalen **63** (1907).
 - ⁴² D. Perez-Garcia, F. Verstraete, M. Wolf, and J. Cirac, Quantum Inf. Comput. **7**, 401 (2007).
 - ⁴³ F. Verstraete, J. J. García-Ripoll, and J. I. Cirac, Phys. Rev. Lett. **93**, 207204 (2004).
 - ⁴⁴ G. Vidal, Phys. Rev. Lett. **101**, 110501 (2008).
 - ⁴⁵ H. Jiang, Z. Weng, and T. Xiang, Phys. Rev. Lett **101**, 090603 (2008).
 - ⁴⁶ L. Wang, I. Pizorn, and F. Verstraete, Phys. Rev. B **83**, 134421 (2011).
 - ⁴⁷ S. Singh, R. N. C. Pfeifer, and G. Vidal, Phys. Rev. A , 050301 (2010).
 - ⁴⁸ S. Singh, arXiv:1203.2222 .
 - ⁴⁹ Z.-C. Gu and X.-G. Wen, Phys. Rev. B **80**, 155131 (2009).
 - ⁵⁰ L. Fidkowski and A. Kitaev, Phys. Rev. B **81**, 134509 (2010).
 - ⁵¹ A. M. Turner, F. Pollmann, and E. Berg, arXiv:1008.4346 .
 - ⁵² X. Chen, Z.-C. Gu, and X.-G. Wen, Phys. Rev. B **83**, 035107 (2011).
 - ⁵³ X. Chen, Z.-C. Gu, and X.-G. Wen, Phys. Rev. B **84**, 235128 (2011).

5 Summary and Outlook

In this thesis we have demonstrated the application of numerical algorithms based on matrix product states to different problems in more than one dimension. In the process we have introduced new algorithms based on tensor product states and modified existing algorithms to deal with large systems. Additionally, we have learned how tensor networks can be modified to treat fermions and how single-site DMRG can be parallelized. All of these advances enable the simulation of large two-dimensional systems on high-performance computing clusters.

The highly efficient $SU(2)$ symmetric DMRG algorithm allowed us to study the ground state of the kagome lattice Heisenberg antiferromagnet with very good accuracy and precision in both the spin $S = 0$ and the spin $S = 1$ sectors of the system, thereby yielding the spin gap in a reliable manner. Having access to the resulting wave functions in their MPS representation enabled us to study various ground state properties of this system. By performing a careful analysis of the massive amounts of data we were able to exclude the presence of any conventional order in this system. At the same time, the generalization of the entanglement entropy to arbitrary Renyi indices made it possible for us to show for the first time the applicability of this quantum information measure to realistic problems, thereby identifying topological order. Altogether, this study presents a very complete characterization of the kagome lattice Heisenberg antiferromagnet and its properties, while also giving a very competitive ground state energy.

Even though numerics can contribute significantly to the study of previously unknown ground states, it is still the analytical theory that explains why and how these observations fit together. This phenomenological theory is still missing in the case of the kagome HAFM. While there are many proposals for a gapped spin liquid with a total quantum dimension of 2, it is not clear yet which of those proposals is the one that actually constitutes the ground states. Likely candidates include a doubled semion theory or a $Z_2 \times Z_2$ theory. To determine the exact type of low-energy theory we need to compute the exchange statistics of the topological quasi-particles. This calculation has been performed for some models using different methods, but the characterization of the topological quantum field theory underlying the kagome HAFM still remains to be done.

Furthermore, the investigation of the applicability of the tensor product algorithms to the Bethe lattice marks one of the first applications of the novel tensor product algorithms to systems with non-conventional order in more than one dimension. Employing this new method with enlarged unit cells enabled us to investigate the full phase diagram, finding both conventional order and a realization of the Haldane phase in higher-dimensional systems. By analyzing various observables, such as the entanglement spectrum and edge spins as well as string order we were able to conclusively

show this phase to exhibit symmetry-protected topological order.

These applications showcase just two examples in a field that is rapidly evolving. Where a few years ago quantum Monte Carlo dominated the study of two-dimensional system we now have the tools available to also treat frustrated and fermionic models that are close off to QMC due to the sign problem. At the same time the concept of topological order has matured and with the influx of new ideas from quantum information theory offers a wealth of interesting problems. Some of these problems are related to old questions concerning the validity of topological order at finite temperatures and the robustness of spin liquids. Studying these models with finite-temperature methods and after finite times we may be in a position to answer some of these questions.

Bibliography

- [1] K. G. Wilson, The renormalization group: Critical phenomena and the Kondo problem, *Rev. Mod. Phys.* **47**, 773–840 (1975).
- [2] J. Bardeen, L. N. Cooper, and J. R. Schrieffer, Theory of Superconductivity, *Phys. Rev.* **108**, 1175–1204 (1957).
- [3] M. H. Anderson, J. R. Ensher, M. R. Matthews, C. E. Wieman, and E. A. Cornell, Observation of Bose-Einstein Condensation in a Dilute Atomic Vapor, *Science* **269**, 198–201 (1995).
- [4] E. Kim and M. H. W. Chan, Observation of Superflow in Solid Helium, *Science* **305**, 1941–1944 (2004).
- [5] J. G. Bednorz and K. A. Müller, Possible high T_C superconductivity in the *BaLaCuO* system, *Zeitschrift für Physik B* **64**, 189–193 (1986).
- [6] B. Blok and X. G. Wen, Effective theories of the fractional quantum Hall effect: Hierarchy construction, *Physical Review B* **42**, 8145–8156 (1990).
- [7] F. D. M. Haldane and E. H. Rezayi, Periodic Laughlin-Jastrow wave functions for the fractional quantized Hall effect, *Physical Review B* **31**, 2529–2531 (1985).
- [8] T. Hansson, V. Oganesyan, and S. Sondhi, Superconductors are topologically ordered, *Annals of Physics* **313**, 497–538 (2004).
- [9] V. Kalmeyer and R. B. Laughlin, Equivalence of the resonating-valence-bond and fractional quantum Hall states, *Physical Review Letters* **59**, 2095–2098 (1987).
- [10] X. G. Wen, Gapless boundary excitations in the quantum Hall states and in the chiral spin states, *Physical Review B* **43**, 11025–11036 (1991).
- [11] X. G. Wen and Q. Niu, Ground-state degeneracy of the fractional quantum Hall states in the presence of a random potential and on high-genus Riemann surfaces, *Physical Review B* **41**, 9377–9396 (1990).
- [12] X.-G. Wen, Quantum orders and symmetric spin liquids, *Physical Review B* **65**, 165113 (2002).
- [13] E. Witten, Quantum field theory and the Jones polynomial, *Communications in Mathematical Physics* **121**, 351–399 (1989).

- [14] X.-G. Wen, Topological Order: From Long-Range Entangled Quantum Matter to a Unified Origin of Light and Electrons, *ISRN Condensed Matter Physics* **2013**, 1–20 (2013).
- [15] L. Amico, R. Fazio, A. Osterloh, and V. Vedral, Entanglement in many-body systems, *Rev. Mod. Phys.* **80**, 517–576 (2008).
- [16] D. Gottesman and M. B. Hastings, Entanglement versus gap for one-dimensional spin systems, *New Journal of Physics* **12**, 025002 (2010).
- [17] M. B. Hastings, Entropy and entanglement in quantum ground states, *Physical Review B* **76**, 035114 (2007).
- [18] P. Ye and X.-G. Wen, 2D Lattice Model Construction of Symmetry-Protected Topological Phases, *arXiv:1212.2121* (2012).
- [19] X. G. Wen, Mean-field theory of spin-liquid states with finite energy gap and topological orders, *Physical Review B* **44**, 2664–2672 (1991).
- [20] X. Chen, Z.-C. Gu, and X.-G. Wen, Local unitary transformation, long-range quantum entanglement, wave function renormalization, and topological order, *Physical Review B* **82**, 155138 (2010).
- [21] P. W. Anderson, The Resonating Valence Bond State in La_2CuO_4 and Superconductivity, *Science* **235**, 1196–1198 (1987).
- [22] P. W. Anderson, G. Baskaran, Z. Zou, and T. Hsu, Resonating-valence-bond theory of phase transitions and superconductivity in La_2CuO_4 -based compounds, *Physical Review Letters* **58**, 2790–2793 (1987).
- [23] G. Baskaran, Z. Zou, and P. Anderson, The resonating valence bond state and high- T_c superconductivity — A mean field theory, *Solid State Communications* **63**, 973–976 (1987).
- [24] S. A. Kivelson and D. S. Rokhsar, Bogoliubov quasiparticles, spinons, and spin-charge decoupling in superconductors, *Physical Review B* **41**, 11693–11696 (1990).
- [25] S. A. Kivelson, D. S. Rokhsar, and J. P. Sethna, Topology of the resonating valence-bond state: Solitons and high- T_c superconductivity, *Physical Review B* **35**, 8865–8868 (1987).
- [26] G. Kotliar and J. Liu, Superexchange mechanism and d-wave superconductivity, *Physical Review B* **38**, 5142–5145 (1988).
- [27] X. G. Wen, F. Wilczek, and A. Zee, Chiral spin states and superconductivity, *Physical Review B* **39**, 11413–11423 (1989).
- [28] X. G. Wen, Vacuum degeneracy of chiral spin states in compactified space, *Physical Review B* **40**, 7387–7390 (1989).

-
- [29] A. Kitaev, Fault-tolerant quantum computation by anyons, *Annals of Physics* **303**, 2–30 (2003).
- [30] S. Das Sarma, M. Freedman, and C. Nayak, Topologically Protected Qubits from a Possible Non-Abelian Fractional Quantum Hall State, *Phys. Rev. Lett.* **94**, 166802 (2005).
- [31] I. Bloch, J. Dalibard, and W. Zwerger, Many-body physics with ultracold gases, *Reviews of Modern Physics* **80**, 885 (2008).
- [32] M. P. A. Fisher, P. B. Weichman, G. Grinstein, and D. S. Fisher, Boson localization and the superfluid-insulator transition, *Phys. Rev. B* **40**, 546–570 (1989).
- [33] M. Lewenstein, A. Sanpera, V. Ahufinger, B. Damski, A. Sen, and U. Sen, Ultracold atomic gases in optical lattices: mimicking condensed matter physics and beyond, *Advances in Physics* **56**, 243 – 379 (2007).
- [34] F. C. Coomer, A. Harrison, G. S. Oakley, J. Kulda, J. R. Stewart, J. A. Stride, B. Fåk, J. W. Taylor, and D. Visser, Inelastic neutron scattering study of magnetic excitations in the kagome antiferromagnet potassium jarosite, *Journal of Physics: Condensed Matter* **18**, 8847 (2006).
- [35] J. S. Helton, Y. Chen, G. L. Bychkov, S. N. Barilo, N. Rogado, R. J. Cava, and J. W. Lynn, Evolution of the commensurate and incommensurate magnetic phases of the $S = 3/2$ kagome staircase $\text{Co}_3\text{V}_2\text{O}_8$ in an applied field, *Journal of Physics: Condensed Matter* **24**, 016003 (2012).
- [36] E. Lhotel, V. Simonet, J. Ortloff, B. Canals, C. Paulsen, E. Suard, T. Hansen, D. J. Price, P. T. Wood, A. K. Powell, and R. Ballou, Domain-Wall Spin Dynamics in Kagome Antiferromagnets, *Phys. Rev. Lett.* **107**, 257205 (2011).
- [37] R. Z. Bachrach, *Synchrotron radiation research: advances in surface and interface science. Techniques*, volume 1, Plenum Pub Corp (1992).
- [38] J. Braun, The theory of angle-resolved ultraviolet photoemission and its applications to ordered materials, *Reports on Progress in Physics* **59**, 1267 (1996).
- [39] J. D. Koralek, J. F. Douglas, N. C. Plumb, Z. Sun, A. V. Fedorov, M. M. Murnane, H. C. Kapteyn, S. T. Cundiff, Y. Aiura, K. Oka, H. Eisaki, and D. S. Dessau, Laser Based Angle-Resolved Photoemission, the Sudden Approximation, and Quasiparticle-Like Spectral Peaks in $\text{Bi}_2\text{Sr}_2\text{CaCu}_2\text{O}_{8+\delta}$, *Phys. Rev. Lett.* **96**, 017005 (2006).
- [40] R. M. Noack and S. R. Manmana, Diagonalization- and Numerical Renormalization-Group-Based Methods for Interacting Quantum Systems, in A. Avella and F. Mancini, editors, *LECTURES ON THE PHYSICS OF HIGHLY CORRELATED ELECTRON SYSTEMS IX: Ninth Training Course*

- in the Physics of Correlated Electron Systems and High-Tc Superconductors*, volume 789, pages 93–163, AIP (2005).
- [41] D. M. Ceperley and B. J. Alder, Ground State of the Electron Gas by a Stochastic Method, *Phys. Rev. Lett.* **45**, 566–569 (1980).
- [42] W. M. C. Foulkes, L. Mitas, R. J. Needs, and G. Rajagopal, Quantum Monte Carlo simulations of solids, *Rev. Mod. Phys.* **73**, 33–83 (2001).
- [43] J. Oitmaa, C. Hamer, and W. Zheng, *Series Expansion Methods for Strongly Interacting Lattice Models*, Cambridge University Press, Cambridge, England (2006).
- [44] M. Rigol, T. Bryant, and R. R. P. Singh, Numerical linked-cluster algorithms. I. Spin systems on square, triangular, and kagomé lattices, *Phys. Rev. E* **75**, 061118 (2007).
- [45] S. R. White, Density matrix formulation for quantum renormalization groups, *Phys. Rev. Lett.* **69**, 2863–2866 (1992).
- [46] S. Östlund and S. Rommer, Thermodynamic Limit of Density Matrix Renormalization, *Phys. Rev. Lett.* **75**, 3537–3540 (1995).
- [47] S. Rommer and S. Östlund, Class of ansatz wave functions for one-dimensional spin systems and their relation to the density matrix renormalization group, *Phys. Rev. B* **55**, 2164–2181 (1997).
- [48] I. P. McCulloch, From density-matrix renormalization group to matrix product states, *Journal of Statistical Mechanics: Theory and Experiment* **2007**, P10014–P10014 (2007).
- [49] U. Schollwöck, The density-matrix renormalization group, *Reviews of Modern Physics* **77**, 259 (2005).
- [50] U. Schollwöck, The density-matrix renormalization group in the age of matrix product states, *Annals of Physics* **326**, 96–192 (2011).
- [51] G. Evenbly and G. Vidal, A real space decoupling transformation for quantum many-body systems, *arXiv:1205.0639* (2012).
- [52] G. Evenbly and G. Vidal, Quantum Criticality with the Multi-scale Entanglement Renormalization Ansatz, *1109.5334* (2011).
- [53] G. Evenbly and G. Vidal, Tensor Network States and Geometry, *Journal of Statistical Physics* **145**, 891–918 (2011).
- [54] P. Corboz, S. R. White, G. Vidal, and M. Troyer, Stripes in the two-dimensional t - J model with infinite projected entangled-pair states, *Phys. Rev. B* **84**, 041108 (2011).

-
- [55] V. Murg, F. Verstraete, Ö. Legeza, and R. M. Noack, Simulating strongly correlated quantum systems with tree tensor networks, *Physical Review B* **82**, 205105 (2010).
- [56] G. Evenbly and G. Vidal, Frustrated Antiferromagnets with Entanglement Renormalization: Ground State of the Spin-1/2 Heisenberg Model on a Kagome Lattice, *Physical Review Letters* **104**, 187203 (2010).
- [57] R. Orus, A. C. Doherty, and G. Vidal, First order phase transition in the anisotropic quantum orbital compass model, *Phys. Rev. Lett.* **102**, 077203 (2009).
- [58] R. N. C. Pfeifer, G. Evenbly, and G. Vidal, Entanglement renormalization, scale invariance, and quantum criticality, *Phys. Rev. A* **79**, 040301 (2009).
- [59] J. Jordan, R. Orús, and G. Vidal, Numerical study of the hard-core Bose-Hubbard model on an infinite square lattice, *Phys. Rev. B* **79**, 174515 (2009).
- [60] G. Vidal, A class of quantum many-body states that can be efficiently simulated, *Physical Review Letters* **101**, 110501 (2008).
- [61] J. Jordan, R. Orús, G. Vidal, F. Verstraete, and J. I. Cirac, Classical Simulation of Infinite-Size Quantum Lattice Systems in Two Spatial Dimensions, *Physical Review Letters* **101**, 250602 (2008).
- [62] G. Evenbly and G. Vidal, Entanglement Renormalization in Two Spatial Dimensions, *Phys. Rev. Lett.* **102**, 180406 (2009).
- [63] M. Aguado and G. Vidal, Entanglement Renormalization and Topological Order, *Physical Review Letters* **100**, 070404 (2008).
- [64] Y.-Y. Shi, L.-M. Duan, and G. Vidal, Classical simulation of quantum many-body systems with a tree tensor network, *Physical Review A* **74**, 022320 (2006).
- [65] L. Wang, D. Poilblanc, Z.-C. Gu, X.-G. Wen, and F. Verstraete, Constructing gapless spin liquid state for the spin-1/2 J1-J2 Heisenberg model on a square lattice, *arXiv:1301.4492* (2013).
- [66] V. Murg, V. E. Korepin, and F. Verstraete, Algebraic Bethe ansatz and tensor networks, *Phys. Rev. B* **86**, 045125 (2012).
- [67] L. Wang, Z.-C. Gu, X.-G. Wen, and F. Verstraete, Possible spin liquid state in the spin 1/2 J1-J2 antiferromagnetic Heisenberg model on square lattice: A tensor product state approach, *1112.3331* (2011).
- [68] L. Wang and F. Verstraete, Cluster update for tensor network states, *1110.4362* (2011).

- [69] J. I. Cirac, D. Poilblanc, N. Schuch, and F. Verstraete, Entanglement spectrum and boundary theories with projected entangled-pair states, *Physical Review B* **83**, 245134 (2011).
- [70] M. Schwarz, K. Temme, and F. Verstraete, Preparing Projected Entangled Pair States on a Quantum Computer, *Phys. Rev. Lett.* **108**, 110502 (2012).
- [71] I. Pižorn, L. Wang, and F. Verstraete, Time evolution of projected entangled pair states in the single-layer picture, *Phys. Rev. A* **83**, 052321 (2011).
- [72] J. Haegeman, T. J. Osborne, H. Verschelde, and F. Verstraete, Entanglement Renormalization for Quantum Fields in Real Space, *Phys. Rev. Lett.* **110**, 100402 (2013).
- [73] L. Wang, I. Pižorn, and F. Verstraete, Monte Carlo simulation with tensor network states, *Phys. Rev. B* **83**, 134421 (2011).
- [74] Z.-C. Gu, F. Verstraete, and X.-G. Wen, Grassmann tensor network states and its renormalization for strongly correlated fermionic and bosonic states, *1004.2563* (2010).
- [75] V. Murg, F. Verstraete, and J. I. Cirac, Exploring frustrated spin systems using projected entangled pair states, *Phys. Rev. B* **79**, 195119 (2009).
- [76] V. Murg, F. Verstraete, and J. I. Cirac, Variational study of hard-core bosons in a two-dimensional optical lattice using Projected Entangled Pair States, *Physical Review A (Atomic, Molecular, and Optical Physics)* **75**, 033605 (2007).
- [77] F. Verstraete, M. M. Wolf, D. Perez-Garcia, and J. I. Cirac, Criticality, the Area Law, and the Computational Power of Projected Entangled Pair States, *Physical Review Letters* **96**, 220601 (2006).
- [78] F. Verstraete, J. J. García-Ripoll, and J. I. Cirac, Matrix Product Density Operators: Simulation of Finite-Temperature and Dissipative Systems, *Phys. Rev. Lett.* **93**, 207204 (2004).
- [79] F. Verstraete and J. I. Cirac, Renormalization algorithms for Quantum-Many Body Systems in two and higher dimensions, *cond-mat/0407066* (2004).
- [80] W. Li, J. von Delft, and T. Xiang, Efficient simulation of infinite tree tensor network states on the Bethe lattice, *Physical Review B* **86**, 195137 (2012).
- [81] H. H. Zhao, Z. Y. Xie, Q. N. Chen, Z. C. Wei, J. W. Cai, and T. Xiang, Renormalization of tensor-network states, *Physical Review B* **81**, 174411 (2010).
- [82] H. C. Jiang, Z. Y. Weng, and T. Xiang, Accurate Determination of Tensor Network State of Quantum Lattice Models in Two Dimensions, *Physical Review Letters* **101**, 090603 (2008).

-
- [83] Z. Y. Xie, H. C. Jiang, Q. N. Chen, Z. Y. Weng, and T. Xiang, Second Renormalization of Tensor-Network States, *Phys. Rev. Lett.* **103**, 160601 (2009).
- [84] M. Fannes, B. Nachtergaele, and R. Werner, Finitely Correlated States on Quantum Spin Chains, *Communications in Mathematical Physics* **144**, 443–490 (1992).
- [85] M. B. Hastings, Light-cone matrix product, *Journal of Mathematical Physics* **50**, 095207–095207–17 (2009).
- [86] D. Perez-Garcia, F. Verstraete, M. M. Wolf, and J. I. Cirac, Matrix Product State Representations, *Quantum Inf. Comput.* **7**, 401 (2007).
- [87] N. Schuch, M. M. Wolf, F. Verstraete, and J. I. Cirac, Entropy Scaling and Simulability by Matrix Product States, *Phys. Rev. Lett.* **100**, 030504 (2008).
- [88] F. Verstraete, J. I. Cirac, J. I. Latorre, E. Rico, and M. M. Wolf, Renormalization-Group Transformations on Quantum States, *Physical Review Letters* **94**, 140601 (2005).
- [89] J. I. Cirac and G. Sierra, Infinite matrix product states, conformal field theory, and the Haldane-Shastry model, *Physical Review B* **81**, 104431 (2010).
- [90] S. R. White and A. E. Feiguin, Real-Time Evolution Using the Density Matrix Renormalization Group, *Phys. Rev. Lett.* **93**, 076401 (2004).
- [91] A. J. Daley, C. Kollath, U. Schollwöck, and G. Vidal, Time-dependent density-matrix renormalization-group using adaptive effective Hilbert spaces, *Journal of Statistical Mechanics: Theory and Experiment* **2004**, P04005 (2004).
- [92] P. E. Dargel, A. Honecker, R. Peters, R. M. Noack, and T. Pruschke, Adaptive Lanczos-vector method for dynamic properties within the density matrix renormalization group, *Phys. Rev. B* **83**, 161104 (2011).
- [93] S. R. White and D. J. Scalapino, Density Matrix Renormalization Group Study of the Striped Phase in the 2D t-J Model, *Physical Review Letters* **80**, 1272–1275 (1998).
- [94] S. R. White, Spin Gaps in a Frustrated Heisenberg Model for CaV_4O_9 , *Physical Review Letters* **77**, 3633–3636 (1996).
- [95] E. M. Stoudenmire, L. O. Wagner, S. R. White, and K. Burke, One-Dimensional Continuum Electronic Structure with the Density-Matrix Renormalization Group and Its Implications for Density-Functional Theory, *Phys. Rev. Lett.* **109**, 056402 (2012).
- [96] E. M. Stoudenmire and S. R. White, Studying Two-Dimensional Systems with the Density Matrix Renormalization Group, in Langer, JS, editor, *ANNUAL REVIEW OF CONDENSED MATTER PHYSICS, VOL 3*, volume 3 of *Annual Review of Condensed Matter Physics*, pages 111–128 (2012).

- [97] A. Weichselbaum and S. R. White, Incommensurate correlations in the anisotropic triangular Heisenberg lattice, *Phys. Rev. B* **84**, 245130 (2011).
- [98] Z. Zhu, D. A. Huse, and S. R. White, Weak Plaquette Valence Bond Order in the $S=1/2$ Honeycomb J_1-J_2 Heisenberg Model, *Phys. Rev. Lett.* **110**, 127205 (2013).
- [99] D. J. Scalapino and S. R. White, Stripe Structures in the t-t'-J Model, *arXiv:1204.5212* (2012).
- [100] S. Yan, D. A. Huse, and S. R. White, Spin-Liquid Ground State of the $S = 1/2$ Kagome Heisenberg Antiferromagnet, *Science* **332**, 1173–1176 (2011).
- [101] S. R. White and A. L. Chernyshev, Néel Order in Square and Triangular Lattice Heisenberg Models, *Physical Review Letters* **99**, 127004 (2007).
- [102] S. R. White and D. J. Scalapino, Energetics of Domain Walls in the 2D t-J Model, *Physical Review Letters* **81**, 3227–3230 (1998).
- [103] A. Ekert and P. L. Knight, Entangled quantum systems and the Schmidt decomposition, *American Journal of Physics* **63**, 415–423 (1995).
- [104] E. Schmidt, Zur Theorie der linearen und nichtlinearen Integralgleichungen, *Mathematische Annalen* **63**, 433–476 (1907).
- [105] M. Nielsen and I. Chuang, *Quantum Computation and Quantum Information*, Cambridge University Press, Cambridge, England (2000).
- [106] L. Tagliacozzo, T. R. de Oliveira, S. Iblisdir, and J. I. Latorre, Scaling of entanglement support for matrix product states, *Physical Review B (Condensed Matter and Materials Physics)* **78**, 024410 (2008).
- [107] F. Verstraete, V. Murg, and J. Cirac, Matrix product states, projected entangled pair states, and variational renormalization group methods for quantum spin systems, *Advances In Physics* **57**, 143–224 (2008).
- [108] F. Verstraete and J. I. Cirac, Matrix product states represent ground states faithfully, *Physical Review B* **73**, 094423 (2006).
- [109] G. Vidal, Efficient Classical Simulation of Slightly Entangled Quantum Computations, *Phys. Rev. Lett.* **91**, 147902 (2003).
- [110] G. Vidal, Efficient Simulation of One-Dimensional Quantum Many-Body Systems, *Phys. Rev. Lett.* **93**, 040502 (2004).
- [111] G. Vidal, Classical simulation of infinite-size quantum lattice systems in one spatial dimension, *Phys. Rev. Lett.* **98**, 070201 (2007).
- [112] I. P. McCulloch, Infinite size density matrix renormalization group, revisited, *arXiv:0804.2509* (2008).

-
- [113] H. N. Phien, G. Vidal, and I. P. McCulloch, Infinite boundary conditions for matrix product state calculations, *Phys. Rev. B* **86**, 245107 (2012).
- [114] H. N. Phien, G. Vidal, and I. P. McCulloch, Dynamical windows for real-time evolution with matrix product states, *arXiv:1207.0678* (2012).
- [115] R. Orús and G. Vidal, Infinite time-evolving block decimation algorithm beyond unitary evolution, *Physical Review B* **78**, 155117 (2008).
- [116] J. I. Cirac and F. Verstraete, Renormalization and tensor product states in spin chains and lattices, *Journal of Physics A: Mathematical and Theoretical* **42**, 504004 (2009).
- [117] G. Evenbly, Foundations and Applications of Entanglement Renormalization, *1109.5424* (2011).
- [118] L. Cincio, J. Dziarmaga, and M. M. Rams, Multiscale Entanglement Renormalization Ansatz in Two Dimensions: Quantum Ising Model, *Physical Review Letters* **100**, 240603 (2008).
- [119] C. M. Dawson, J. Eisert, and T. J. Osborne, Unifying Variational Methods for Simulating Quantum Many-Body Systems, *Physical Review Letters* **100**, 130501 (2008).
- [120] A. Gendiar, T. Nishino, and R. Derian, Estimation of the Magnetic Critical Exponent by Tensor Product Variational Approach, *Acta Phys. Slov.* **55**, 141 (2005).
- [121] A. Gendiar, N. Maeshima, and T. Nishino, Stable Optimization of a Tensor Product Variational State, *Progress of Theoretical Physics* **110**, 691–699 (2003).
- [122] T. Nishino, K. Okunishi, Y. Hieida, N. Maeshima, Y. Akutsu, and A. Gendiar, Two-Dimensional Tensor Product Variational Formulation, *Progress of Theoretical Physics* **105**, 409–417 (2001).
- [123] T. Nishino, K. Okunishi, Y. Hieida, N. Maeshima, and Y. Akutsu, Self-Consistent Tensor Product Variational Approximation for 3D Classical Models, *Nuclear Physics B* **575**, 504–512 (2000).
- [124] T. Barthel, M. Kliesch, and J. Eisert, Real-Space Renormalization Yields Finite Correlations, *Phys. Rev. Lett.* **105**, 010502 (2010).
- [125] R. Orús, Exploring corner transfer matrices and corner tensors for the classical simulation of quantum lattice systems, *Physical Review B* **85**, 205117 (2012).
- [126] S. Dusuel, M. Kamfor, R. Orús, K. P. Schmidt, and J. Vidal, Robustness of a Perturbed Topological Phase, *Physical Review Letters* **106**, 107203 (2011).

- [127] R. Orús, T.-C. Wei, and H.-H. Tu, Phase diagram of the $SO(n)$ bilinear-biquadratic chain from many-body entanglement, *Phys. Rev. B* **84**, 064409 (2011).
- [128] B. Bauer, P. Corboz, A. M. Läuchli, L. Messio, K. Penc, M. Troyer, and F. Mila, Three-sublattice order in the $SU(3)$ Heisenberg model on the square and triangular lattice, *Phys. Rev. B* **85**, 125116 (2012).
- [129] A. J. Ferris and G. Vidal, Perfect sampling with unitary tensor networks, *Phys. Rev. B* **85**, 165146 (2012).
- [130] B. Bauer, G. Vidal, and M. Troyer, Assessing the accuracy of projected entangled-pair states on infinite lattices, *Journal of Statistical Mechanics: Theory and Experiment* **2009**, P09006 (2009).
- [131] T. Barthel, C. Pineda, and J. Eisert, Contraction of fermionic operator circuits and the simulation of strongly correlated fermions, *Physical Review A* **80**, 042333 (2009).
- [132] P. Corboz, J. Jordan, and G. Vidal, Simulation of fermionic lattice models in two dimensions with projected entangled-pair states: Next-nearest neighbor Hamiltonians, *Physical Review B* **82**, 245119 (2010).
- [133] P. Corboz, G. Evenbly, F. Verstraete, and G. Vidal, Simulation of interacting fermions with entanglement renormalization, *Physical Review A* **81**, 010303 (2010).
- [134] P. Corboz and G. Vidal, Fermionic multiscale entanglement renormalization ansatz, *Physical Review B* **80**, 165129 (2009).
- [135] I. Pižorn and F. Verstraete, Fermionic implementation of projected entangled pair states algorithm, *Physical Review B* **81**, 245110 (2010).
- [136] C. V. Kraus, N. Schuch, F. Verstraete, and J. I. Cirac, Fermionic projected entangled pair states, *Physical Review A* **81**, 052338 (2010).
- [137] Z.-C. Gu, Efficient simulation of Grassmann Tensor Product States, *1109.4470* (2011).
- [138] C. Pineda, T. Barthel, and J. Eisert, Unitary circuits for strongly correlated fermions, *Phys. Rev. A* **81**, 050303 (2010).
- [139] I. P. McCulloch and M. Gulácsi, The non-Abelian density matrix renormalization group algorithm, *EPL (Europhysics Letters)* **57**, 852 (2002).
- [140] S. Singh and G. Vidal, Symmetry protected entanglement renormalization, *arXiv:1303.6716* (2013).
- [141] S. Singh and G. Vidal, Tensor network states and algorithms in the presence of a global $SU(2)$ symmetry, *Phys. Rev. B* **86**, 195114 (2012).

-
- [142] S. Singh, Tensor Network States and Algorithms in the presence of Abelian and non-Abelian Symmetries, *arXiv:1203.2222* (2012).
- [143] S. Singh, H.-Q. Zhou, and G. Vidal, Simulation of one-dimensional quantum systems with a global SU(2) symmetry, *New Journal of Physics* **12**, 033029 (2010).
- [144] S. Singh, R. N. C. Pfeifer, and G. Vidal, Tensor network decompositions in the presence of a global symmetry, *Phys. Rev. A* **82**, 050301 (2010).
- [145] G. M. Crosswhite, A. C. Doherty, and G. Vidal, Applying matrix product operators to model systems with long-range interactions, *Phys. Rev. B* **78**, 035116 (2008).
- [146] G. M. Crosswhite and D. Bacon, Finite automata for caching in matrix product algorithms, *Phys. Rev. A* **78**, 012356 (2008).
- [147] S. R. White, Density matrix renormalization group algorithms with a single center site, *Physical Review B* **72**, 180403 (2005).
- [148] E. M. Stoudenmire and S. R. White, Real-space parallel density matrix renormalization group, *Physical Review B* **87**, 155137 (2013).
- [149] T. Grover, Entanglement Entropy and Strongly Correlated Topological Matter, *Modern Physics Letters A* **28**, 1330001 (2013).
- [150] T. Grover, Y. Zhang, and A. Vishwanath, Entanglement entropy as a portal to the physics of quantum spin liquids, *New Journal of Physics* **15**, 025002 (2013).
- [151] Y. Zhang, T. Grover, and A. Vishwanath, Entanglement Entropy of Critical Spin Liquids, *Physical Review Letters* **107**, 067202 (2011).
- [152] Y. Zhang, T. Grover, and A. Vishwanath, Topological entanglement entropy of Z_2 spin liquids and lattice Laughlin states, *Physical Review B* **84**, 075128 (2011).
- [153] L. Balents, Spin liquids in frustrated magnets, *Nature* **464**, 199–208 (2010).
- [154] N. Read and B. Chakraborty, Statistics of the excitations of the resonating-valence-bond state, *Physical Review B* **40**, 7133–7140 (1989).
- [155] N. Read and S. Sachdev, Large-N expansion for frustrated quantum antiferromagnets, *Physical Review Letters* **66**, 1773–1776 (1991).
- [156] S. Sachdev, Kagome- and triangular-lattice Heisenberg antiferromagnets: Ordering from quantum fluctuations and quantum-disordered ground states with unconfined bosonic spinons, *Physical Review B* **45**, 12377–12396 (1992).
- [157] P. Anderson, Resonating valence bonds: A new kind of insulator?, *Materials Research Bulletin* **8**, 153–160 (1973).

- [158] T. Senthil, A. Vishwanath, L. Balents, S. Sachdev, and M. P. A. Fisher, Deconfined Quantum Critical Points, *Science* **303**, 1490–1494 (2004).
- [159] X.-G. Wen, Quantum order: a quantum entanglement of many particles, *Physics Letters A* **300**, 175–181 (2002).
- [160] X. G. Wen and A. Zee, Gapless fermions and quantum order, *Physical Review B* **66**, 235110 (2002).
- [161] Y. Ran, M. Hermele, P. A. Lee, and X.-G. Wen, Projected-Wave-Function Study of the Spin-1/2 Heisenberg Model on the Kagomé Lattice, *Physical Review Letters* **98**, 117205 (2007).
- [162] P. A. Lee, From high temperature superconductivity to quantum spin liquid: progress in strong correlation physics, *Reports on Progress in Physics* **71**, 012501 (2008).
- [163] P. A. Lee and N. Nagaosa, Gauge theory of the normal state of high- T_c superconductors, *Physical Review B* **46**, 5621–5639 (1992).
- [164] M. Hermele, T. Senthil, M. P. A. Fisher, P. A. Lee, N. Nagaosa, and X.-G. Wen, Stability of U(1) spin liquids in two dimensions, *Physical Review B* **70**, 214437 (2004).
- [165] M. Hermele, Y. Ran, P. A. Lee, and X.-G. Wen, Properties of an algebraic spin liquid on the kagome lattice, *Physical Review B* **77**, 224413 (2008).
- [166] C. Lhuillier, Frustrated Quantum Magnets, *cond-mat/0502464* (2005).
- [167] J. B. Marston and C. Zeng, SpinPeierls and spinliquid phases of Kagomé quantum antiferromagnets, *Journal of Applied Physics* **69**, 5962–5964 (1991).
- [168] S. Okumura, H. Kawamura, T. Okubo, and Y. Motome, Novel Spin-Liquid States in the Frustrated Heisenberg Antiferromagnet on the Honeycomb Lattice, *Journal of the Physical Society of Japan* **79**, 114705 (2010).
- [169] G. Misguich, C. Lhuillier, M. Mambrini, and P. Sindzingre, Degeneracy of the ground-state of antiferromagnetic spin-1/2 Hamiltonians, *The European Physical Journal B - Condensed Matter and Complex Systems* **26**, 167–183 (2002).
- [170] P. Sindzingre, C. Lhuillier, and J. B. Fouet, Quantum phases in two-dimensional frustrated spin-1/2 antiferromagnets, *cond-mat/0110283* (2001).
- [171] M. Tamura, A. Nakao, and R. Kato, Frustration-Induced Valence-Bond Ordering in a New Quantum Triangular Antiferromagnet Based on $[\text{Pd}(\text{dmit})_2]$, *Journal of the Physical Society of Japan* **75**, 093701 (2006).

-
- [172] Y. Kohsaka, C. Taylor, K. Fujita, A. Schmidt, C. Lupien, T. Hanaguri, M. Azuma, M. Takano, H. Eisaki, H. Takagi, S. Uchida, and J. C. Davis, An Intrinsic Bond-Centered Electronic Glass with Unidirectional Domains in Underdoped Cuprates, *Science* **315**, 1380–1385 (2007).
- [173] V. Kalmeyer and R. B. Laughlin, Theory of the spin liquid state of the Heisenberg antiferromagnet, *Phys. Rev. B* **39**, 11879–11899 (1989).
- [174] V. A. Zyuzin and G. A. Fiete, Spatially anisotropic kagome antiferromagnet with Dzyaloshinskii-Moriya interaction, *Phys. Rev. B* **85**, 104417 (2012).
- [175] A. Zorko, F. Bert, A. Ozarowski, J. van Tol, D. Boldrin, A. S. Wills, and P. Mendels, Suppression of Quantum Fluctuations by the Dzyaloshinsky-Moriya Interaction in a Kagome Antiferromagnet, *arXiv:1304.3238* (2013).
- [176] M. E. Zhitomirsky, Octupolar ordering of classical kagome antiferromagnets in two and three dimensions, *Physical Review B* **78**, 094423 (2008).
- [177] S.-L. Yu and J.-X. Li, Chiral superconducting phase and chiral spin-density-wave phase in a Hubbard model on the kagome lattice, *Phys. Rev. B* **85**, 144402 (2012).
- [178] D. Wulferding, P. Lemmens, H. Yoshida, Y. Okamoto, and Z. Hiroi, Tuning the spin dynamics of kagome systems, *1111.2167* (2011).
- [179] J. Wildeboer and A. Seidel, Correlation Functions in SU(2)-Invariant Resonating-Valence-Bond Spin Liquids on Nonbipartite Lattices, *Phys. Rev. Lett.* **109**, 147208 (2012).
- [180] Y. Wan and O. Tchernyshyov, Phenomenological Z_2 lattice gauge theory of the spin-liquid state of the kagome Heisenberg antiferromagnet, *arXiv:1301.5008* (2013).
- [181] T. Tay and O. I. Motrunich, Variational study of $J_1 - J_2$ Heisenberg model on kagome lattice using projected Schwinger-boson wave functions, *Physical Review B* **84**, 020404 (2011).
- [182] T. Tay and O. I. Motrunich, Sign structures for short-range RVB states on small kagome clusters, *Phys. Rev. B* **84**, 193102 (2011).
- [183] R. Suttner, C. Platt, J. Reuther, and R. Thomale, Renormalization group analysis of competing quantum phases in the J_1 - J_2 Heisenberg model on the kagome lattice, *arXiv:1303.0579* (2013).
- [184] M. Spenke and S. Guertler, Classical J_1 - J_2 Heisenberg model on the kagome lattice, *Phys. Rev. B* **86**, 054440 (2012).
- [185] R. R. P. Singh and D. A. Huse, Triplet and singlet excitations in the valence bond crystal phase of the kagome lattice Heisenberg model, *Physical Review B* **77**, 144415 (2008).

- [186] R. R. P. Singh and J. Oitmaa, High-temperature series expansion study of the Heisenberg antiferromagnet on the hyperkagome lattice: Comparison with $\text{Na}_4\text{Ir}_3\text{O}_8$, *Phys. Rev. B* **85**, 104406 (2012).
- [187] R. R. P. Singh and D. A. Huse, Ground state of the spin-1/2 kagome-lattice Heisenberg antiferromagnet, *Physical Review B* **76**, 180407 (2007).
- [188] P. Sindzingre and C. Lhuillier, Low-energy excitations of the kagome antiferromagnet and the spin-gap issue, *EPL (Europhysics Letters)* **88**, 27009 (2009).
- [189] D. N. Sheng and L. Balents, Numerical Evidences of Fractionalization in an Easy-Axis Two-Spin Heisenberg Antiferromagnet, *Physical Review Letters* **94**, 146805 (2005).
- [190] V. R. Shaginyan, A. Z. Msezane, and K. G. Popov, Thermodynamic properties of the kagome lattice in herbertsmithite, *Phys. Rev. B* **84**, 060401 (2011).
- [191] D. Schwandt, M. Mambrini, and D. Poilblanc, Generalized hard-core dimer model approach to low-energy Heisenberg frustrated antiferromagnets: General properties and application to the kagome antiferromagnet, *Phys. Rev. B* **81**, 214413 (2010).
- [192] N. Schuch, D. Poilblanc, J. I. Cirac, and D. Pérez-García, Resonating valence bond states in the PEPS formalism, *Physical Review B* **86**, 115108 (2012).
- [193] T. Sakai and H. Nakano, Critical magnetization behavior of the triangular- and kagome-lattice quantum antiferromagnets, *Phys. Rev. B* **83**, 100405 (2011).
- [194] S. Ryu, O. I. Motrunich, J. Alicea, and M. P. A. Fisher, Algebraic vortex liquid theory of a quantum antiferromagnet on the kagome lattice, *Physical Review B* **75**, 184406 (2007).
- [195] A. Rahmani and G.-W. Chern, Universal Renyi mutual information in classical systems: the case of kagome ice, *arXiv:1304.4160* (2013).
- [196] J. A. Quilliam, F. Bert, R. H. Colman, D. Boldrin, A. S. Wills, and P. Mendels, Ground state and intrinsic susceptibility of the kagome antiferromagnet vesignieite as seen by ^{51}V NMR, *Phys. Rev. B* **84**, 180401 (2011).
- [197] D. Poilblanc and N. Schuch, Simplex \mathbb{Z}_2 spin liquids on the kagome lattice with projected entangled pair states: Spinon and vison coherence lengths, topological entropy, and gapless edge modes, *Phys. Rev. B* **87**, 140407 (2013).
- [198] D. Poilblanc, N. Schuch, D. Pérez-García, and J. I. Cirac, Topological and entanglement properties of resonating valence bond wave functions, *Phys. Rev. B* **86**, 014404 (2012).
- [199] D. Poilblanc and G. Misguich, Competing valence bond crystals in the kagome quantum dimer model, *Phys. Rev. B* **84**, 214401 (2011).

-
- [200] A. Olariu, P. Mendels, F. Bert, F. Duc, J. C. Trombe, M. A. de Vries, and A. Harrison, ^{17}O NMR Study of the Intrinsic Magnetic Susceptibility and Spin Dynamics of the Quantum Kagome Antiferromagnet $\text{ZnCu}_3(\text{OH})_6\text{Cl}_2$, *Physical Review Letters* **100**, 087202 (2008).
- [201] P. Nikolic and T. Senthil, Physics of low-energy singlet states of the Kagome lattice quantum Heisenberg antiferromagnet, *Physical Review B* **68**, 214415 (2003).
- [202] H. Nakano and T. Sakai, Numerical-Diagonalization Study of Spin Gap Issue of the Kagome Lattice Heisenberg Antiferromagnet, *Journal of the Physical Society of Japan* **80**, 053704 (2011).
- [203] H. Nakano, T. Shimokawa, and T. Sakai, Collapse of Ferrimagnetism in Two-Dimensional Heisenberg Antiferromagnet due to Frustration, *Journal of the Physical Society of Japan* **80**, 033709 (2011).
- [204] G. Misguich, D. Serban, and V. Pasquier, Quantum Dimer Model on the Kagome Lattice: Solvable Dimer-Liquid and Ising Gauge Theory, *Physical Review Letters* **89**, 137202 (2002).
- [205] L. Messio, C. Lhuillier, and G. Misguich, Time reversal symmetry breaking chiral spin liquids: Projective symmetry group approach of bosonic mean-field theories, *Phys. Rev. B* **87**, 125127 (2013).
- [206] L. Messio, O. Cépas, and C. Lhuillier, Schwinger-boson approach to the kagome antiferromagnet with Dzyaloshinskii-Moriya interactions: Phase diagram and dynamical structure factors, *Phys. Rev. B* **81**, 064428 (2010).
- [207] L. Messio, B. Bernu, and C. Lhuillier, Kagome Antiferromagnet: A Chiral Topological Spin Liquid?, *Phys. Rev. Lett.* **108**, 207204 (2012).
- [208] P. Mendels and F. Bert, Quantum kagome antiferromagnet : $\text{ZnCu}_3(\text{OH})_6\text{Cl}_2$, *Journal of Physics: Conference Series* **320**, 012004 (2011).
- [209] J.-W. Mei, E. Tang, and X.-G. Wen, Chiral spin states in polarized kagome spin systems with spin-orbit coupling, *arXiv:1102.2406* (2011).
- [210] K. Matan, B. M. Bartlett, J. S. Helton, V. Sikolenko, S. Mat'áš, K. Prokeš, Y. Chen, J. W. Lynn, D. Grohol, T. J. Sato, M. Tokunaga, D. G. Nocera, and Y. S. Lee, Dzyaloshinskii-Moriya interaction and spin reorientation transition in the frustrated kagome lattice antiferromagnet, *Phys. Rev. B* **83**, 214406 (2011).
- [211] Y.-M. Lu, Y. Ran, and P. A. Lee, Z_2 spin liquids in the $S=1/2$ Heisenberg model on the kagome lattice: A projective symmetry-group study of Schwinger fermion mean-field states, *Physical Review B* **83**, 224413 (2011).

- [212] Y. sheng Li and Q. ming Zhang, Structure and magnetism of $S=1/2$ kagome antiferromagnets $\text{NiCu}_3(\text{OH})_6\text{Cl}_2$ and $\text{CoCu}_3(\text{OH})_6\text{Cl}_2$, *Journal of Physics: Condensed Matter* **25**, 026003 (2013).
- [213] T. Li, The spin - $1/2$ Heisenberg model on Kagome lattice as a quantum critical system, *1106.6134* (2011).
- [214] A. M. Läuchli, J. Sudan, and E. S. Sørensen, Ground-state energy and spin gap of spin- $\frac{1}{2}$ Kagomé-Heisenberg antiferromagnetic clusters: Large-scale exact diagonalization results, *Phys. Rev. B* **83**, 212401 (2011).
- [215] A. Laeuchli and C. Lhuillier, Dynamical Correlations of the Kagome $S=1/2$ Heisenberg Quantum Antiferromagnet, *0901.1065* (2009).
- [216] E. Khatami, R. R. P. Singh, and M. Rigol, Thermodynamics and phase transitions for the Heisenberg model on the pinwheel distorted kagome lattice, *Phys. Rev. B* **84**, 224411 (2011).
- [217] H. Kawamura, Z_2 -vortex order of frustrated Heisenberg antiferromagnets in two dimensions, *Journal of Physics: Conference Series* **320**, 012002 (2011).
- [218] H. Ju and L. Balents, Finite size effects in the Z_2 spin liquid on the kagome lattice, *arXiv:1302.2636* (2013).
- [219] G.-B. Jo, J. Guzman, C. K. Thomas, P. Hosur, A. Vishwanath, and D. M. Stamper-Kurn, Ultracold Atoms in a Tunable Optical Kagome Lattice, *Phys. Rev. Lett.* **108**, 045305 (2012).
- [220] H. C. Jiang, Z. Y. Weng, and D. N. Sheng, Density Matrix Renormalization Group Numerical Study of the Kagome Antiferromagnet, *Physical Review Letters* **101**, 117203 (2008).
- [221] H. O. Jeschke, F. Salvat-Pujol, and R. Valenti, First-principles determination of Heisenberg Hamiltonian parameters for the spin- $1/2$ kagome antiferromagnet $\text{ZnCu}_3(\text{OH})_6\text{Cl}_2$, *arXiv:1303.1310* (2013).
- [222] M. Jeong, F. Bert, P. Mendels, F. Duc, J. C. Trombe, M. A. de Vries, and A. Harrison, Field-Induced Freezing of a Quantum Spin Liquid on the Kagome Lattice, *Phys. Rev. Lett.* **107**, 237201 (2011).
- [223] Y. Iqbal, F. Becca, and D. Poilblanc, Valence-bond crystals in the kagome spin- $1/2$ Heisenberg antiferromagnet: a symmetry classification and projected wave function study, *New Journal of Physics* **14**, 115031 (2012).
- [224] Y. Iqbal, F. Becca, and D. Poilblanc, Valence-bond crystal in the extended kagome spin- $1/2$ quantum Heisenberg antiferromagnet: A variational Monte Carlo approach, *Physical Review B* **83**, 100404 (2011).

-
- [225] Y. Iqbal, F. Becca, and D. Poilblanc, Projected wave function study of Z_2 spin liquids on the kagome lattice for the spin-1/2 quantum Heisenberg antiferromagnet, *Physical Review B* **84**, 020407 (2011).
- [226] Y. Iqbal, F. Becca, S. Sorella, and D. Poilblanc, Gapless spin-liquid phase in the kagome spin- $\frac{1}{2}$ Heisenberg antiferromagnet, *Phys. Rev. B* **87**, 060405 (2013).
- [227] T. Imai, M. Fu, T. H. Han, and Y. S. Lee, Local spin susceptibility of the $S = \frac{1}{2}$ kagome lattice in $\text{ZnCu}_3(\text{OD})_6\text{Cl}_2$, *Phys. Rev. B* **84**, 020411 (2011).
- [228] K. Hwang, Y. B. Kim, J. Yu, and K. Park, Spin cluster operator theory for the kagome lattice antiferromagnet, *Phys. Rev. B* **84**, 205133 (2011).
- [229] Y. Huh, M. Punk, and S. Sachdev, Vison states and confinement transitions of Z_2 spin liquids on the kagome lattice, *Physical Review B* **84**, 094419 (2011).
- [230] Y. Huh, M. Punk, and S. Sachdev, Optical conductivity of visons in Z_2 spin liquids close to a VBS transition on the kagome lattice, *arXiv:1303.7235* (2013).
- [231] Z. Hao and O. Tchernyshyov, Spin-1/2 Heisenberg antiferromagnet on kagome: a Z_2 spin liquid with fermionic spinons, *arXiv:1301.3261* (2013).
- [232] T. Han, S. Chu, and Y. S. Lee, Refining the Spin Hamiltonian in the Spin- $\frac{1}{2}$ Kagome Lattice Antiferromagnet $\text{ZnCu}_3(\text{OH})_6\text{Cl}_2$ Using Single Crystals, *Phys. Rev. Lett.* **108**, 157202 (2012).
- [233] S. Guertler and H. Monien, Doping on the kagome lattice: A variational Monte Carlo study of the t - J model, *Phys. Rev. B* **84**, 174409 (2011).
- [234] O. Götze, D. J. J. Farnell, R. F. Bishop, P. H. Y. Li, and J. Richter, Heisenberg antiferromagnet on the kagome lattice with arbitrary spin: A higher-order coupled cluster treatment, *Phys. Rev. B* **84**, 224428 (2011).
- [235] B. Fåk, E. Kermarrec, L. Messio, B. Bernu, C. Lhuillier, F. Bert, P. Mendels, B. Koteswararao, F. Bouquet, J. Ollivier, A. D. Hillier, A. Amato, R. H. Colman, and A. S. Wills, Kapellasite: A Kagome Quantum Spin Liquid with Competing Interactions, *Phys. Rev. Lett.* **109**, 037208 (2012).
- [236] N. Elstner and A. P. Young, Spin-1/2 Heisenberg antiferromagnet on the kagome lattice: High-temperature expansion and exact-diagonalization studies, *Physical Review B* **50**, 6871–6876 (1994).
- [237] J.-C. Domenge, C. Lhuillier, L. Messio, L. Pierre, and P. Viot, Chirality and Z_2 vortices in a Heisenberg spin model on the kagome lattice, *Physical Review B* **77**, 172413 (2008).
- [238] T. Dodds, S. Bhattacharjee, and Y. B. Kim, Quantum spin liquids in the absence of spin-rotation symmetry: application to Herbertsmithite, *arXiv:1303.1154* (2013).

- [239] L. Dang, S. Inglis, and R. G. Melko, Quantum spin liquid in a spin- $\frac{1}{2}$ XY model with four-site exchange on the kagome lattice, *Phys. Rev. B* **84**, 132409 (2011).
- [240] G.-W. Chern and O. Tchernyshyov, Magnetic charge and ordering in kagome spin ice, *Philosophical Transactions of the Royal Society A: Mathematical, Physical and Engineering Sciences* **370**, 5718–5737 (2012).
- [241] O. Cépas and A. Ralko, Resonating color state and emergent chromodynamics in the kagome antiferromagnet, *Phys. Rev. B* **84**, 020413 (2011).
- [242] B. Bernu, C. Lhuillier, E. Kermarrec, F. Bert, P. Mendels, R. H. Colman, and A. S. Wills, Exchange energies of kapellasite from high-temperature series analysis of the kagome lattice $J_1 - J_2 - J_d$ -Heisenberg model, *Phys. Rev. B* **87**, 155107 (2013).
- [243] B. H. Bernhard, B. Canals, and C. Lacroix, Green’s function approach to the magnetic properties of the kagomé antiferromagnet, *Phys. Rev. B* **66**, 104424 (2002).
- [244] V. Elser, Nuclear antiferromagnetism in a registered ^3He solid, *Phys. Rev. Lett.* **62**, 2405–2408 (1989).
- [245] C. Zeng and V. Elser, Numerical studies of antiferromagnetism on a Kagomé net, *Phys. Rev. B* **42**, 8436–8444 (1990).
- [246] J. T. Chalker and J. F. G. Eastmond, Ground-state disorder in the spin-1/2 kagomé Heisenberg antiferromagnet, *Phys. Rev. B* **46**, 14201–14204 (1992).
- [247] J. T. Chalker, P. C. W. Holdsworth, and E. F. Shender, Hidden order in a frustrated system: Properties of the Heisenberg Kagomé antiferromagnet, *Physical Review Letters* **68**, 855–858 (1992).
- [248] V. Elser and C. Zeng, Kagome spin-1/2 antiferromagnets in the hyperbolic plane, *Phys. Rev. B* **48**, 13647–13653 (1993).
- [249] J. Richter, J. Schulenburg, and A. Honecker, Quantum magnetism in two dimensions: From semi-classical Néel order to magnetic disorder, in U. Schollwöck, J. Richter, D. J. J. Farnell, and R. F. Bishop, editors, *Quantum Magnetism*, number 645 in Lecture Notes in Physics, pages 85–153, Springer Berlin Heidelberg (2004).
- [250] J. Robert, B. Canals, V. Simonet, and R. Ballou, Propagation and Ghosts in the Classical Kagome Antiferromagnet, *Phys. Rev. Lett.* **101**, 117207 (2008).
- [251] J.-C. Domenge, P. Sindzingre, C. Lhuillier, and L. Pierre, Twelve sublattice ordered phase in the J_1 - J_2 model on the kagomé lattice, *Phys. Rev. B* **72**, 024433 (2005).

-
- [252] C. Waldtmann, H.-U. Everts, B. Bernu, C. Lhuillier, P. Sindzingre, P. Lecheminant, and L. Pierre, First excitations of the spin 1/2 Heisenberg antiferromagnet on the kagom lattice, *The European Physical Journal B - Condensed Matter and Complex Systems* **2**, 501–507 (1998).
- [253] P. Lecheminant, B. Bernu, C. Lhuillier, L. Pierre, and P. Sindzingre, Order versus disorder in the quantum Heisenberg antiferromagnet on the kagomé lattice using exact spectra analysis, *Physical Review B* **56**, 2521–2529 (1997).
- [254] E. S. Sørensen, M. J. Lawler, and Y. B. Kim, Néel and valence-bond crystal order on a distorted kagome lattice: Implications for Zn-paratacamite, *Phys. Rev. B* **79**, 174403 (2009).
- [255] F. Wang and A. Vishwanath, Spin-liquid states on the triangular and Kagomé lattices: A projective-symmetry-group analysis of Schwinger boson states, *Physical Review B* **74**, 174423 (2006).
- [256] S. Sachdev, Quantum magnetism and criticality, *Nature Physics* **4**, 173–185 (2008).
- [257] A. M. Essin and M. Hermele, Classifying fractionalization: Symmetry classification of gapped Z_2 spin liquids in two dimensions, *Physical Review B* **87**, 104406 (2013).
- [258] G. Chen, A. Essin, and M. Hermele, Majorana spin liquids and projective realization of $SU(2)$ spin symmetry, *Phys. Rev. B* **85**, 094418 (2012).
- [259] M. P. Zaletel, R. S. K. Mong, and F. Pollmann, Topological characterization of fractional quantum Hall ground states from microscopic Hamiltonians, *arXiv:1211.3733* (2012).
- [260] X. G. Wen, Non-Abelian statistics in the fractional quantum Hall states, *Physical Review Letters* **66**, 802–805 (1991).
- [261] T. Senthil and M. P. A. Fisher, Fractionalization in the Cuprates: Detecting the Topological Order, *Physical Review Letters* **86**, 292–295 (2001).
- [262] S. Sachdev, What Can Gauge-Gravity Duality Teach Us About Condensed Matter Physics?, volume 3 of *Annual Review of Condensed Matter Physics*, pages 9–33 (2012).
- [263] A. Kitaev and J. Preskill, Topological Entanglement Entropy, *Physical Review Letters* **96**, 110404 (2006).
- [264] M. Levin and X.-G. Wen, Detecting Topological Order in a Ground State Wave Function, *Phys. Rev. Lett.* **96**, 110405 (2006).
- [265] Y. Zhang, T. Grover, A. Turner, M. Oshikawa, and A. Vishwanath, Quasiparticle statistics and braiding from ground-state entanglement, *Phys. Rev. B* **85**, 235151 (2012).

- [266] Y. Zhang and A. Vishwanath, Establishing non-Abelian topological order in Gutzwiller-projected Chern insulators via entanglement entropy and modular \mathcal{S} -matrix, *Phys. Rev. B* **87**, 161113 (2013).
- [267] M. P. Zaletel, J. H. Bardarson, and J. E. Moore, Logarithmic Terms in Entanglement Entropies of 2D Quantum Critical Points and Shannon Entropies of Spin Chains, *Phys. Rev. Lett.* **107**, 020402 (2011).
- [268] X. G. Wen, TOPOLOGICAL ORDERS IN RIGID STATES, *International Journal of Modern Physics B* **04**, 239–271 (1990).
- [269] F. Liu, Z. Wang, Y.-Z. You, and X.-G. Wen, Quantum fidelity, modular transformations, and topological orders in two dimensions, *arXiv:1303.0829* (2013).
- [270] M. A. Levin and X.-G. Wen, String-net condensation: A physical mechanism for topological phases, *Phys. Rev. B* **71**, 045110 (2005).
- [271] O. Buerschaper, M. Aguado, and G. Vidal, Explicit tensor network representation for the ground states of string-net models, *Physical Review B* **79**, 085119 (2009).
- [272] M. B. Hastings, Dirac structure, RVB, and Goldstone modes in the kagomé antiferromagnet, *Physical Review B* **63**, 014413 (2000).
- [273] K. Yang, L. K. Warman, and S. M. Girvin, Possible spin-liquid states on the triangular and kagomé lattices, *Phys. Rev. Lett.* **70**, 2641–2644 (1993).
- [274] C. Zeng and V. Elser, Quantum dimer calculations on the spin-1/2 kagome Heisenberg antiferromagnet, *Phys. Rev. B* **51**, 8318–8324 (1995).
- [275] A. F. Albuquerque, D. Schwandt, B. Hetényi, S. Capponi, M. Mambrini, and A. M. Läuchli, Phase diagram of a frustrated quantum antiferromagnet on the honeycomb lattice: Magnetic order versus valence-bond crystal formation, *Phys. Rev. B* **84**, 024406 (2011).
- [276] S. Capponi, V. R. Chandra, A. Auerbach, and M. Weinstein, $p6$ chiral resonating valence bonds in the kagome antiferromagnet (2013).
- [277] H.-C. Jiang, Z. Wang, and L. Balents, Identifying topological order by entanglement entropy, *Nature Physics* **8**, 902–905 (2012).
- [278] S.-H. Lee, H. Kikuchi, Y. Qiu, B. Lake, Q. Huang, K. Habicht, and K. Kiefer, Quantum-spin-liquid states in the two-dimensional kagome antiferromagnets $\text{ZnxCu}_{4-x}(\text{OD})_6\text{Cl}_2$, *Nat Mater* **6**, 853–857 (2007).
- [279] O. Ofer, A. Keren, E. A. Nytko, M. P. Shores, B. M. Bartlett, D. G. Nocera, C. Baines, and A. Amato, Ground state and excitation properties of the quantum kagomé system $\text{ZnCu}_3(\text{OH})_6\text{Cl}_2$ investigated by local probes, *arXiv:cond-mat/0610540* (2006).

-
- [280] J. S. Helton, K. Matan, M. P. Shores, E. A. Nytko, B. M. Bartlett, Y. Yoshida, Y. Takano, A. Suslov, Y. Qiu, J.-H. Chung, D. G. Nocera, and Y. S. Lee, Spin Dynamics of the Spin-1/2 Kagome Lattice Antiferromagnet $\text{ZnCu}_3(\text{OH})_6\text{Cl}_2$, *Phys. Rev. Lett.* **98**, 107204 (2007).
- [281] F. Bert, S. Nakamae, F. Ladieu, D. L'Hôte, P. Bonville, F. Duc, J.-C. Trombe, and P. Mendels, Low temperature magnetization of the $S = \frac{1}{2}$ kagome antiferromagnet $\text{ZnCu}_3(\text{OH})_6\text{Cl}_2$, *Phys. Rev. B* **76**, 132411 (2007).
- [282] V. R. Shaginyan, A. Z. Msezane, K. G. Popov, G. S. Japaridze, and V. A. Stephanovich, Identification of strongly correlated spin liquid in herbertsmithite, *EPL (Europhysics Letters)* **97**, 56001 (2012).
- [283] S. Pujari and M. Lawler, Effect of Dirac spinons on angle-resolved photoemission signatures of herbertsmithite, *Phys. Rev. B* **87**, 104415 (2013).
- [284] O. Cépas, C. M. Fong, P. W. Leung, and C. Lhuillier, Quantum phase transition induced by Dzyaloshinskii-Moriya interactions in the kagome antiferromagnet, *Phys. Rev. B* **78**, 140405 (2008).
- [285] O. Janson, J. Richter, and H. Rosner, Modified Kagome Physics in the Natural Spin-1/2 Kagome Lattice Systems: Kapellasite $\text{Cu}_3\text{Zn}(\text{OH})_6\text{Cl}_2$ and Haydeeite $\text{Cu}_3\text{Mg}(\text{OH})_6\text{Cl}_2$, *Phys. Rev. Lett.* **101**, 106403 (2008).
- [286] O. Janson, J. Richter, and H. Rosner, Intrinsic peculiarities of real material realizations of a spin-1/2 kagomé lattice, *Journal of Physics: Conference Series* **145**, 012008 (2009).
- [287] S. Maegawa, R. Kaji, S. Kanou, A. Oyamada, and M. Nishiyama, Spin dynamics in classical and quantum Kagome lattice magnets studied by NMR, *Journal of Physics: Condensed Matter* **19**, 145250 (2007).
- [288] W. Schweika, M. Valldor, and P. Lemmens, Approaching the Ground State of the Kagomé Antiferromagnet, *Phys. Rev. Lett.* **98**, 067201 (2007).
- [289] P. Mendels, F. Bert, M. A. de Vries, A. Olariu, A. Harrison, F. Duc, J. C. Trombe, J. S. Lord, A. Amato, and C. Baines, Quantum Magnetism in the Paratacamite Family: Towards an Ideal Kagomé Lattice, *Physical Review Letters* **98**, 077204 (2007).
- [290] S. Dommange, M. Mambrini, B. Normand, and F. Mila, Static impurities in the $S = 1/2$ kagome lattice: Dimer freezing and mutual repulsion, *Phys. Rev. B* **68**, 224416 (2003).
- [291] Y. Hu, S. D. Stirling, and Y.-S. Wu, Ground-state degeneracy in the Levin-Wen model for topological phases, *Physical Review B* **85**, 075107 (2012).
- [292] T. Grover, Chiral Symmetry Breaking, Deconfinement and Entanglement Monotonicity, *arXiv:1211.1392* (2012).

- [293] T. Grover, Quantum Entanglement and Detection of Topological Order in Numerics, *1112.2215* (2011).
- [294] T. Grover, A. M. Turner, and A. Vishwanath, Entanglement entropy of gapped phases and topological order in three dimensions, *Physical Review B* **84**, 195120 (2011).
- [295] X. Chen, Z.-C. Gu, Z.-X. Liu, and X.-G. Wen, Symmetry-Protected Topological Orders in Interacting Bosonic Systems, *Science* **338**, 1604–1606 (2012).
- [296] D. V. Else, S. D. Bartlett, and A. C. Doherty, The hidden symmetry-breaking picture of symmetry-protected topological order, *arXiv:1304.0783* (2013).
- [297] Z.-C. Gu and X.-G. Wen, Tensor-entanglement-filtering renormalization approach and symmetry-protected topological order, *Physical Review B* **80**, 155131 (2009).
- [298] X.-G. Wen, Symmetry-protected topological phases in noninteracting fermion systems, *Physical Review B* **85**, 085103 (2012).
- [299] X.-G. Wen, Topological invariants of symmetry-protected and symmetry-enriched topological phases of interacting bosons or fermions, *arXiv:1301.7675* (2013).
- [300] L. Cincio and G. Vidal, Characterizing Topological Order by Studying the Ground States on an Infinite Cylinder, *Physical Review Letters* **110**, 067208 (2013).
- [301] S. T. Flammia, A. Hamma, T. L. Hughes, and X.-G. Wen, Topological Entanglement Rényi Entropy and Reduced Density Matrix Structure, *Physical Review Letters* **103**, 261601 (2009).
- [302] F. Haldane, Continuum dynamics of the 1-D Heisenberg antiferromagnet: Identification with the $O(3)$ nonlinear sigma model, *Physics Letters A* **93**, 464–468 (1983).
- [303] I. Affleck, T. Kennedy, E. Lieb, and H. Tasaki, Valence bond ground states in isotropic quantum antiferromagnets, *Communications in Mathematical Physics* **115**, 477–528 (1988).
- [304] A. Kitaev, Periodic table for topological insulators and superconductors, *AIP Conference Proceedings* **1134**, 22–30 (2009).
- [305] N. Schuch, D. Pérez-García, and I. Cirac, Classifying quantum phases using matrix product states and projected entangled pair states, *Physical Review B* **84**, 165139 (2011).
- [306] J. Wang and X.-G. Wen, Boundary Degeneracy of Topological Order, *arXiv:1212.4863* (2012).

-
- [307] F. D. M. Haldane, Nonlinear Field Theory of Large-Spin Heisenberg Antiferromagnets: Semiclassically Quantized Solitons of the One-Dimensional Easy-Axis Néel State, *Phys. Rev. Lett.* **50**, 1153–1156 (1983).
- [308] I. Affleck, T. Kennedy, E. H. Lieb, and H. Tasaki, Rigorous results on valence-bond ground states in antiferromagnets, *Physical Review Letters* **59**, 799 (1987).
- [309] T.-C. Wei, I. Affleck, and R. Raussendorf, Two-dimensional Affleck-Kennedy-Lieb-Tasaki state on the honeycomb lattice is a universal resource for quantum computation, *Physical Review A* **86**, 032328 (2012).
- [310] M. Hagiwara, K. Katsumata, I. Affleck, B. I. Halperin, and J. P. Renard, Observation of $S = 1/2$ degrees of freedom in an $S = 1$ linear-chain Heisenberg antiferromagnet, *Phys. Rev. Lett.* **65**, 3181–3184 (1990).
- [311] F. Pollmann, E. Berg, A. M. Turner, and M. Oshikawa, Symmetry protection of topological phases in one-dimensional quantum spin systems, *Phys. Rev. B* **85**, 075125 (2012).
- [312] F. Pollmann and A. M. Turner, Detection of symmetry-protected topological phases in one dimension, *Phys. Rev. B* **86**, 125441 (2012).
- [313] F. Pollmann, A. M. Turner, E. Berg, and M. Oshikawa, Entanglement spectrum of a topological phase in one dimension, *Physical Review B* **81**, 064439 (2010).
- [314] C.-Y. Huang, X. Chen, and F.-L. Lin, Symmetry Protected Quantum State Renormalization, *arXiv:1303.4190* (2013).
- [315] Y. A. Fridman, O. A. Kosmachev, A. K. Kolezhuk, and B. A. Ivanov, Spin Nematic and Antinematic States in a Spin-3/2 Isotropic Non-Heisenberg Magnet, *Physical Review Letters* **106**, 097202 (2011).

Curriculum Vitae

Name Stefan Depenbrock
Date of birth 28/07/1985
Place of birth Dortmund, Germany
Nationality German
Address Germersheimer Straße 38,
80687 München,
Germany

Education

- 2009-today: PhD Student with Prof. Schollwöck
- 2004-2009: Diploma in Physics at RWTH Aachen, graded “sehr gut”
- 2004: Abitur at Stadtgymnasium Dortmund

Acknowledgments

Many people have contributed to the work on this thesis and shall not remain unmentioned. Special thanks go to:

- Ulrich Schollwöck for the opportunity to work in his group for both my diploma and PhD thesis, for the support, for introducing me to the field of numerical simulations of quantum many-body systems, giving me a chance to attend so many interesting conferences, as well as his wry humor in the face of academia.
- Michael Wolf for his kind readiness to co-examine this thesis.
- Fabian Heidrich-Meisner for continued support with so many things in the daily life of a PhD student, while keeping up his good humor.
- Ian McCulloch for sharing his impressive toolkit with me and helping with some of the trickier modifications.
- my flatmate, office mate, and friend Stephan Langer for many an enjoyable evening in the kitchen.
- Tim and Janosch for the care they took to repeatedly point out that some mathematicians view numerical physics as not much different from manual labor.
- Stephan Grap for making many days more enjoyable and showing me his LaTeX magic.
- the rest of the group, especially Alex, Carlos, Fabian K., Lev, Lode, Peter, Thomas, and Vincenzo for sharing their knowledge even after suffering more than one kagome talk.
- the von Delft lunch group (Mensa section) for many discussions over and about mediocre food.
- Cordula Weber for facilitating life in the administrative jungle of the university and making everything so much easier.
- the German Research Foundation (DFG) for substantial financial support.
- my family for their support and motivation.
- Dagmar Hummel for her patience with physics at late hours, willingness to look for internet when the clusters needed attention, and so much more that I could write another thesis about it.

No PhD students were harmed in the making of this thesis.

Selbstständigkeitserklärung

Hiermit versichere ich, dass ich die vorliegende Arbeit selbstständig und ohne Benutzung anderer als der angegebenen Quellen und Hilfsmittel verfasst habe. Die den benutzten Werken wörtlich oder inhaltlich entnommenen Stellen sind als solche kenntlich gemacht.

München, im Mai 2013

Stefan Depenbrock